

SMC Bulletin

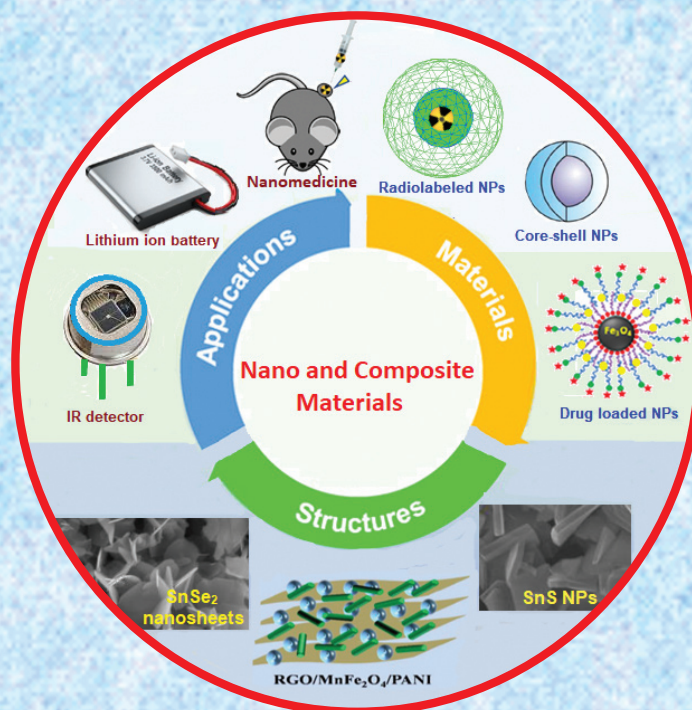
ISSN 2394-5087

A Publication of the Society for Materials Chemistry

Volume 12

No. 1

April 2021



Special Issue on Nano and Composite Materials: Properties and Applications



Society for Materials Chemistry

Society for Materials Chemistry was mooted in 2007 with following aims and objectives:

- to help the advancement, dissemination and application of the knowledge in the field of materials chemistry,
- to promote active interaction among all material scientists, bodies, institutions and industries interested in achieving the advancement, dissemination and application of the knowledge of materials chemistry,
- to disseminate information in the field of materials chemistry by publication of bulletins, reports, newsletters, journals.
- to provide a common platform to young researchers and active scientists by arranging seminars, lectures, workshops, conferences on current research topics in the area of materials chemistry,
- to provide financial and other assistance to needy deserving researchers for participation to present their work in symposia, conference, etc.
- to provide an incentive by way of cash awards to researchers for best thesis, best paper published in journal/national/international conferences for the advancement of materials chemistry,
- to undertake and execute all other acts as mentioned in the constitution of SMC.

Executive Committee

President

Dr. A. K. Tyagi

Bhabha Atomic Research Centre
Trombay, Mumbai – 400 085
Email: aktyagi@barc.gov.in

Vice-Presidents

Prof. Kulamani Parida

Siksha 'O' Anusandhan University
Bhubaneswar – 751 030, Odisha
Email: kulamaniparida@soa.ac.in

Dr. P. A. Hassan

Bhabha Atomic Research Centre
Trombay, Mumbai – 400 085
Email: hassan@barc.gov.in

Secretary

Dr. Sandeep Nigam

Bhabha Atomic Research Centre
Trombay, Mumbai – 400 085
Email: snigam@barc.gov.in

Treasurer

Dr. K. C. Barick

Bhabha Atomic Research Centre
Trombay, Mumbai – 400 085
Email: kcbarick@barc.gov.in

Members

Prof. Amreesh Chandra

Indian Institute of Technology
Kharagpur Kharagpur – 721 302

Dr. Chandra N. Patra

Bhabha Atomic Research Centre
Trombay, Mumbai – 400 085

Dr. Deepak Tyagi

Bhabha Atomic Research Centre
Trombay, Mumbai – 400 085

Prof. (Smt.) Kanchana V.

Indian Institute of Technology
Hyderabad Kandi-502284, Sangareddy,
Telangana

Dr. (Smt.) Mrinal R. Pai

Bhabha Atomic Research Centre
Trombay, Mumbai – 400 085

Dr. Pranesh Senguta

Bhabha Atomic Research Centre
Trombay, Mumbai – 400 085

Dr. R. K. Vatsa

Department of Atomic Energy Mumbai
Mumbai – 400 001

Dr. Sukhendu Nath

Bhabha Atomic Research Centre
Trombay, Mumbai – 400 085

Prof. Tokeer Ahmad

Jamia Millia Islamia
Jamia Nagar, New Delhi – 110 025

Dr. V. K. Jain,

UM-DAE Centre for Excellence in Basic
Sciences, University of Mumbai
Kalina Campus, Mumbai – 400098

Dr. (Smt.) Vinita G. Gupta

Bhabha Atomic Research Centre
Trombay, Mumbai – 400 085

Prof. Vivek Polshettiwar

Tata Institute of Fundamental
Research Mumbai – 400 005

Dr. Y. K. Bhardwaj

Bhabha Atomic Research Centre
Trombay, Mumbai – 400 085

Co-opted Members

Dr. Adish Tyagi

Bhabha Atomic Research Centre
Trombay, Mumbai – 400 085

Prof. G. Mugesh

Indian Institute of Science Bangalore
Bangalore – 560 012

Dr. Pramod Sharma

Bhabha Atomic Research Centre
Trombay, Mumbai – 400 085

Prof. Sandeep Verma

Indian Institute of Technology Kanpur
Kanpur – 208 016

Contact address

Society for Materials Chemistry

C/o Chemistry Division

Bhabha Atomic Research Centre, Trombay, Mumbai, 400 085, India

Tel: +91-22-25592001, E-mail: socmatchem@gmail.com

SMC Bulletin

A Publication of the Society for Materials Chemistry

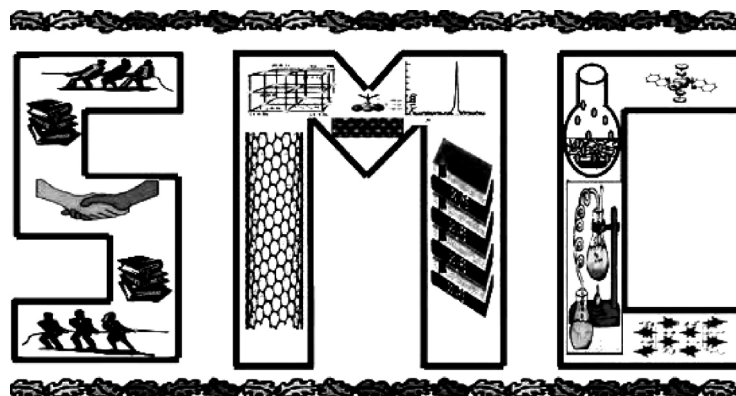
Volume 12

No. 1

April 2021

Special Issue on

Nano and Composite Materials: Properties and Applications



SOCIETY FOR MATERIALS CHEMISTRY

SMC Bulletin

Vol. 12

No. 1

April 2021

Guest Editors

Dr. K. C. Barick
Chemistry Division
Bhabha Atomic Research Centre
Trombay, Mumbai - 400 085
Email: kckbarick@barc.gov.in

Dr. Sandeep Nigam
Chemistry Division
Bhabha Atomic Research Centre
Trombay, Mumbai - 400 085
Email: snigam@barc.gov.in

Dr. Lalita Ledwani
Manipal University Jaipur
Jaipur, Rajasthan - 303007
Email: lalita.ledwani@jaipur.
manipal.edu

Editorial Board	
Dr. C. Majumder (Editor-in-Chief) Chemistry Division Bhabha Atomic Research Centre Trombay, Mumbai - 400 085 Email: chimaju@barc.gov.in	Dr. Arvind Kumar Tripathi Chemistry Division Bhabha Atomic Research Centre Trombay, Mumbai, 400 085 e-mail: catal@barc.gov.in
Dr. (Smt.) S. N. Sawant Chemistry Division Bhabha Atomic Research Centre Trombay, Mumbai - 400 085 Email: stawde@barc.gov.in	Dr. (Smt.) Mrinal Pai Chemistry Division Bhabha Atomic Research Centre Trombay, Mumbai - 400 085 Email: mrinalr@barc.gov.in
Dr. (Kum.) Manidipa Basu Chemistry Division Bhabha Atomic Research Centre Trombay, Mumbai, 400 085 e-mail: deepa@barc.gov.in	Prof. (Smt.) Kanchana V. Department of Physics Indian Institute of Technology Hyderabad Kandi-502284, Sangareddy, Telangana Email: kanchana@phy.iith.ac.in
Dr. Kaustava Bhattacharyya Chemistry Division Bhabha Atomic Research Centre Trombay, Mumbai - 400 085 Email: kaustava@barc.gov.in	Dr. (Smt.) Gunjan Verma Chemistry Division Bhabha Atomic Research Centre Trombay, Mumbai - 400 085 Email: gunjanv@barc.gov.in

Published by

Society for Materials Chemistry
C/o. Chemistry Division
Bhabha Atomic Research Centre, Trombay, Mumbai, 400 085
E-mail: socmatchem@gmail.com,
Tel: +91-22-25592001

Please note that the authors of the paper are alone responsible for the technical contents of papers and references cited therein. Front cover shows the materials, structures and applications of nano and composite materials (cover page is designed by assembling figures reported in this issue of SMC Bulletin)

Guest Editorial



Dr. K. C. Barick



Dr. Lalita Ledwani



Dr. Sandeep Nigam

Nano and composite materials have found tremendous applications in various field ranging from energy, environmental to biomedical sciences etc. Most of these applications are driven by the exciting properties which emerge due to the presence of multiphase components and dimensional constraints. Therefore, today research in the area of nano and composite materials is proven to be a very fertile ground for great scientific and technological discoveries. In order to recognize the potential applications of these materials, evolutionary progress and revolutionary breakthrough are required in the fabrication and understanding of their fundamental properties. The keen interest of research in these areas is stimulated by its tremendous economical, technological and scientific impact. In this special issue, we bring together articles covering the areas of synthesis, properties and potential applications of nano and composite materials in the field of energy, health care and environment. The present issue is collection of articles received from the speakers/participants of National Workshops on Materials Chemistry (NWMC-2019) organized by Society for Materials Chemistry (SMC) in collaboration with Department of Chemistry, School of Basic Sciences, Manipal University, Jaipur, Rajasthan during November 8 - 9, 2019 under the theme of 'Nano and Composite Materials'.

It has been our great pleasure to act as guest editors for this special issue on "Nano and Composite Materials: Properties and Applications". Our sincere thanks to Dr. A. K. Tyagi, President, SMC and all executive committee members for giving us this opportunity. We also thank all the authors for their contribution to the current issue of the bulletin. We hope the readers enjoy reading the articles in this issue and find them informative.

From the desks of the President and Secretary



Dr. A. K. Tyagi



Dr. Sandeep Nigam

Dear SMC Members, Colleagues and Readers,

Warm greetings from the Executive Council of the Society for Materials Chemistry (SMC)!

Society for Materials Chemistry (SMC) organizes biennial National Workshops on Materials Chemistry to promote the field of material science to the young researchers and providing them key inputs required in the fields. To broaden the horizon, the 5th workshop in the NWMC series was first time organized outside Mumbai, in collaboration with Department of Chemistry, School of Basic Sciences, Manipal University, Jaipur, Rajasthan during November 8 - 9, 2019. The theme of the workshop was 'Nano and Composite Materials'. The present issue is collection of articles received from the speakers/participants of NWMC-2019 under the same theme.

The articles in this issue deal with synthesis, functionality, processing, characterization, properties of Nano and Composite Materials and their applications in the field of energy, sensing and health care. First article discussed the structural aspects of composite materials based on phosphate and silicate glasses, along with nanoparticles incorporated glasses. Two article presents the utilization of nanoparticles/nanoplatforms for cancer therapy. Other two articles evaluated the potential of metal and metal chalcogenides nanoparticles for antibacterial and energy applications respectively. The characterisation nano material properties via electrochemical measurements have been summarized in one of the articles. Finally, an article in this issue covers the quantum cutting materials prepared via ionic liquids and their optical applications.

We would like to thank the guest editors who agreed to guest edit this issue and put in efforts to bring out this special issue. We also acknowledge the efforts of all the contributing authors for submitting their informative articles. We also thank all the members of SMC for their continued support and cooperation in the growth of the Society for Materials Chemistry

CONTENTS

Sr. No	Feature Articles	Page No.
1	Glasses and composites based on phosphate and silicate glasses <i>V. Sudarsan</i>	1
2	Intrinsically radiolabeled nanoplatfoms for cancer theranostics <i>Rubel Chakravarty</i>	11
3	Synthesis and characterization of metallic nanoparticles using <i>Rheum emodi</i> roots and investigation of its antibacterial and cytotoxic potential <i>Deepika Sharma, Naveen Kumar, Priyanka Pareek and Lalita Ledwani</i>	19
4	Exploring the gravity of tin chalcogenides as potential energy materials <i>Gourab Karmakar, Adish Tyagi and G. Kedarnath</i>	25
5	Electrochemical techniques in evaluation of processes for energy and sensing applications <i>S. Manna, Abhishek Sharma, Srikant Sahoo and A. K. Satpati</i>	33
6	Quantum cutting nanomaterials via ionic liquids <i>Pushpal Ghosh</i>	45
7	Development of surface functionalized nanoparticles for cancer therapy <i>S. B. Shelar, K. C. Barick and P. A. Hassan</i>	55

Glasses and Composites based on phosphate and silicate glasses

V. Sudarsan

Chemistry Division, Bhabha Atomic Research Centre, Trombay, Mumbai

E-mail: vsudar@barc.gov.in

Abstract

Structural aspects of composite materials based on phosphate and silicate glasses are the subject matter of discussion in the present article. Composition of Ag_2O in $\text{Ag}_2\text{O-P}_2\text{O}_5$ glass has got a strong influence on the extent of Ag metal particle formation in the glass matrix. Annealing in hydrogen environment leads to the formation of Ag nanoparticles of varying sizes in both binary $\text{Ag}_2\text{O-P}_2\text{O}_5$ and ternary $\text{Ag}_2\text{O-PbO-P}_2\text{O}_5$ glasses and the particles exhibit surface Plasmon resonance. Heating binary $\text{Ag}_2\text{O-P}_2\text{O}_5$ glass in hydrogen at 150°C and above leads to destabilization of phosphate network and formation of $\text{P}_2\text{O}_5/\text{P-OH}$ linkages. Unlike this, $\text{Ag}_2\text{O-PbO-P}_2\text{O}_5$ based glasses and composites are thermally stable up to 360°C as revealed by X-ray diffraction (XRD) and ^{31}P Magic Angle Spinning Nuclear Magnetic Resonance (MAS NMR) studies.

Introduction

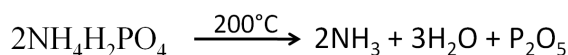
Glasses and composite materials are the most ancient materials used by mankind. It has become part and parcel of human civilizations over the last many years. Generally glasses are defined as amorphous non-crystalline materials which exhibit a phenomenon called glass transition [1]. Composite materials are produced from the combination of two or materials. Typical examples include: concrete, wood, bricks made of straw and mud, bone etc. Glass ceramics which show both the properties of glass and crystalline materials also belong to the category of composite material. Composite materials have been classified according to their composition, structure or on the type of applications. Another commonly encountered classification of glassy or composite materials is based on their structure, namely the amorphous and crystalline phases. Both amorphous and crystalline materials (solids) can be either single phase or a combination of number of phases; the latter material is also called as a composite material. There are many instances, wherein a synergistic mechanism operates and a composite material has many advantages over the corresponding single phase components. Typical examples of such materials include metal supported on oxides such as TiO_2 , Al_2O_3 etc., which have wide application in the area of heterogeneous catalysis [2]. Composite materials also find wide variety of applications and are commonly employed as luminescent materials, glass ceramics, gas /hydrogen storage materials etc [3-5]. In this article a brief description of glass and glass-ceramics along with nanoparticles incorporated glasses, composite materials consisting of silicates etc., will be discussed in detail. Technique used in the present study to characterize such materials is mainly solid state NMR. Brief working principle of solid state NMR is also described in this article.

Phosphate glasses and composites containing Ag^+ ions

Glasses containing Ag^+ ions have potential application as solid state electrolytes in charge storage devices and batteries [6]. High mobility of Ag^+ ion is mainly responsible for such applications [7,8]. Binary $\text{Ag}_2\text{O-P}_2\text{O}_5$ glasses have been well studied for their electrical properties and structural aspects [7-8]. It has been confirmed from these studies that stable glass formation occurs over the region of 65% to 35 mol % of P_2O_5 in $\text{Ag}_2\text{O-P}_2\text{O}_5$ glasses. In general phosphate glasses with high P_2O_5 contents are moisture sensitive and while heating phosphoric acid evaporates out from such glasses, leading to loss in phosphorous contents. These glasses are also prone to crystallizations upon high temperatures heat treatment resulting in the formation of composite materials. It may be also noted that, Ag-O-P bonds present in $\text{Ag}_2\text{O-P}_2\text{O}_5$ glasses are quite different from the P-O-Na bond present in $\text{Na}_2\text{O-P}_2\text{O}_5$ glasses and this can be explained based on difference in the polarisability of Na^+ and Ag^+ ions in the P-O-Na/P-O-Ag linkages. Unlike Na^+ ion containing glasses, $\text{Ag}_2\text{O-P}_2\text{O}_5$ glasses with higher Ag^+ ions, there is possibility of formation of Ag metal nanoparticles as confirmed earlier by Rindone and Weyl [9]. Increased number of non-bridging oxygen atoms formed due to the extended incorporation of Ag^+ ions in the glass, facilitates the reduction of Ag^+ to Ag metal nanoparticles in the glass matrix. Electrical conductivity and dielectric relaxation studies carried out on these glasses revealed non-linear variation in the properties as a function of compositions, which probably can be attributed to the formation of silver metal nanoparticles in the glass matrix [10]. Glasses, particularly the phosphate glasses with metal nanoparticles exhibit high non linear index of refraction or optical susceptibility ($\chi^3 \approx 10^{-8}$ esu)

[11] and are potential candidates for opto-electronic applications. Surface plasmon resonance exhibited by these nanoparticles is responsible for the improvement in the nonlinear properties of these glasses. Sizes of the metal particles play major role in deciding the optical properties of these glasses. As binary phosphate glasses such as $\text{Ag}_2\text{O-P}_2\text{O}_5$ are less stable compared to silicate glasses under ambient conditions, additives like AgI are generally added to make a composite materials which are stable [12-15]. Another way to make the system more stable under ambient conditions is to heat the binary phosphate glasses at higher temperatures so that the crystalline phosphate phases are formed in the glass matrix thereby reducing the phosphorus content in the glassy phase. This results in the stabilization of the glassy phase. In the present study a similar approach has been followed to make Ag nanoparticle incorporated glass composites. Two representative glass systems namely $\text{Ag}_2\text{O-P}_2\text{O}_5$ and $\text{Ag}_2\text{O-PbO-P}_2\text{O}_5$ were prepared and characterised. These glass systems were converted to composite materials by nucleating Ag nanoparticles in the glass matrix by annealing in hydrogen environment. XRD and ^{31}P Magic Angle Spinning Nuclear Magnetic Resonance (MAS NMR) techniques have been used to characterize both glasses and composites. Preparation methods of glasses and composites are mentioned in the following section. As NMR technique is mainly used to characterize different structural units present in these materials, a brief principle of the technique is also mentioned in the article.

Glasses and glass composites were prepared from the starting materials $\text{NH}_4\text{H}_2\text{PO}_4$ (ADP), $\text{Pb}(\text{NO}_3)_2$ and AgNO_3 . The constituents in the required mole or weight ratios were mixed and heated initially at 200°C for the complete decomposition of ADP to P_2O_5 based on the following reaction:



The reaction product obtained at 200°C was heated further to higher temperatures in the range of $700\text{-}800^\circ\text{C}$ and quenched between two brass plates. Glass with less than 40 mol % P_2O_5 are found to form composite phase where as those with more than 65% P_2O_5 are found to be highly moisture sensitive. Samples were mainly characterised by different techniques such as XRD, UV-Visible optical absorption and ^{31}P MAS NMR techniques.

Magic Angle Spinning Nuclear Magnetic Resonance (MAS NMR): MAS NMR technique involves rotating the powder samples at high speeds, at an angle of 54.7° (magic angle) with respect to the applied magnetic field (B_0) direction. When $\theta=54.7^\circ$, the term $3\cos^2\theta$ becomes unity

and hence the term $3\cos^2\theta - 1$ becomes zero. Different inter-nuclear interactions such as dipole-dipole, quadrupolar and chemical shift anisotropy etc., average out up on fast spinning under 54.7° , as all these interactions have an angular dependence of $3\cos^2\theta - 1$ in their Hamiltonian (mentioned below). This is also schematically shown in Fig.1 and explained below.

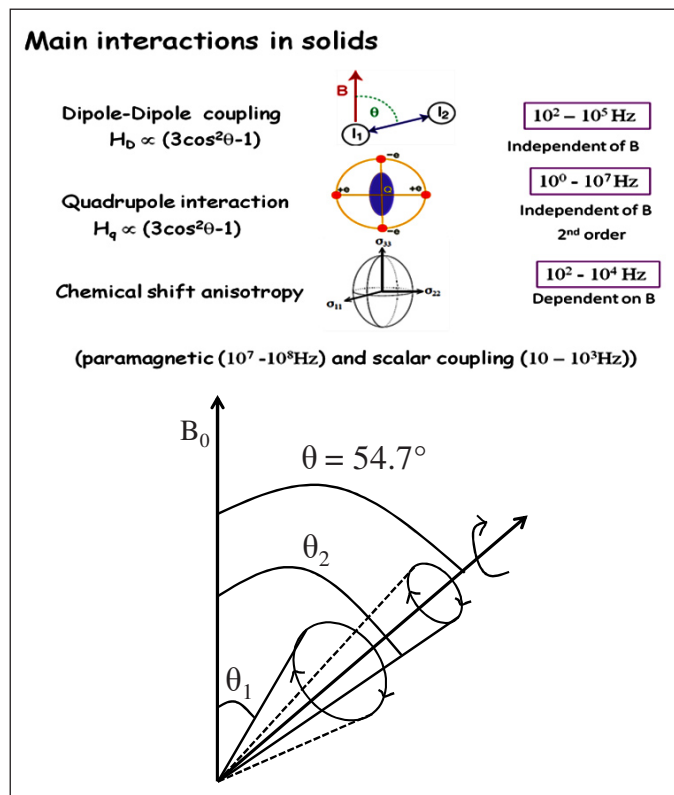


Fig. 1 Principle of MAS NMR experiment

At sufficiently fast spinning speeds, the NMR interaction tensor orientations with initial angles of θ_1 and θ_2 relative to B_0 have orientation averages of 54.7° , resulting in the conversion of $3\cos^2\theta - 1$ term in expressions corresponding to various interactions to a very small value, thereby giving rise to sharp NMR peaks. Thus the MAS NMR technique provides high resolution solid state NMR patterns and chemical environments can be correlated with corresponding chemical shift values [16, 17].

Although, MAS is an efficient technique employed for getting high resolution NMR patterns from solid samples, in many cases, due to spinning, side bands, which are mirror images of the isotropic peak and spread from the isotropic peak by integer multiples of the spinning frequency, appear along with the central isotropic peak. This happens particularly for nuclei having wide range of chemical shift values. Side bands and isotropic peak can be distinguished by varying the spinning speeds

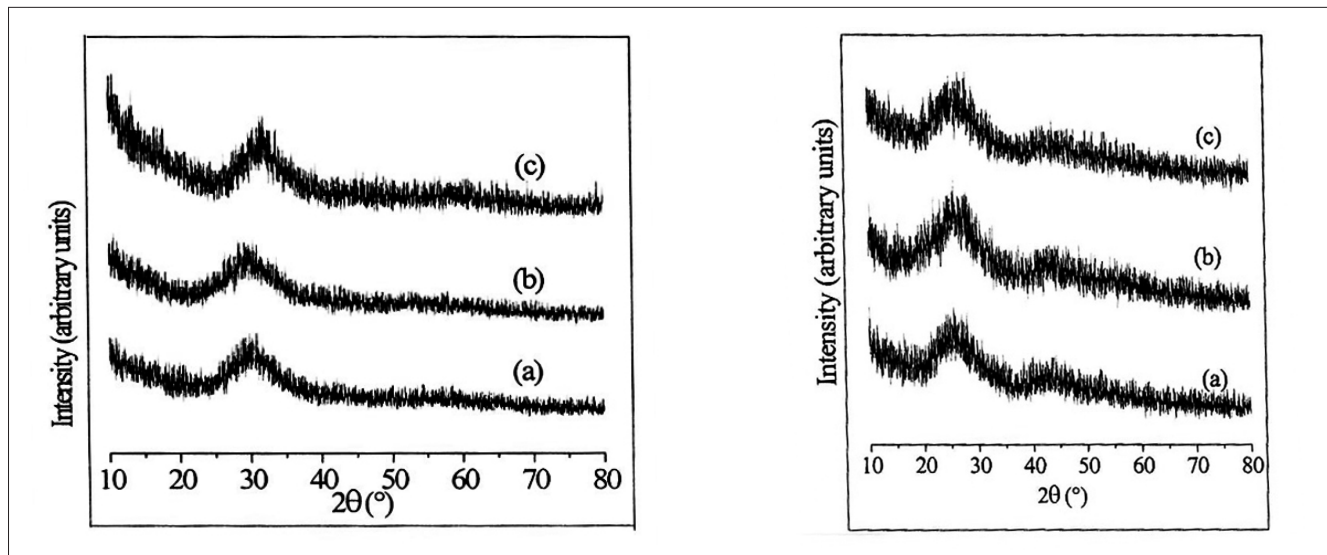


Figure 2. XRD patterns of $(\text{Ag}_2\text{O})_{1-x}(\text{P}_2\text{O}_5)_x$ glasses (right) with (a) $x=0.50$, (b) $x=0.45$ and (c) $x=0.40$. Corresponding patterns for $(\text{PbO})_{1-x}(\text{P}_2\text{O}_5)_x$ glasses with (a) $x=0.50$, (b) $x=0.45$ and (c) $x=0.40$ are shown in the left side of Fig. 2

and recording the NMR spectrum. Unlike the position of isotropic peak, the position of side bands shifts with variation in frequency. In the present study, ^{31}P MAS NMR patterns were recorded using a 400 MHz BrukerAvance machine with a ^{31}P basic frequency of 161.92 MHz. The samples were packed inside 4 mm rotor and subjected to a spinning speed of 10000 Hz. The chemical shift values are expressed with respect to 85% H_3PO_4 solution. The typical 90° pulse duration and relaxation delay are 4 μs and 5s respectively.

Results and discussion

Figure 2 shows the XRD patterns of both $\text{Ag}_2\text{O}-\text{P}_2\text{O}_5$ and $\text{PbO}-\text{P}_2\text{O}_5$ glasses. Patterns corresponding to both the series of glasses showed a broad hump over the 2θ range $25-35^\circ$ characteristic of the amorphous nature the glass compositions. XRD patterns were also recorded for the glass samples prepared in different batches and no sharp peaks characteristic of crystalline phase could be detected from the patterns, confirming the glassy nature of the samples (at least to the detection limit of XRD technique). In the case of $\text{PbO}-\text{P}_2\text{O}_5$ glasses, Ag_2O was incorporated up to 25 wt.% and it is observed that beyond 25 wt% Ag_2O incorporation, glass formation does not occur.

Figure 3(right) shows the UV visible optical absorption spectra recorded from $\text{Ag}_2\text{O}-\text{P}_2\text{O}_5$ glasses as a function of composition. The glass with composition $(\text{Ag}_2\text{O})_{0.45}(\text{P}_2\text{O}_5)_{0.55}$ is characterised by a broad absorption edge with onset of absorption around 316 nm and this corresponds to an optical gap of around 3.67 eV. With increase in Ag_2O content in the glass, onset wavelength corresponding

to optical absorption edge shifts to higher wavelengths. For example the value changes to 337,370 and 461 nm for $(\text{Ag}_2\text{O})_{0.50}(\text{P}_2\text{O}_5)_{0.50}$, $(\text{Ag}_2\text{O})_{0.55}(\text{P}_2\text{O}_5)_{0.45}$ and $(\text{Ag}_2\text{O})_{0.60}(\text{P}_2\text{O}_5)_{0.40}$ glasses (Fig. 3(left)). Optical absorption observed in these glasses can be attributed to the combined effect of glass matrix and silver nanoparticles present in the matrix. Glass sample with composition $(\text{Ag}_2\text{O})_{0.55}(\text{P}_2\text{O}_5)_{0.45}$ (and also $(\text{Ag}_2\text{O})_{0.60}(\text{P}_2\text{O}_5)_{0.40}$) are characterised by light yellow colour whereas other glass samples with more than 45% P_2O_5 are found to be colour less. Yellow colour from 45 mol% P_2O_5 and less than 45 mol % P_2O_5 containing glasses has been attributed to the silver nanoparticles present in it. Hence except for the glass with 45 mol% and 40 mol% P_2O_5 for all the remaining glasses, the optical absorption edge is mainly constituted by the glass network namely P-O-P linkages. Absorption from the glass matrix can be considered as excitation of electrons from the 2p levels of oxygen atoms/ions in the glass to higher energy levels. It will be much easier to excite electrons from oxygen when it is having a negative charge compared to neutral state (state with no charge). Oxygen with negative charge is considered as non-bridging oxygen and that with neutral charge is nothing but bridging oxygen. Hence with increase in concentration of non-bridging oxygen atoms, it is expected that the value of optical gap should decrease. Indeed with increase in Ag_2O content, optical gap decreases as revealed by the increase in wavelength corresponding to the onset of absorption as mentioned above. A similar trend is also observed for binary $\text{PbO}-\text{P}_2\text{O}_5$ glasses which showed increase in the onset wavelength corresponding to optical absorption with increase in PbO content in the glass as can be seen from Figure 3(left).

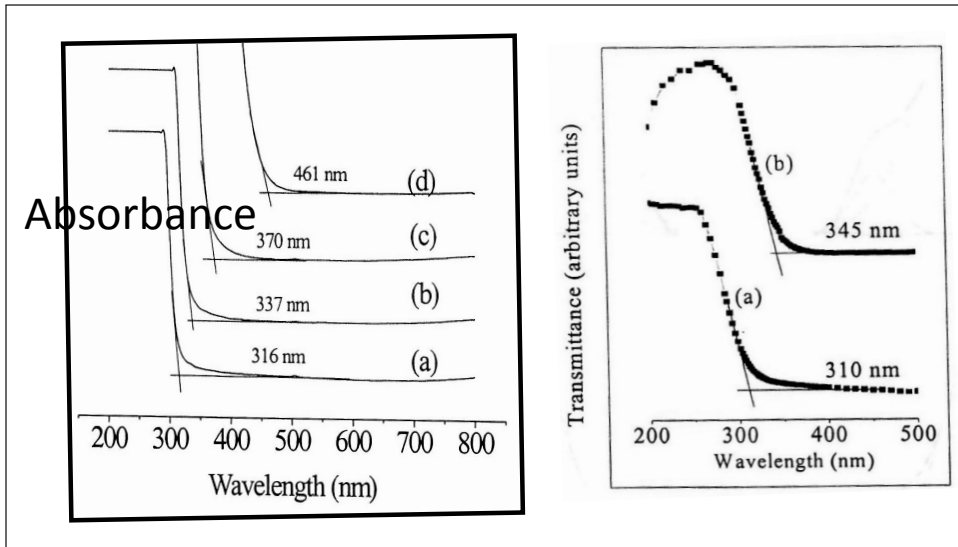


Figure 3. Optical absorption spectra of $(Ag_2O)_{1-x}(P_2O_5)_x$ glasses (left) with (a) $x=0.55$, (b) $x=0.50$, (c) $x=0.45$ and (d) $x=0.40$. Corresponding patterns for $(PbO)_{1-x}(P_2O_5)_x$ glasses with (a) $x=0.60$ and (b) $x=0.40$ are shown in the left side of Fig. 3

To confirm the formation of Ag nanoparticles in the glass matrix, the $(Ag_2O)_{0.60}(P_2O_5)_{0.40}$ glass sample was heated in hydrogen environment and its UV-Visible optical absorption spectrum is shown in Fig. 4. It is interesting to note that a shoulder peak is seen in the UV-Visible absorption spectrum for the glass sample heated in hydrogen at 65°C for 30 minutes.

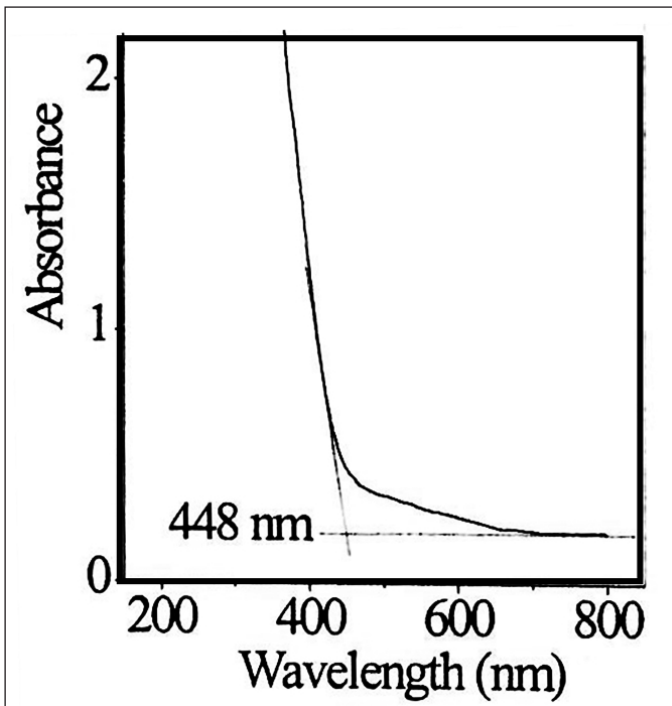


Figure 4. UV visible optical absorption spectrum of $(Ag_2O)_{0.6}(P_2O_5)_{0.4}$ glass sample heated in hydrogen at 64°C for 30 minutes.

The shoulder peak which overlaps with the optical absorption edge has been attributed to the surface Plasmon resonance from the Ag nanoparticles. Heating in hydrogen resulted in the increase in concentration of Ag metal nanoparticles. Subsequently clustering of the particles occurs, leading to increase in particles size. This explains observation of shoulder peak in the UV-Visible spectrum (Fig. 4). Such shoulder peaks are not seen for the glass samples which are not heated in hydrogen probably due to the low concentration of Ag nanoparticles combined with its smaller size. XRD patterns of glasses heated at 65°C for 30 minutes did not

show the presence of Ag nanoparticle also due to the low concentration of nanoparticles. To further establish the formation of Ag nanoparticles in glass matrix, the samples were heated in hydrogen atmosphere at higher temperatures for longer durations and figure 5(a and b) shows the XRD patterns of $(Ag_2O)_{0.60}(P_2O_5)_{0.40}$ and $(Ag_2O)_{0.50}(P_2O_5)_{0.50}$ glasses subjected to higher heat treatment temperatures for longer durations. The temperature was varied from 25 to 150°C with a time duration of 4h at each temperature. For sample heated above 60°C a sharp peak around 2θ value of 38.11° appeared in the XRD pattern and the same has been attributed to the Ag metal nanoparticles. Based on the Debye-Scherrer equation average crystallite size has been evaluated and found to vary from 30 to 57 nm with increase in temperature from 25°C up to 150°C. Evaluated crystallite sizes are mentioned in Fig. 5(a and b). A similar trend is also observed for $(Ag_2O)_{0.50}(P_2O_5)_{0.50}$ glasses, although the particle size varied from 20 to ~50 nm for these glasses as can be seen from Fig. 5(b). Upon heating the sample beyond 150°C, slight opacity was developed in both the glass samples indicating partial devitrification or phase separation. Further, glass samples also showed increase in moisture absorption above an annealing temperature of 150°C.

With increase in temperatures, diffusion rate of Ag^+ ions in the glass increases leading to clustering. Clustered Ag^+ ions in hydrogen environment undergo reduction to form silver metal particles. In $Ag_2O-P_2O_5$ glasses, Ag^+ ions exist in the interstitial positions and neutralize the negative charge of non-bridging oxygen atoms. Due to the conversion of Ag^+ ions to Ag metal particles, sufficient

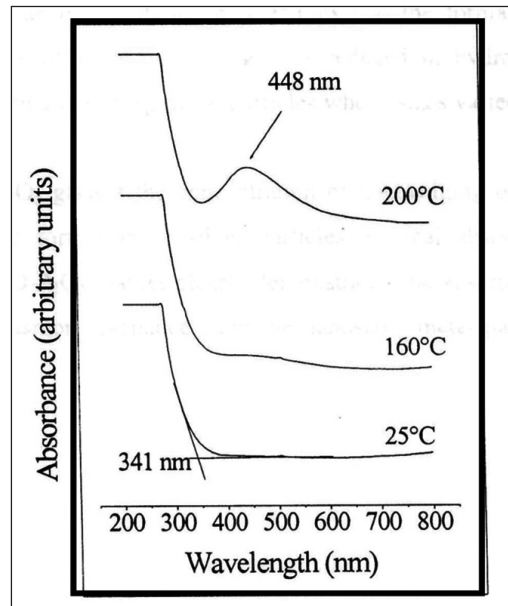
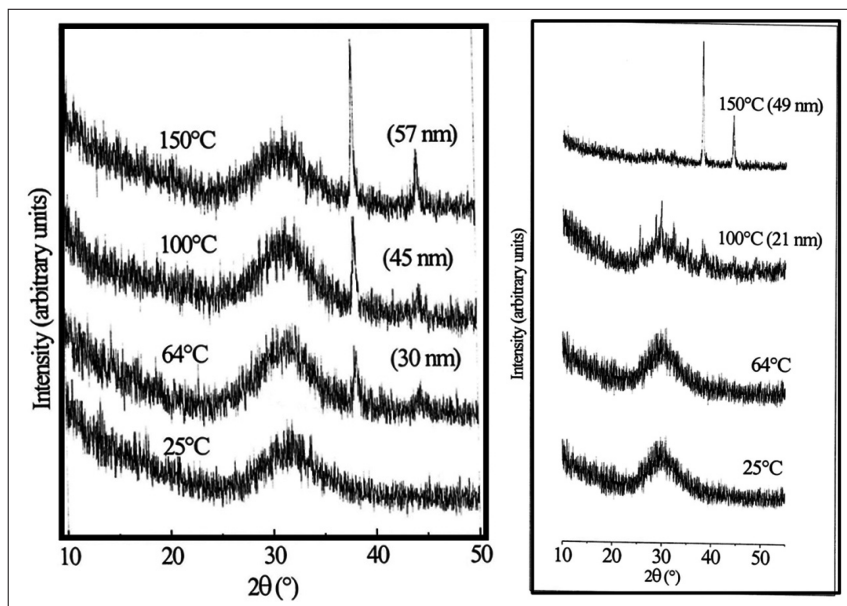


Figure 5. XRD patterns of $(Ag_2O)_{0.60}(P_2O_5)_{0.40}$ (a) and $(Ag_2O)_{0.50}(P_2O_5)_{0.50}$ (b) glasses up on heat treatment at different temperatures for different durations.

Figure 6. UV-Visible optical absorption spectra of 10 wt.% Ag_2O doped $(PbO)_{0.5}(P_2O_5)_{0.5}$ glass heated at different temperatures under flowing hydrogen environment.

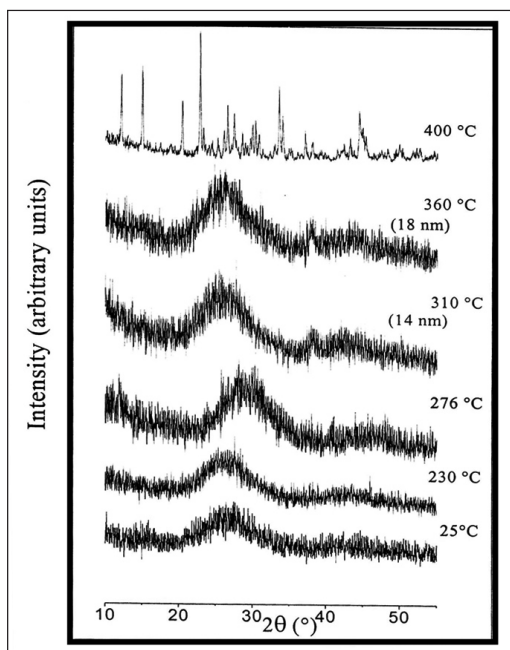


Figure 7. XRD patterns corresponding to 10 wt.% Ag_2O incorporated $(PbO)_{0.5}(P_2O_5)_{0.5}$ glass heated in hydrogen environment at different temperatures.

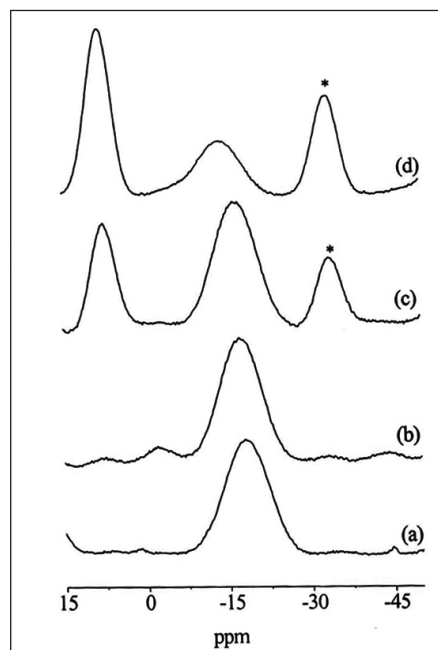


Figure 8. ^{31}P MAS NMR patterns of as prepared glass sample with composition (a) $(Ag_2O)_{0.45}(P_2O_5)_{0.55}$ (b) $(Ag_2O)_{0.50}(P_2O_5)_{0.50}$ (c) $(Ag_2O)_{0.55}(P_2O_5)_{0.45}$ (d) $(Ag_2O)_{0.60}(P_2O_5)_{0.40}$. The peaks marked "*" correspond to spinning side bands

Ag^+ ions are not available for neutralizing the negative charge of non-bridging oxygen atoms (ions) and this leads to moisture attack on the glass thereby forming P-OH linkages. This must be the reason for the increase in moisture sensitiveness of the glass with increase in annealing temperatures.

For $(PbO)_{0.5}(P_2O_5)_{0.5}$ glass containing 10 wt.% Ag_2O , no clear absorption peak is observed for the as prepared sample. But upon heating at temperatures above $150^\circ C$, the surface Plasmon peak over the region of 420-500nm with peak maximum around 450 nm appeared as can be seen from Fig. 6. The

peak become more predominant for the 200°C heated sample

XRD patterns of the heated samples were recorded to check whether any crystalline phase is appearing up on heat treatment. It is observed that the glass is found to be quite stable up to temperature of 360°C and beyond which crystallization of $Pb(PO_3)_2$ phase occurred. This is clear from the sharp diffraction peaks in the XRD patterns shown in Figure 7 (top pattern).

To understand the effect of heat treatment under hydrogen environment on different P structural units present in these glasses, ^{31}P MAS NMR studies were carried out and the results are described in the following section

^{31}P MAS NMR studies

^{31}P MAS NMR patterns of as prepared $Ag_2O-P_2O_5$ glasses are shown in Fig. 8. A single broad peak around -18 ppm is observed for $(Ag_2O)_{0.45}(P_2O_5)_{0.55}$ and $(Ag_2O)_{0.50}(P_2O_5)_{0.50}$ glasses (Figure 8 (a and b)). Unlike this for glass sample with more than 50% Ag_2O , (i.e. for $(Ag_2O)_{0.55}(P_2O_5)_{0.45}$ and $(Ag_2O)_{0.60}(P_2O_5)_{0.40}$ glasses), another peak (which is relatively sharper than -18 ppm) started appearing around 8 ppm (Fig. 8(c and d)).

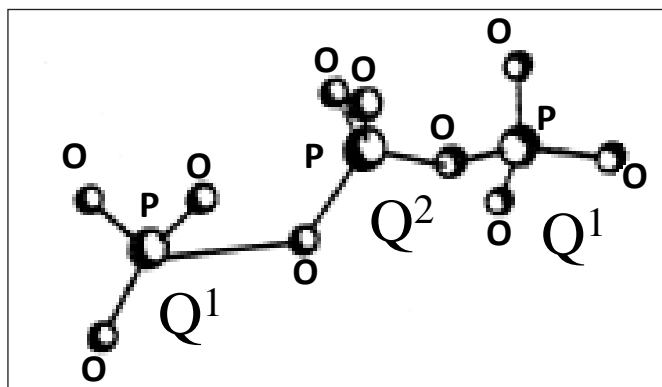


Figure 9. Schematic representation of P-O-P network consisting of Q² and Q¹ structural units of P (middle and end structural units respectively) existing in phosphate glasses.

Based on earlier studies on phosphate glasses [18,19], the peak round -18 ppm has been attributed to Q² structural units of P (phosphorus structural units with 2 bridging oxygen atoms) and that around 8 ppm to Q¹ structural units (i.e P structural units with one bridging oxygen atoms and 3 non bridging oxygen atoms). These structural units are schematically shown in Fig. 9.

With increase in Ag_2O content, there is slight increase in the chemical shift values of Q² and Q¹ structural units and this has been attributed to decrease in P-O-P chain length brought about by the network modifying action of Ag_2O .

For $(Ag_2O)_{0.45}(P_2O_5)_{0.55}$ and $(Ag_2O)_{0.50}(P_2O_5)_{0.50}$ glasses ^{31}P MAS NMR line shapes are identical confirming that the incorporated Ag^+ ions do not affect the P structural units and must be occupying the network modifying sites (interstitial sites) in the glass network. In other words the relative concentrations of non-bridging oxygen atoms attached with P is nearly same for $(Ag_2O)_{0.45}(P_2O_5)_{0.55}$ and $(Ag_2O)_{0.50}(P_2O_5)_{0.50}$ glasses and this is also reflected in the marginal shift in wavelength corresponding to onset of absorption observed in the UV-Visible absorption spectra (Fig.3(left)). ^{31}P MAS NMR patterns confirm that there is increase in relative concentration of Q¹ structural units and associated increase in the non-bridging oxygen atoms in $(Ag_2O)_{0.55}(P_2O_5)_{0.45}$

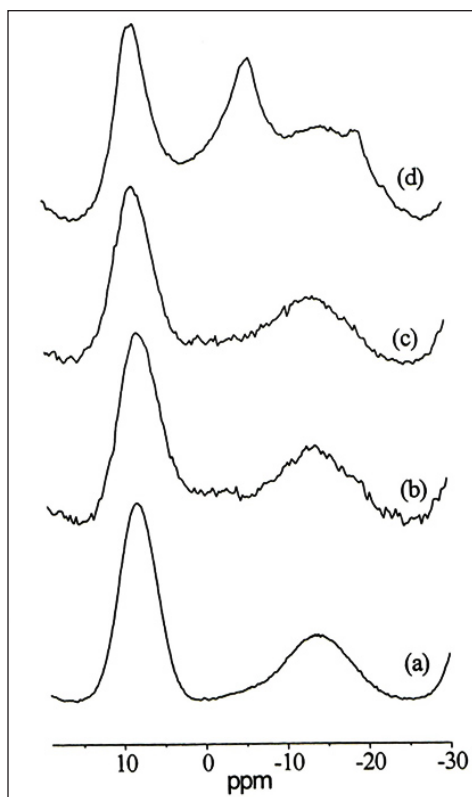


Fig. 10(left): ^{31}P MAS NMR patterns of $(Ag_2O)_{0.60}(P_2O_5)_{0.40}$ glass heated at different temperatures in hydrogen environment: (a) as prepared (b) 64°C (c) 100°C and (d) 150°C.

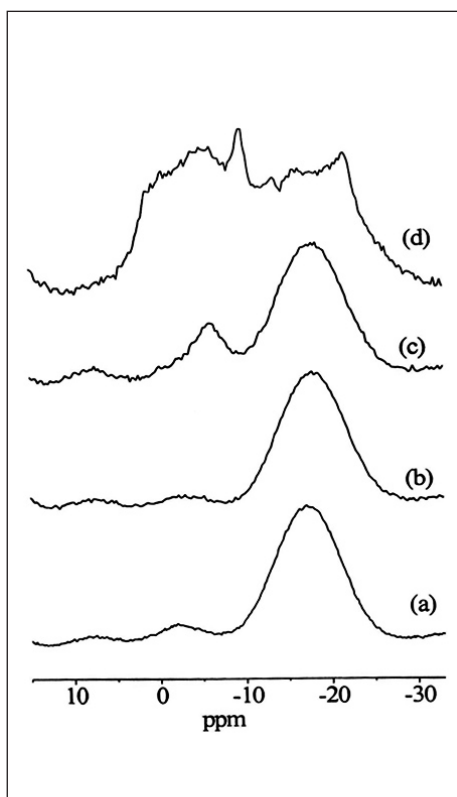


Fig. 10(right): ^{31}P MAS NMR patterns of $(Ag_2O)_{0.50}(P_2O_5)_{0.50}$ glass heated at different temperatures in hydrogen environment: (a) as prepared (b) 64°C (c) 100°C and (d) 150°C.

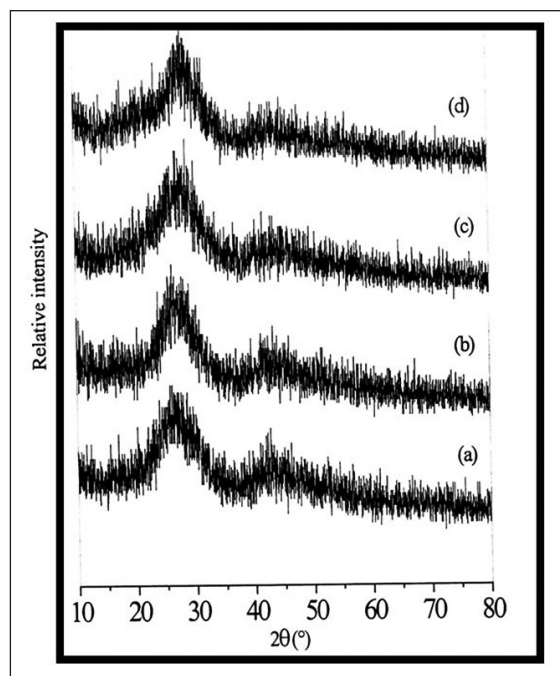


Figure 11. XRD patterns of $(\text{PbO})_{0.55}(\text{P}_2\text{O}_5)_{0.45}$ glasses containing (a) 0 wt.% Ag_2O (b) 6 wt.% Ag_2O (c) 12 wt.% Ag_2O and (d) 25 wt.% Ag_2O

and $(\text{Ag}_2\text{O})_{0.60}(\text{P}_2\text{O}_5)_{0.40}$ glasses. This is reflected as significant increase in the onset wavelength of absorption as can be seen from Fig. 3(left).

NMR studies were also carried out on hydrogen heated samples of $\text{Ag}_2\text{O}-\text{P}_2\text{O}_5$ glasses and representative NMR patterns of $(\text{Ag}_2\text{O})_{0.50}(\text{P}_2\text{O}_5)_{0.50}$ and $(\text{Ag}_2\text{O})_{0.60}(\text{P}_2\text{O}_5)_{0.40}$ glasses are shown in Figure 10 (left and right).

Temperature range at which the samples were heated varied over 25 to 150°C. Changes in NMR line shapes are observed for $(\text{Ag}_2\text{O})_{0.60}(\text{P}_2\text{O}_5)_{0.40}$ glass around 150°C and above, whereas for $(\text{Ag}_2\text{O})_{0.50}(\text{P}_2\text{O}_5)_{0.50}$ glass, even annealing at 100°C, structural units undergo change (viz. Fig.10(right)). Structural changes occur in terms of appearance of peaks around -6.5 ppm characteristic of P-OH linkages. From the results it is inferred that formation of Ag nanoparticles makes $\text{Ag}_2\text{O}-\text{P}_2\text{O}_5$ glasses more susceptible to moisture absorption and this occurs possibly due to the conversion of charge neutralizing Ag^+ ions to Ag or Ag^0 species, leaving the P-O linkages susceptible for moisture attack. Effect of Ag^+ ions doping in $\text{PbO}-\text{P}_2\text{O}_5$ glasses were also investigated and the results are described in the following section.

Figure 11 shows the XRD patterns of $(\text{PbO})_{0.55}(\text{P}_2\text{O}_5)_{0.45}$ glasses containing up to 25 wt.% Ag_2O .

A broad asymmetric peak with a peak a maximum around 26° was observed for the samples indicating its amorphous nature. No sharp peaks characteristic of Ag

As described earlier in this article and also based on previous studies [18, 19] the peak around -24 and -10 ppm have been attributed to Q^2 and Q^1 structural units of P. Network modifying action of PbO is responsible for the significant increase in the concentration of Q^1 structural units. For glass samples with less than 50mol % PbO , the ^{31}P MAS NMR line shapes are nearly same suggesting that PbO act as a network former in these glasses. For limited concentrations of Pb^{2+} , it can be accommodated in the phosphate network as PbO_4^{2-} structural units and above this concentration, Pb^{2+} occupies the interstitial positions and is expected to have higher coordination numbers (6 and above). It may be also noted that Wang and Zhang [20], based XPS studies, reported the network forming and modifying action of PbO in lead silicate glasses. Our

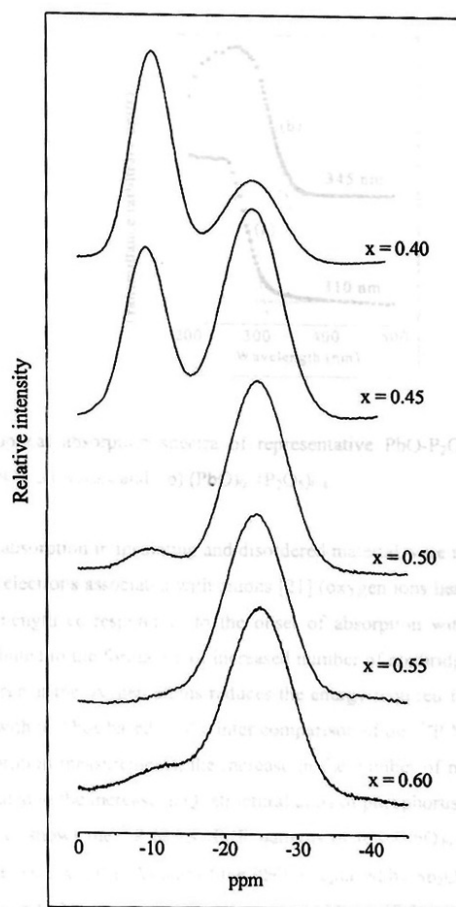


Figure 12. ^{31}P MAS NMR patterns of $(\text{PbO})_{1-x}(\text{P}_2\text{O}_5)_x$ glasses

nanoparticles could be seen in the XRD patterns. This probably may be due to the low concentration of Ag nanoparticles in the matrix.

Figure 12 shows the ^{31}P MAS NMR patterns of $(\text{PbO})_{1-x}(\text{P}_2\text{O}_5)_x$ glasses with $0.4 \leq x \leq 0.6$. The glass with composition $(\text{PbO})_{0.4}(\text{P}_2\text{O}_5)_{0.6}$ is characterized by a broad peak around

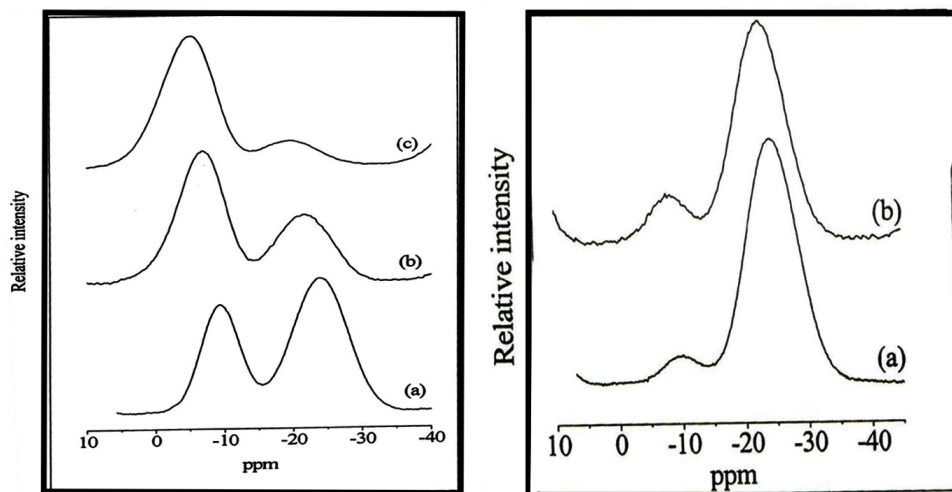


Figure 13 (left). ^{31}P MAS NMR patterns of $(\text{PbO})_{0.55}(\text{P}_2\text{O}_5)_{0.45}$ glass containing (a) 0 wt.%, (b) 10 wt.% and (c) 25 wt.% Ag_2O . Corresponding patterns for $(\text{PbO})_{0.50}(\text{P}_2\text{O}_5)_{0.50}$ glass with (a) 0 wt.% and (b) 10 wt.% Ag_2O are shown in Fig. 13(right)

inferences further confirm the dual role of Pb^{2+} in glasses.

^{31}P MAS NMR patterns of Ag_2O containing $\text{PbO-P}_2\text{O}_5$ glasses having two representative compositions namely $(\text{PbO})_{0.5}(\text{P}_2\text{O}_5)_{0.5}$ and $(\text{PbO})_{0.55}(\text{P}_2\text{O}_5)_{0.45}$ and containing up to 25 wt.% Ag_2O are shown in Fig. 13 (left and right). The glasses are found to be stable up to 360°C as can be seen from the identical ^{31}P MAS NMR patterns.

In the case of $(\text{PbO})_{0.55}(\text{P}_2\text{O}_5)_{0.45}$ glass, Q^1 structural units increase at the expense of Q^2 structural units with increase in Ag_2O content in the glass. Unlike this for

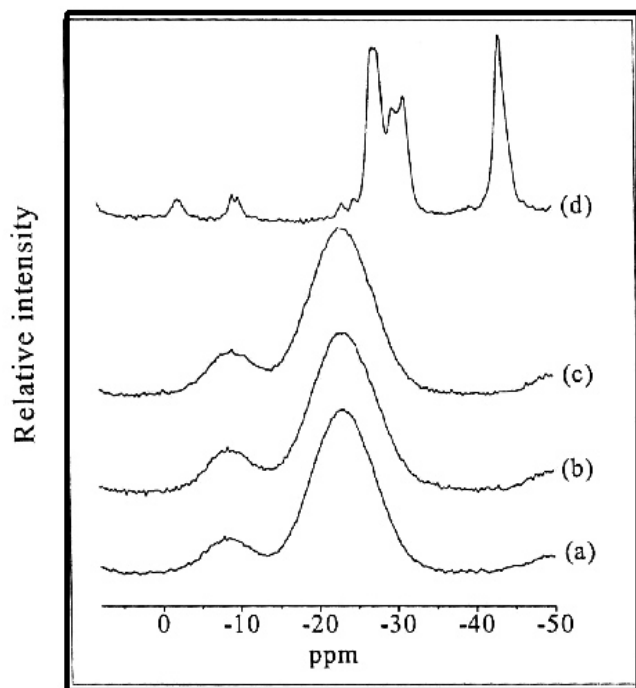


Figure 14. ^{31}P MAS NMR patterns of $(\text{PbO})_{0.50}(\text{P}_2\text{O}_5)_{0.50}$ glass sample containing 10 wt.% Ag_2O and heated in hydrogen at different temperatures for 4h. (a) 25°C (b) 260°C (c) 360°C and (d) 400°C

-24 ppm with a shoulder around -10 ppm. As the PbO concentration increases in the glass above 50 mol %, the intensity of peak around -10 ppm increases significantly and for glass sample with 60 mol % PbO peak around -24 ppm becomes less intense compared to that of the peak around -10 ppm. There is also a slight increase in the chemical shift values of both the peaks with increase in PbO content in the glass.

$(\text{PbO})_{0.50}(\text{P}_2\text{O}_5)_{0.50}$ glass, phosphorus structural units namely Q^2 and Q^1 units, remained nearly same in terms of chemical shift values and line shapes. For higher concentration of Ag_2O , free flowing melt could not be obtained and hence glasses could not be prepared. In the case of $(\text{PbO})_{0.50}(\text{P}_2\text{O}_5)_{0.50}$ glasses sufficient number of Q^2 structural units with longer chain length and two non-bridging oxygen atoms attached to each P provide enough sites for the incorporation of Ag^+ ions at the network modifying positions. In the case of $(\text{PbO})_{0.55}(\text{P}_2\text{O}_5)_{0.45}$ glass, significant quantity of Q^2 structural units have been converted to Q^1 structural units and Q^2 chain lengths become smaller and added Ag_2O exhibits a behaviour similar to PbO leading to modification of network. Possible reason for this could be difference in the network modifying site and its charge density for the $(\text{PbO})_{0.55}(\text{P}_2\text{O}_5)_{0.45}$ glass compared to $(\text{PbO})_{0.50}(\text{P}_2\text{O}_5)_{0.50}$ glass. NMR patterns were also recorded for hydrogen heated glass samples of $\text{PbO-P}_2\text{O}_5$ containing Ag_2O and the results are discussed in the following section

^{31}P MAS NMR patterns of 10 wt.% Ag_2O doped $(\text{PbO})_{0.50}(\text{P}_2\text{O}_5)_{0.50}$ glasses subjected to heat treatment at different temperatures in hydrogen environment are shown in Fig. 14. It is clear from the NMR patterns that P structural units are unaffected for the sample heated up to 360°C . However, above 360°C , partial crystallization of glass resulted into the appearance of sharp peaks around -27.8, -28.7, -30.5, and -31.8 and -43 ppm. Based on earlier ^{31}P MAS NMR studies these peaks, except -43 ppm, have been attributed to the four crystallographically different P atoms present in $\text{Pb}(\text{PO}_3)_2$ phase [21,22]. The peak around -43 ppm is arising due to the P_2O_5 phase. These inferences

are further confirmed by the XRD patterns discussed earlier (Fig. 7).

Glass ceramics based on silicate glasses

As mentioned in the introduction part, Glass-ceramics is another example of a composite material. They are produced as a result of controlled crystallization of glass with the addition of suitable nucleating agents. In some cases without the addition of nucleating agents also glass ceramics can be prepared. A glass ceramics consist of crystalline phases to the extent of 30-90% and the remaining is glass. Glass ceramics possesses the advantages of both glasses and ceramics. For example, glasses are generally brittle in nature and it is not possible to machine them. However, glass ceramics made with certain annealing conditions are machine-able. An example of machine-able glass ceramics is magnesium alumino silicate (MAS). By addition of suitable nucleating agents such as Al_2O_3 , crystallization of a phase called potassium fluorophlogopite occurs in the glass. This phase exists in layered structure and is responsible for the machine-able property. Presence of such phases can be identified and their relative concentration can be evaluated based on solid state nuclear magnetic resonance technique. Here ^{29}Si has been used as the probe nuclei to get an idea regarding the formation of potassium fluorophlogopite phase. Representative ^{29}Si MAS NMR spectrum for MAS glass ceramic prepared with addition of 8 mol% of Al_2O_3 is shown in Fig. 15. Sharp peaks are superimposed over a broad peak in the ^{29}Si MAS NMR spectrum, as can be seen from Fig. 15. The sharp peaks are characteristic of Potassium fluorophlogopite phase [4]. Depending up on concentration of this phase, extent machine-ability of glass ceramic is found to change [4].

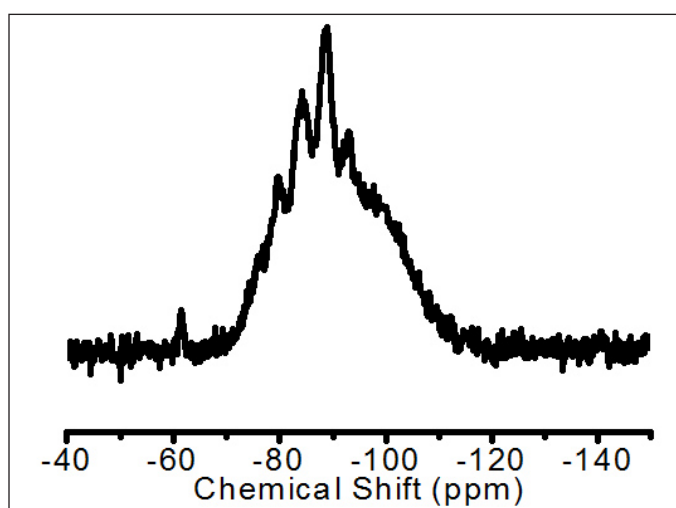


Figure 15. ^{29}Si MAS NMR pattern of Magnesium Alumino Silicate glass ceramics obtained by adding 8 mol % Al_2O_3

Conclusions

Composite materials based of $\text{Ag}_2\text{O-P}_2\text{O}_5$ and $\text{Ag}_2\text{O-PbO-P}_2\text{O}_5$ glasses have been prepared and characterised. All these glasses are constituted by Q^2 and Q^1 structural units of P and their relative concentrations affect the thermal stability of glass and size of Ag nanoparticles. $\text{Ag}_2\text{O-P}_2\text{O}_5$ glass is less stable under annealing in hydrogen environment compared to $\text{PbO-P}_2\text{O}_5$ glasses doped with different amounts of Ag_2O . In the case of silicate based glass-ceramics, NMR studies have confirmed that extent fluorophlogopite phase present in the glass-ceramics decides the mechanical properties of the composite.

References

1. S. W. Martin, "Glass" world book online America, Eds. 2000
2. S. J. Tauster, S. C. Fung, R. T. K. Baker, J. A. Horsley, Science 211(1981) 1121
3. T. Wehner, M. T. Seuffert, J. R. Sorg M. Schneider, K. Mandel, G. Sextl and K. Müller-Buschbaum, J. Mater. Chem C. 5 (2017) 10133
4. M. Goswami, G. P. Kothiyal, V. Sudarsan and S. K. Kulshreshtha Glass Technol. 46 (2005) 341.
5. Seemita Banerjee, Asheesh Kumar, P. Ruz, P. Sengupta, Int J. Hydrogen Energy, 41 (2016) 18130.
6. J. S. Mckechnie, L. D. S. Turner, C. A. Vincent, M. Lazzari and B. Scrosati J. Chern. Educ. 55 (1978) 203.
7. K. P. Muller, Glasstechn. Ber. 42 (1969) 8.
8. Bartholomew, J. Non-Cryst. Solids 7 (1972) 221
9. G. E. Rindone and W. A. Weyl, J. Am. Ceram. Soc. 33 (1950) 91.
10. Tsuchiya-T, Horiuchi-T and Moriya-T, Yogyo-Kyokai-Shi. 85 (1977) 127.
11. K. Uchida, S. Kaneko. S. Omi, C. Hata, H. Tanji, Y. Asahara and A. J. Ikushima, T. Tokizaki and A. Nakamura J. Opt. Soc. Am. B 11 (1994) 1236.
12. J. D. Wicks, L. Borjesson, G. Bushnell-Wye and W. S. Howells, R. L. Mcgreivy Phys. Rev. Lett. 74 (1995) 726.
13. J. D. Wicks, Ph.D thesis, Oxford University, 1993.
14. L. Borjesson, R. L. Mcgreivy and J. Wicks, J. Phys.(Paris) IV C2 (1992) 107.
15. H. Takahashi, E. Matsubara, Y. Waseda, J. Mater. Sci. 29 (1994) 2536.
16. M. E. Smith, E. R. H. van eck, Prog. NMR Spectrosc. 34 (1999) 159
17. F. A. Bovey, L. Jelinski, P. A. Mirau, Nuclear magnetic resonance spectroscopy, 2nd edition, Academic Press, New York 1988
18. S. Prabhakar, K. J. Rao, C. N. R. Rao, Chem. Phys. Lett. 139 (1987) 96
19. M. Villa, M. Scagliotti, G. Chiodelli, J. Non-Cryst. Solids 94 (1987) 101
20. P.W.Wang, L.Zhang, J.Non-Cryst. Solids194 (1996)129
21. K. H. Jost, Acta. Crystallogr. 17 (1964) 1539.
22. F. Fayon, C. Bessada, J. P. Coutures and D. Massiot, Inorg. Chern. 38 (1999) 5212.



Dr. V. Sudarsan joined Chemistry Division of BARC in the year 1994 after graduating from 37th batch of BARC training school. He received his Ph. D degree in Chemistry from Mumbai University in the year 2002 for his work on structural aspects of inorganic glasses. Subsequently he worked for a period of two years at the University of Victoria, British Columbia, Canada in the area of structural aspects and luminescence of lanthanide ions doped nanoparticles of inorganic hosts. Currently he is working on optical properties of nanoparticles and glassy materials.

Intrinsically radiolabeled nanoplatforms for cancer theranostics

Rubel Chakravarty

Radiopharmaceuticals Division, Bhabha Atomic Research Centre, Trombay, Mumbai 400085, India

Homi Bhabha National Institute, Anushaktinagar, Mumbai 400094, India

E-mail: rubelc@barc.gov.in

Abstract

Over the last few years, a plethora of radiolabeled nanoparticles have been developed and evaluated for their potential use in cancer theranostics. Radiolabeled nanoparticles represent an emerging paradigm in cancer management, allowing the incorporation of various imaging modalities, targeting ligands, and therapeutic payloads into a single vector. A major challenge in this endeavor is to develop disease-specific nanoparticles with facile and robust radiolabeling strategies. Also, the radiolabeled nanoparticles should demonstrate adequate *in vitro* and *in vivo* stability, enhanced sensitivity for detection of disease at an early stage, optimized *in vivo* pharmacokinetics for reduced non-specific organ uptake, and improved targeting for achieving high efficacy. This short article focusses on the synthesis of intrinsically radiolabeled nanoparticles and describes the latest advances from our laboratory towards synthesis of such advanced materials for cancer theranostics using reactor produced radioisotopes.

Keywords: Cancer, intrinsically radiolabeled, nanoparticles, reactor produced radioisotopes, theranostics

1. Introduction

In the recent times, synthesis of functionalized nanoplatforms has demonstrated tremendous potential to greatly enhance the clinical armamentarium for cancer theranostics [1,2]. Extensive research efforts at the interface between materials science and biology have resulted in exceptional accomplishments toward syntheses of various types of nanoplatforms that can directly be used for biomedical research. Today, increasing numbers of nanoparticle-based diagnostic or therapeutic agents are either being commercialized or have reached the clinical stage, thereby, achieving important milestones in “bench-to bedside” translation of nanotechnology [3,4]. The overwhelming interest of the scientific community in this arena is manifested by the fact that over 264,600 papers on “nanoparticles” have been reported in PubMed as of October 2021, out of which > 60 % of the papers have been published in the last one decade.

Nanoparticles exhibit unique size-dependent physical and chemical properties, which if properly harnessed can address unsolved challenges in clinical oncology. Particularly, they possess large functional surface area, easily controllable surface chemistry that facilitates surface functionalization to achieve tailored characteristics for effective use in personalized cancer management [5-7]. In the endeavor toward translating this promise into clinical reality, visualization of the distribution of nanoparticle-based carriers in the body following systemic administration through any route is of paramount importance. Presently, the most prudent approach that

provides quantitative information about the whole body biodistribution is by incorporating suitable radioisotopes in the nanoparticles – a process known as “radiolabeling”. After administration of the radiolabeled nanoparticles in living subjects, their *in vivo* biodistribution can be non-invasively monitored by molecular imaging techniques such as single photon emission computed tomography (SPECT), positron emission tomography (PET), Cerenkov luminescence (CL), Cerenkov resonance energy transfer (CRET), etc., that are now been widely explored for cancer imaging in preclinical and/or clinical settings.

The advantages of using radiolabeled nanoparticles for molecular imaging applications are many-fold [5-7]. Radiolabeled nanoparticles can act as signal amplifiers, leading toward enhanced contrast indices and increased sensitivity compared to conventional radiopharmaceuticals. Owing to the large surface area of nanoparticles, they can be conjugated with different targeting ligands for targeted detection of various types of cancers. Also, nanoparticles offer the scope of multimodality imaging which provides synergistic advantages over any one single molecular imaging modality alone. The third advantage lies in the ability of nanoparticles to combine both diagnostic and therapeutic capabilities onto the same nanoplatform, giving rise to the emerging concept of “image-guided drug delivery”. Additionally, different therapeutic agents (chemotherapeutic drugs as well as suitable therapeutic radioisotopes) can be incorporated in the same nanoplatform which might be a viable option toward multimodality targeted therapy for improved cancer management.

2. Intrinsic radiolabeling of nanoparticles

Numerous methods of radiolabeling have been reported in the literature, among which the methods based on the use of exogenous chelators have been the most widely used [5]. However, the chelator based radiolabelling approaches have their inherent limitations [8]. Optimization of a uniform strategy for radiolabelling of nanoplatforms with a variety of diagnostic or therapeutic radiometals becomes a challenge because different radiometals vary significantly in their coordination chemistry, making selection of the right chelator tricky or sometimes even impossible. Additionally, the requirement of harsh reaction conditions in certain cases (e.g. high reaction temperature with long time for incubation) might affect the biological efficacy of the targeting ligand attached to the nanoplatform. The possibility of alteration in pharmacokinetics of nanocarriers and potential detachment of radiometals which might lead to undesirable outcomes can also not be ruled out.

In order to circumvent the limitations of the conventional radiolabeling approaches, recent studies have been focussing on development of chelator-free intrinsic radiolabelling strategy of nanoplatforms using “hot” plus “cold” precursors [5,9]. This novel strategy takes advantage of the unique physical and chemical properties of the well-selected nanoplatforms for incorporation of radiometals inside them during the synthesis process and thus offers an easier, faster and highly specific radiolabeling possibility for preparation of a wide range of diagnostic and therapeutic agents. Since, intrinsically radiolabeled nanoparticles are obtained with high radiochemical stability, their biodistribution pattern in animal models reflect the true distribution of the nanoparticles without leakage of radioactivity. This is also a viable strategy for preparation of radiolabeled agents using low specific activity radiometals or the ones presenting unfavourable coordination chemistry, where formulation of conventional target specific radiopharmaceuticals is not feasible.

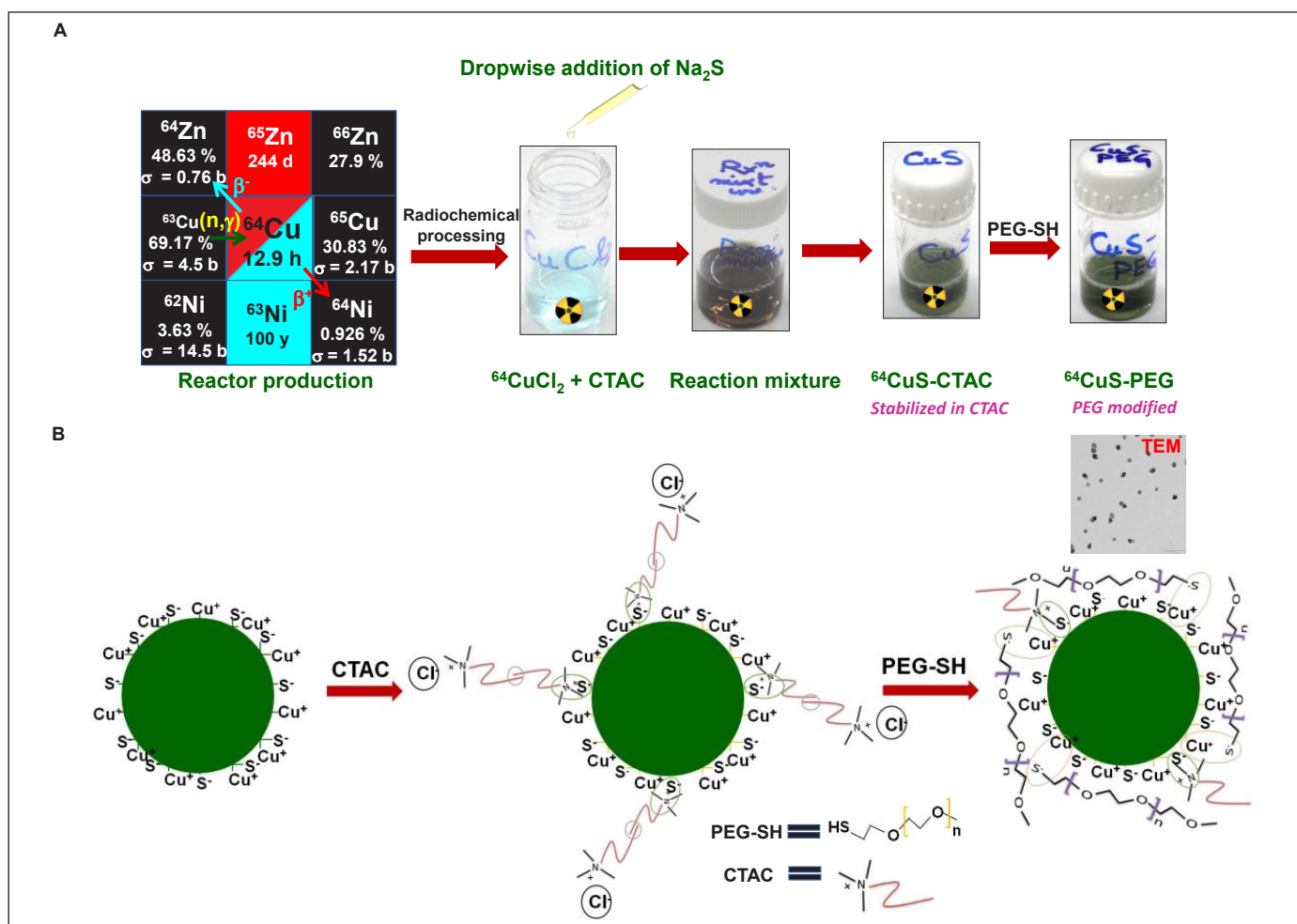


Figure 1. (A) Schematic illustration of production of ^{64}Cu via the neutron activation route and its utilization toward preparation of intrinsically radiolabeled $[^{64}\text{Cu}]\text{CuS}$ nanoparticles. (B) Schematic diagram for interaction between CuS nanoparticles and CTAC molecules and further addition of PEG-SH molecules to CuS-CTAC nanoparticles. Adapted from [9] with permission.

Despite excellent attributes in terms of radiochemical stability, synthesis of clinically relevant doses of intrinsically radiolabeled nanoparticles poses a challenge as large amounts of radioactivity needs to be handled. In order to reduce the radiation exposure to the working personnel, the synthesis procedure should be facile so that it can easily be operated in a shielded facility with remotely operable tongs. A simple procedure for synthesis of intrinsically radiolabeled nanoparticles is also vital towards formulation of doses for possible clinical translation while adhering to current Good Manufacturing Practice (cGMP) regulations. In the following paragraphs, the examples of intrinsically radiolabeled nanoparticles developed from our laboratory and efficacy of which have been established in preclinical settings are briefly described.

2.1 [^{64}Cu]CuS nanoparticles

Copper-64 ($t_{1/2} = 12.7$ h) has attracted significant interest in the nuclear medicine community, particularly because of its unique nuclear decay characteristics [10].

This radioisotope decays via three processes, namely, electron capture (EC), positron, and beta decays (EC 45%, β^+ 17.9%, β^- 37.1%), which allows for its utility both in the preparation of probes for PET imaging and also in the development of radiotherapy agents for treatment of various types of cancers. Another advantage of the unique nuclear characteristics of ^{64}Cu is that the radioisotope can be produced both in a nuclear reactor as well as in a cyclotron. Our group has optimized the protocol for large scale production of ^{64}Cu via $^{63}\text{Cu} (n, \gamma) ^{64}\text{Cu}$ reaction in the Dhruva reactor at BARC [10]. The irradiated target was radiochemically processed by dissolving in HCl medium. Intrinsically radiolabeled [^{64}Cu]CuS nanoparticles were synthesized by reacting the radioactive [^{64}Cu]CuCl₂ solution with Na₂S in presence of cetyltrimethylammonium chloride (CTAC) [9] (Figure 1). A polyethylene glycol (PEG) coating on the nanoparticles was introduced by incubating the synthesized nanoparticles with methoxy PEG thiol (molecular weight 5000 Da). The synthesized nanoparticles were of ~30 nm size and demonstrated excellent colloidal

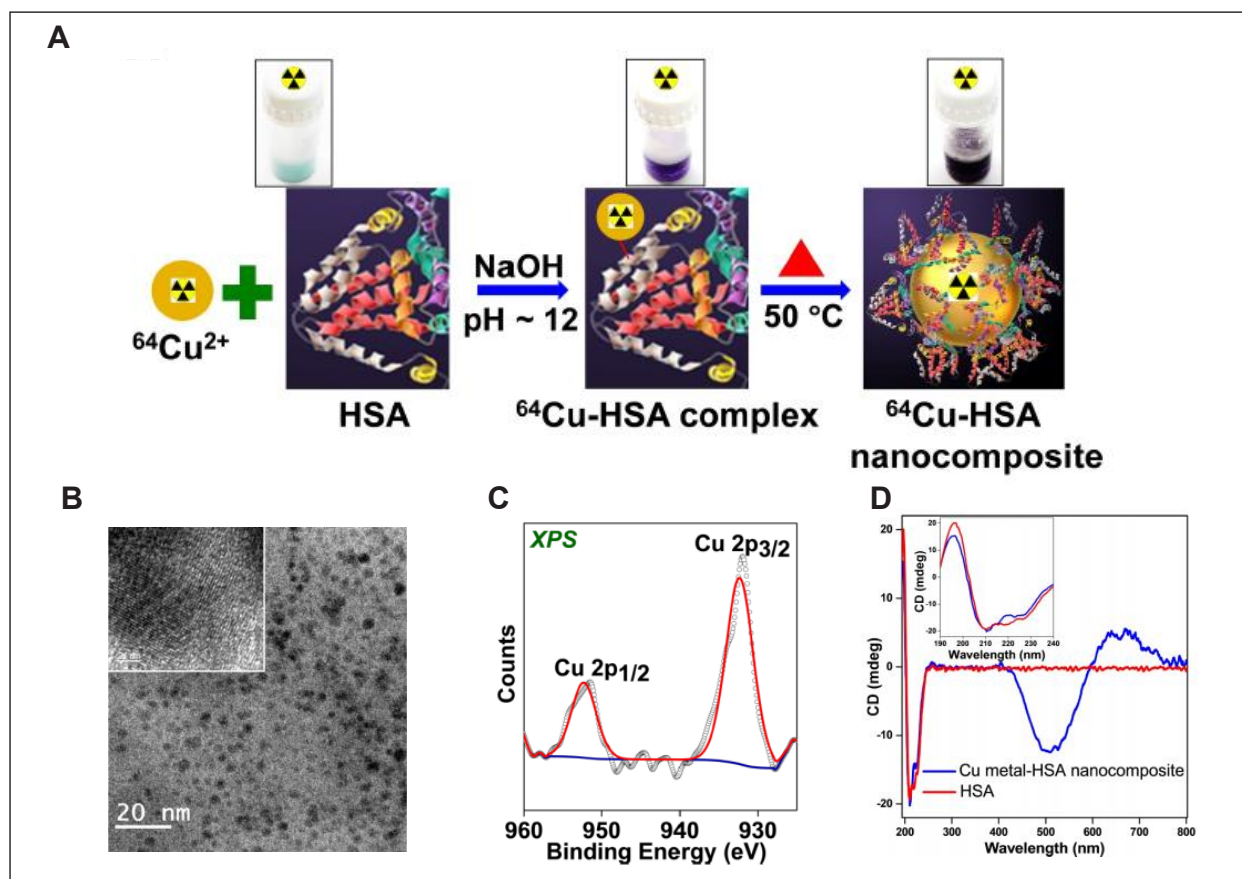


Figure 2: (A) Schematic illustration for synthesis of intrinsically radiolabeled [^{64}Cu]Cu-HSA nanocomposite by reaction of [^{64}Cu]CuCl₂ with HSA. (B) TEM image of Cu-HSA nanocomposite. Inset shows HRTEM image of Cu-HSA nanocomposite which gives a lattice spacing of 0.210 ± 0.014 nm corresponding to the (111) plane of Cu (0). (C) XPS spectrum of Cu 2p electrons in Cu-HSA nanocomposite. The absence of satellite peaks indicated the absence of oxidized Cu²⁺. (D) Circular dichroism spectra of HSA and Cu-HSA nanocomposite in the wavelength range of 190–800 nm. Inset shows the enlarged view of the circular dichroism spectra in the wavelength range of 190–240 nm. Adapted from [11].

stability. The radiochemical stability of the nanoparticles under physiological conditions was established by detailed *in vitro* studies in phosphate buffered saline (PBS) and mouse serum media. The biological efficacy of intrinsically radiolabeled ^{64}Cu CuS nanoparticles was studied in C57BL/6 mice bearing melanoma tumors. The results of the biodistribution studies revealed significant tumor uptake ($4.64\% \pm 1.71\% \text{ID/g}$) within 4 h post-injection (where %ID is the percent injected radioactivity dose), with good tumor-to-background contrast. Overall, the promising results obtained in this study demonstrated that this strategy could be utilized for development of novel agents for cancer theranostics using low specific activity ^{64}Cu produced in a medium flux research reactor.

2.2. ^{64}Cu Cu-human serum albumin nanocomposite

With an objective to synthesize to biocompatible ^{64}Cu -based nanoplatforams for cancer targeting, our group has synthesized intrinsically radiolabeled ^{64}Cu metal nanoparticles capped within human serum albumin (HSA) scaffold (^{64}Cu Cu-HSA nanocomposite) [11]. This

approach tends to mimic the biomaterialization processes and therefore have the benefits of biocompatibility, increased efficiency and mild synthesis conditions. HSA is particularly advantageous, as it is stable, biodegradable, non-toxic, non-immunogenic, and can be readily modified with ligands due to the presence of many functional groups [11]. Facile one-pot synthesis of ^{64}Cu Cu-HSA nanocomposite in aqueous medium was achieved using HSA as the sole reducing and nucleating agent (Figure 2A). The particle size distribution of the nanoparticles was in the range of 2–6 nm, with an average particle size of 4.5 ± 1.3 nm (Figure 2B). In the XPS spectrum, the peaks at 952.1 and 932.7 eV could be assigned to Cu $2p_{1/2}$ and Cu $2p_{3/2}$ which are the characteristic peaks due to Cu (0) (Figure 2C). Additionally, the absence of peak due to Cu^{2+} at 942 eV indicated that the Cu-HSA nanocomposite did not contain Cu^{2+} . Circular dichroism (CD) studies indicated that Cu nanoparticles are embedded in HSA protein forming Cu-HSA nanocomposite (Figure 2D).

The biological efficacy of ^{64}Cu Cu-HSA nanocomposite was demonstrated by biodistribution studies in melanoma

tumor bearing C57BL/6 mice, that showed rapid diffusion and accumulation of the radiotracer into tumor and clearance from the biological system by both renal and hepatobiliary routes. The promising results obtained in this study suggest that this strategy could be employed to facilitate clinical translation of a new class of biocompatible radiotracers derived from metal-based nanoparticles for PET imaging.

2.3 ^{199}Au Au-RGD nanoparticles

Gold-199 ($t_{1/2} = 3.14$ d; $\beta_1 = 462$ keV, 6.0%; $\beta_2 = 296$ keV, 71.6%; $\beta_3 = 250$ keV, 22.4%; $\gamma = 159$ keV, 37%) is an upcoming theranostic radiometal whose potential is yet to be explored in clinical context [12]. This radiometal can be obtained in no-carrier-added (NCA) form by neutron activation of ^{198}Pt target followed by radiochemical separation [13]. Owing to complex coordination chemistry of Au, it cannot be utilized for radiolabeling nanoplatforams by standard

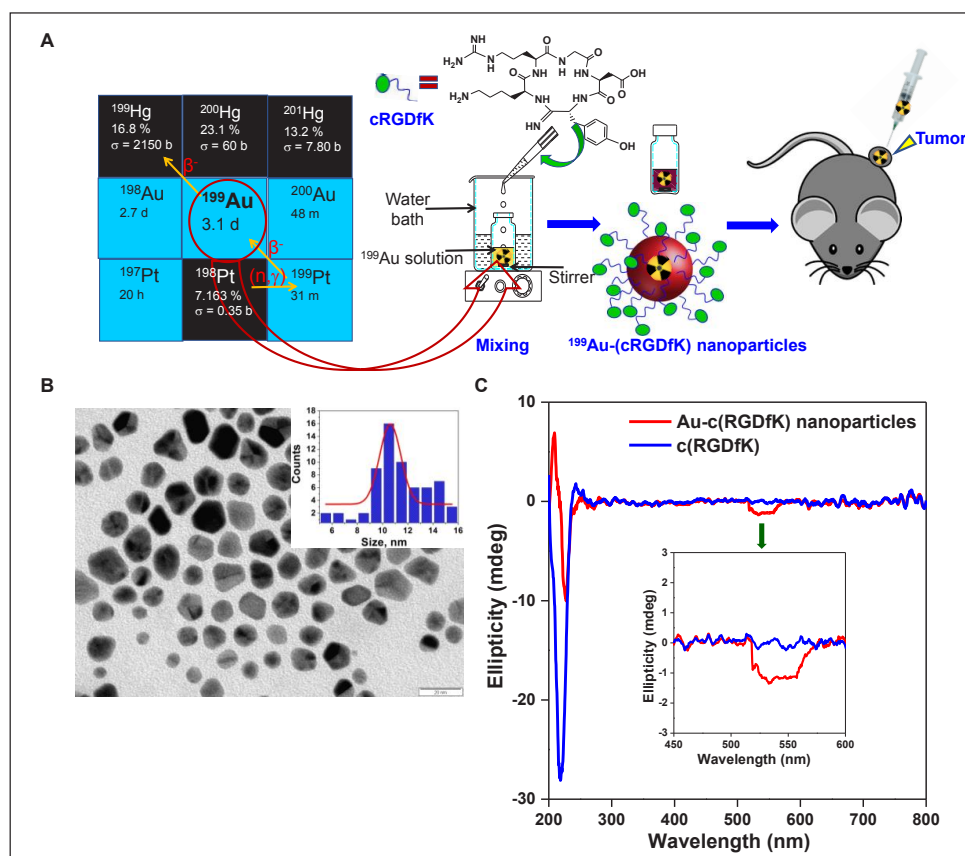


Figure 3: (A) A schematic diagram showing synthesis of intrinsically radiolabeled ^{199}Au Au-RGD nanoparticles by single-step reaction of Au (III) solution with cyclic RGD peptide. (B) TEM micrograph of Au-RGD nanoparticles. (C) Circular dichroism spectra of c(RGDfK) and Au-c(RGDfK) nanoparticles in the wavelength range of 200–800 nm. The amplified view of the CD spectra in the wavelength range of 450–600 nm is shown in the inset. Adapted from [12].

coordination chemistry-based approaches. Therefore, the synthesis of intrinsically radiolabeled nanoparticles is the most viable option toward effective utilization of this excellent radioisotope for clinical benefits. Our group has developed a facile one-pot synthesis protocol for the preparation of cyclic arginine-glycine-aspartate (RGD) conjugated and intrinsically radiolabeled ^{199}Au nanoparticles for targeting integrin $\alpha_v\beta_3$ receptors for potential use in neoadjuvant brachytherapy [12]. Cyclic RGD peptide plays the dual roles of reducing and stabilizing agent towards formation of Au-RGD nanoparticles from Au(III) solution (Figure 3).

The average particle size of the synthesized nanoparticles was estimated to be 11 ± 1 nm with a polydispersity of only $\sim 9\%$. Large-scale synthesis of intrinsically radiolabeled ^{199}Au nanoparticles could be achieved with excellent yield, and they met all the requirements for clinical use. The biological efficacy of the intrinsically radiolabeled ^{199}Au nanoparticles was confirmed by biodistribution studies in C57BL/6 mice having melanoma tumors after intratumoral injection. The results of the biodistribution studies demonstrated high tumor radioactivity concentration of integrin $\alpha_v\beta_3$ targeted ^{199}Au nanoparticles which reduced only marginally over the period of 1 week. Intratumoral administration of 5 MBq and 10 MBq doses of radiolabeled nanoparticles resulted in significant regression of tumor growth in melanoma tumor bearing mice. Apparent body weight loss was not observed in all the treated mice. On the basis of the encouraging results acquired in this study, it was envisaged that this approach would be useful toward clinical translation of this innovative class of radionanomedicine agents for neoadjuvant brachytherapy of selected cancer patients.

2.4 [^{198}Au]Au-RGD nanoparticles

Gold-198 is another interesting theranostic radiometal, which has a suitable half-life and emits β^- particles of desirable energy ($t_{1/2} = 2.7$ d; $\beta_{\text{max}} = 0.96$ MeV) in addition to emission of γ -ray photon (411.8 keV) for SPECT imaging [14]. The radiometal can be produced in large-scale in a medium flux research reactor via $^{197}\text{Au} (n, \gamma) ^{198}\text{Au}$ reaction. Adopting the same strategy as for synthesis of [^{199}Au]Au-RGD nanoparticles, well dispersed and biocompatible nanoparticles (~ 12.5 nm diameter) could be synthesized with excellent radiochemical and colloidal stability [14]. *In vitro* studies exhibited the cell binding affinity and specificity of [^{198}Au]Au-RGD nanoparticles towards melanoma cell line. A high uptake of $8.7 \pm 2.1\%$ ID/g in the tumor was observed within 4 h post-injection (p.i.). Significant decrease in tumor uptake of [^{198}Au]Au-RGD

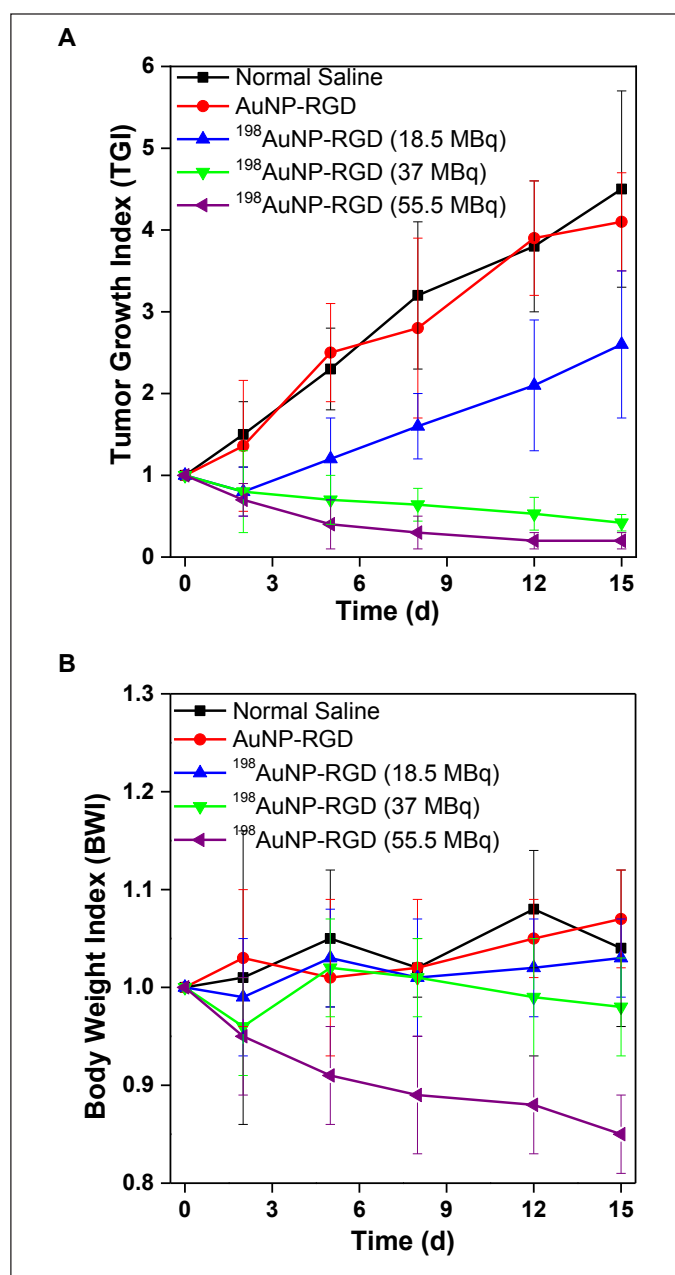


Figure 4: Tumor regression studies with [^{198}Au]Au-RGD nanoparticles. (A) Tumor growth index and (B) body weight index curves of C57BL/6 mice bearing melanoma tumor after intravenous injection of saline (control), Au-RGD nanoparticles (control), 18.5 MBq [^{198}Au]Au-RGD nanoparticles, 37 MBq [^{198}Au]Au-RGD nanoparticles and 55.5 MBq [^{198}Au]Au-RGD nanoparticles. Adapted from [14].

nanoparticles ($2.9 \pm 0.8\%$ ID/g) at 4 h p.i. on co-injection of a blocking dose of the peptide suggested that tumor localization of the intrinsically radiolabeled nanoparticles was receptor mediated. Administration of 37.0 MBq of [^{198}Au]Au-RGD nanoparticles resulted in significant regression of tumor growth with no apparent body weight loss over a period of 15 d (Figure 4). Overall, these promising results demonstrate the suitability of [^{198}Au]Au-

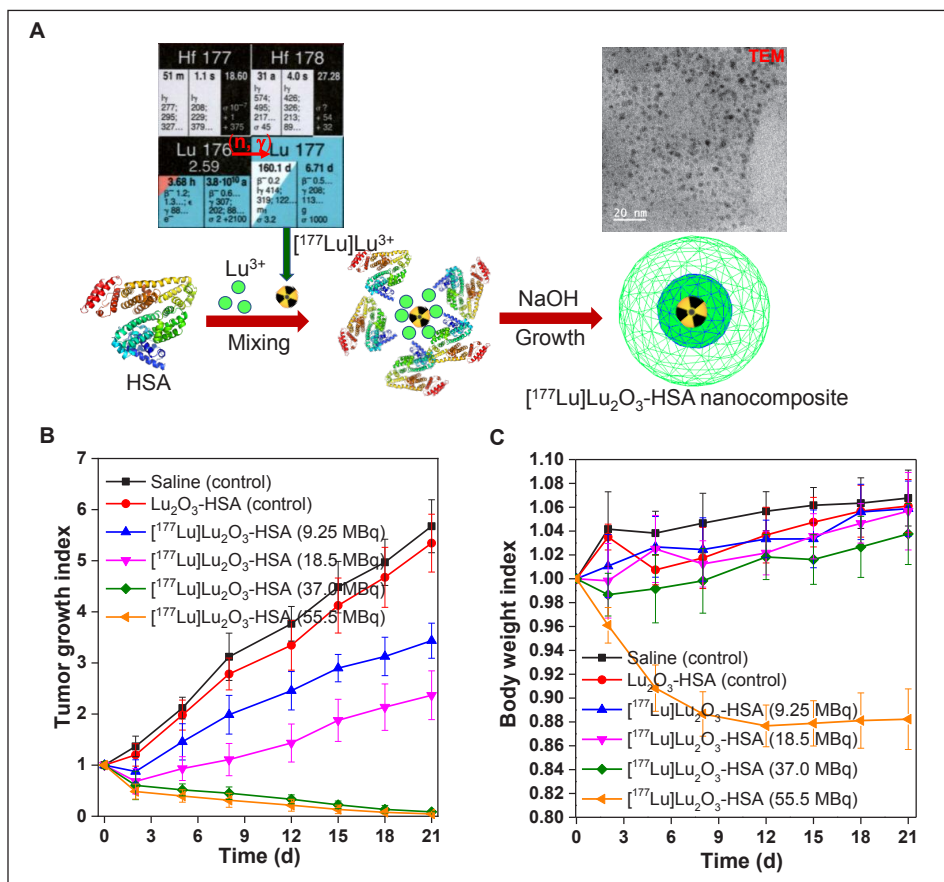


Figure 5: (A) Schematic illustration of synthesis of intrinsically radiolabeled [¹⁷⁷Lu]Lu₂O₃-HSA nanocomposite. Tumor regression studies with [¹⁷⁷Lu]Lu₂O₃-HSA nanocomposite. (B) Tumor growth index and (C) body weight index curves of C57BL/6 mice bearing melanoma tumor after intravenous injection of saline (control), Lu₂O₃-HSA (control), 9.25 MBq of [¹⁷⁷Lu]Lu₂O₃-HSA nanocomposite, 18.5 MBq [¹⁷⁷Lu]Lu₂O₃-HSA nanocomposite, 37.0 MBq [¹⁷⁷Lu]Lu₂O₃-HSA nanocomposite and 55.5 MBq [¹⁷⁷Lu]Lu₂O₃-HSA nanocomposite. Adapted from [15].

RGD nanoparticles as an advanced functional nanoplatform for targeted cancer therapy.

2.5 [¹⁷⁷Lu]Lu₂O₃-HSA nanocomposite

Lutetium-177 is a clinically established theranostic radiometal because of its attractive nuclear decay characteristics ($t_{1/2} = 6.65$ days, $E_{\beta, \text{max}} = 0.497$ MeV, and emits 113 keV (6.4%) and 208 keV (11.0%) γ -photons). This radiometal can be produced in large quantities by a simple ¹⁷⁶Lu (n, γ) ¹⁷⁷Lu reaction in research reactors for cost-effective synthesis of intrinsically radiolabeled nanoparticles [15]. Our group has developed a unique HSA-mediated biomineralization process for synthesis of intrinsically radiolabeled [¹⁷⁷Lu]Lu₂O₃ nanoparticles entrapped in a protein scaffold ([¹⁷⁷Lu]Lu₂O₃-HAS nanocomposite), as schematically illustrated in Figure 5A [15].

The particle size distribution of the Lu₂O₃ nanoparticles embedded in the protein scaffold was in the range of 2–6 nm, with an average particle size of 4.1 ± 1.2 nm. The XPS results clearly indicated the formation of Lu₂O₃-HSA nanocomposites. The intrinsically ¹⁷⁷Lu-labeled nanoparticles demonstrated excellent in vitro and in vivo stability in preclinical settings. Cell binding and toxicity studies demonstrated the binding affinity and specificity of the intrinsically radiolabeled nanoparticles toward melanoma (B16F10) cells for use as a radiotherapeutic agent. Biodistribution studies demonstrated rapid and enhanced accumulation of the radiolabeled nanoparticles in the tumor ($11.7 \pm 2.1\%$ ID/g at 4 h post-injection) with significant retention up to 7 days. The therapeutic efficacy of the [¹⁷⁷Lu]Lu₂O₃-HSA nanocomposite was demonstrated by tumor regression studies performed

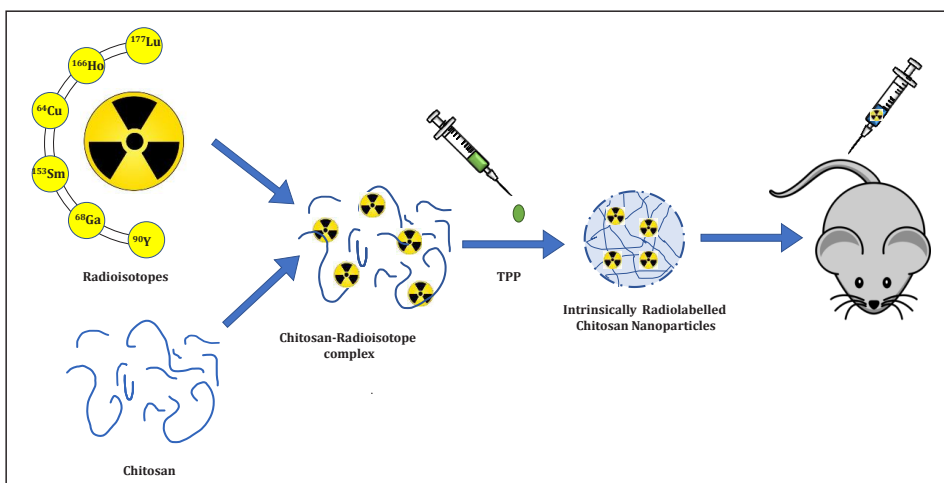


Figure 6: Schematic representation of synthesis of intrinsically radiolabeled chitosan nanoparticles by ionotropic gelation method. Adapted from [16].

over a period of 21 days. It was inferred that a one-time administration of a 37 MBq dose of the [^{177}Lu]Lu₂O₃-HSA nanocomposite was adequate for achieving maximum therapeutic benefits in C57BL/6 mice bearing melanoma tumors (**Figures 5B** and **5C**). The encouraging results obtained in this study demonstrate the potential of the [^{177}Lu]Lu₂O₃-HSA nanocomposite for clinical translation.

2.6 ^{177}Lu -chitosan nanoparticles

In another recent effort, chitosan, a naturally occurring, non-toxic, biodegradable and biocompatible polymer was complexed ^{177}Lu [16]. The radiolabelled chitosan was converted to nanoparticles (50 ± 2 nm particle size) by ionotropic gelation method. The radiolabeled nanoparticles demonstrated excellent *in vitro* and *in vivo* stability. The cell uptake and cytotoxicity of the radiolabeled nanoparticles were evaluated in epithelial lung cancer cell line, which demonstrated their potential as radiotherapeutic agent. Biodistribution studies in normal C57BL/6 mice demonstrated the high *in vivo* stability of the intrinsically radiolabeled nanoparticles. Adopting the same strategy, chitosan could be complexed with other diagnostic and therapeutic radioisotopes (^{64}Cu , ^{68}Ga , ^{90}Y , ^{153}Sm , ^{166}Ho , etc.) and converted into intrinsically radiolabeled nanoparticles, as illustrated in **Figure 6**. The promising results obtained in this study amply demonstrated the suitability of this class of intrinsically radiolabeled nanoparticles for future clinical use for cancer imaging and therapy.

3. Conclusions

In summary, we have provided an overview of the nanoparticles intrinsically radiolabeled with a variety of diagnostic and therapeutic radioisotopes for potential use in cancer theranostics. The intrinsically radiolabeled nanoparticles demonstrated excellent *in vitro* and *in vivo* radiochemical stability, which are desirable for future clinical translation. Biodistribution studies showed rapid and high uptake of the radiolabeled nanoparticles in the tumor and significant retention over a prolonged period of time. Tumor regression studies carried out with nanoparticles labeled with therapeutic radioisotopes established the treatment efficacy of the intrinsically radiolabeled nanoparticles. Although still in the early stages, design and synthesis of intrinsically radiolabeled nanoparticles have shown an attractive potential in offering an easier, faster, more stable, and more specific radiolabeling technique and hence represents an emerging paradigm in cancer care.

Acknowledgements

The author is grateful to Dr. P. K. Pujari, Director, Radiochemistry and Isotope Group, BARC for his valuable

support to this program. Dr. Sudipta Chakraborty, Head, Radiochemicals Section, Radiopharmaceuticals Division, BARC is gratefully acknowledged for his contribution, support and fruitful discussions.

References

1. Toy R, Bauer L, Hoimes C, Ghaghada KB, Karathanasis E. Targeted nanotechnology for cancer imaging. *Adv Drug Deliv Rev* 2014; 76: 79-97.
2. Goel S, England CG, Chen F, Cai W. Positron emission tomography and nanotechnology: A dynamic duo for cancer theranostics. *Adv Drug Deliv Rev* 2017; 113: 157-176.
3. Min Y, Caster JM, Eblan MJ, Wang AZ. Clinical translation of nanomedicine. *Chem Rev* 2015; 115: 11147-90.
4. Etheridge ML, Campbell SA, Erdman AG, Haynes CL, Wolf SM, McCullough J. The big picture on nanomedicine: The state of investigational and approved nanomedicine products. *Nanomedicine* 2013; 9: 1-14.
5. Chakravarty R, Goel S, Dash A, Cai W. Radiolabeled Inorganic Nanoplatfoms for Positron Emission Tomography Imaging of Cancer: An Overview *Q J Nucl Med Mol Imaging* 2017; 61:181-204.
6. Chakravarty R, Hong H, Cai W. Image-Guided Drug Delivery with Single-Photon Emission Computed Tomography: A Review of Literature. *Curr. Drug Targets* 2015; 16: 592-609.
7. Chakravarty R, Hong H, Cai W. Positron Emission Tomography Image-Guided Drug Delivery: Current Status and Future Perspectives. *Mol. Pharm.* 2014; 11: 3777-97.
8. Goel S, Chen F, Ehlerding EB, Cai W. Intrinsically radiolabeled nanoparticles: an emerging paradigm. *Small* 2014; 10(19): 3825-30.
9. Chakravarty R, Chakraborty S, Ningthoujam RS, Nair KVV, Sharma KS, Ballal A, Guleria A, Kunwar A, Sarma HD, Vatsa RK, Dash A. Industrial-Scale Synthesis of Intrinsically Radiolabeled ^{64}CuS Nanoparticles for Use in PET Imaging of Cancer. *Ind Eng Chem Res* 2016; 55: 12407-12419.
10. Chakravarty R, Shetty P, Nair KVV, Rajeswari A, Jagadeesan KC, Sarma HD, Rangarajan V, Krishnatry R, Chakraborty S. Reactor Produced [^{64}Cu]CuCl₂ as a PET Radiopharmaceutical for Cancer Imaging: From Radiochemistry Laboratory to Nuclear Medicine Clinic. *Ann Nucl Med* 2020; 34(12):899-910.
11. Chakravarty R, Chakraborty S, Guleria A, Kunwar A, Sarma HD, Dash A. Facile One-Pot Synthesis of Intrinsically Radiolabeled ^{64}Cu -Human Serum Albumin Nanocomposite for Cancer Targeting. *ChemSelect* 2017; 2: 8043-8051.
12. Chakravarty R, Chakraborty S, Guleria A, Shukla R, Kumar C, Nair KVV, Sarma HD, Tyagi AK, Dash A. Facile one-pot synthesis of intrinsically radiolabeled and cyclic RGD conjugated ^{199}Au nanoparticles for potential use in nanoscale brachytherapy. *Ind Eng Chem Res* 2018; 57: 14337-14346.
13. Vimalnath KV, Chakraborty S, Dash A. Reactor Production of No-Carrier-Added ^{199}Au for Biomedical Applications. *RSC Adv.* 2016; 6: 82832-82841.
14. Chakravarty R, Chakraborty S, Guleria A, Kumar C, Kunwar A, Nair KVV, Sarma HD, Dash A. Clinical Scale Synthesis of Intrinsically Radiolabeled and Cyclic RGD Peptide

- Functionalized ^{198}Au Nanoparticles for Targeted Cancer Therapy. Nucl Med Biol 2019; 72-73: 1-10.
15. Chakravarty R, Guleria A, Jadhav S, Kumar C, Debnath A, Sarma HD, Chakraborty S. Bioinspired Synthesis of Intrinsically ^{177}Lu -Labeled Hybrid Nanoparticles for Potential Cancer Therapy. Ind Eng Chem Res 2020; 59: 22492-22500.
16. Gaikwad G, Rohra N, Kumar C, Jadhav S, Sarma HD, Borade L, Chakraborty S, Bhagwat S, Dandekar P, Jain R, Chakravarty R. A facile strategy for synthesis of a broad palette of intrinsically radiolabeled chitosan nanoparticles for potential use in cancer theranostics. J Drug Discov Sci Technol 2021; 63: 102485



Rubel Chakravarty obtained his M.Sc. (Chemistry) degree from Banaras Hindu University, Varanasi in 2005 and joined BARC in 2006 after successful completion of 1-year orientation course (49th Batch, Chemistry) from the BARC Training School, Mumbai. He obtained his Ph.D. degree in Chemistry from Homi Bhabha National Institute in 2011. He was a Fulbright Visiting Scholar at University of Wisconsin-Madison, United States during 2013-14. His research interests include radioisotope production, separation chemistry, synthesis of nanostructured materials and radiopharmaceutical chemistry. He is a recipient of several awards, including, Scientific and Technical Excellence Award and Young Scientist Award from the Department of Atomic Energy. He has served as Chief Scientific Investigator and Co-investigator in several International Atomic Energy Agency (IAEA)-sponsored Coordinated Research Projects (CRPs). He has co-authored 1 book, 5 book chapters and > 110 papers in peer-reviewed journals.

Synthesis and Characterization of Metallic Nanoparticles using *Rheum emodi* Roots and Investigation of its Antibacterial and Cytotoxic Potential

Deepika Sharma^a, Naveen Kumar^b, Priyanka Pareek^a and Lalita Ledwani^{a*}

^aManipal University Jaipur, Rajasthan, India, 303007^a

^bPanjab Engineering College (Deemed to be University), Chandigarh, India, 160012

*For correspondence: lalita.ledwani@jaipur.manipal.edu; lalitalledwani@gmail.com

Abstract

This present work is a manifestation of antibacterial and cytotoxic potential of Himalayan herb *Rheum emodi*. The phytochemicals present in roots extract of *Rheum emodi* act stabilizing, reducing, and capping agent for synthesizing metal and metal oxide nanoparticles. In the present study, Silver (Ag), Titanium oxide (TiO₂), Hematite (α-Fe₂O₃), Silver-Copper (Ag-Cu) bimetallic alloy, Magnesium hydroxide Mg (OH)₂, and Tin oxide (SnO₂) nanoparticles (NPs) synthesized via green chemistry by making use of *Rheum emodi* roots extract (RERE). Ag NPs showed potent cytotoxic potential against cervical cancer cell line (HeLa), skin cancer cells and breast cancer cell line (MDA-MB-231). Molecular docking technique revealed that Chrysophanic acid present in RERE displayed inhibitory action against CDK-4 and CDK-6 proteins. RERE capped TiO₂ NPs exhibiting anatase crystalline phase, showed remarkable anticancer activity against liver cancer cells (HepG2). Biosynthesized α-Fe₂O₃ NPs depicted excellent antibacterial activity against *Escherichia coli* and *Staphylococcus aureus* strains and also displayed noticeable cytotoxic potential for breast cancer cell line (MDA-MB-231) with low IC₅₀ value (41.90 µg/mL). Bimetallic Ag-Cu NPs were derived via green route and antimicrobial activity of Ag-Cu NPs were carried out against *Escherichia coli* and *Staphylococcus aureus* strains. Phase pure hexagonal shaped Mg (OH)₂ NPs were synthesized using RERE and their *in vitro* investigations were conducted for breast cancer cell line (MDA-MB-231). In the last, structurally enriched tetragonal SnO₂ NPs prepared using RERE displayed outstanding properties such as small size, spherical surface morphology and PL emission peak in the visible region along with potent cytotoxic potential against breast cancer cell (MDA-MB-231).

Introduction

Nanoscale technology is the trending and efficient field of modern materials science, enabling atomic-scale manipulations that give rise to new properties. With a wide range of application areas, the implementation of scientific principles with nanoscale engineering strategies has been a boon to the field of biomedicine and biotechnology for the benefit of human life. Materials at the subatomic scale exhibit designs and characteristics that serve as a pathway to explore new characteristics through imaging, modelling, and various characterization techniques. From an experimental point of view, researchers have exploited various biosynthetic techniques such as electrochemistry, aspirated radiation, reduction in solution and, relatively recently, the ecological green path¹.

Metal nanoparticles such as gold, silver, iron, titanium, copper, and platinum are widely used for human needs. Synthetic biological methods are developing an interest in providing eco-accommodating procedures for nanoparticles, which do not use harmful chemicals². Some natural nanoparticle fusion systems using organisms

such as algae, fungi, enzymes, yeasts, actinomycetes and plants are presented as possible ecological options, unlike chemical and physical techniques. However, the preparation of microbially-mediated nanoparticles limits large-scale production and also requires a specific environment and special conditions, while the use of plants or plant extracts for the synthesis of nanoparticles is more beneficial than the synthesis of microorganisms due to the easy synthesis process and no special atmosphere requirement. Green synthesis of nanoparticles from plant extracts is gaining popularity nowadays because of its one-step synthesis technique, the absence of toxic substances and the presence of natural encapsulating agents.

Himalayan Rhubarb (*Rheum emodi*) is a perennial herbaceous plant found in the temperate, subalpine and alpine region of the Himalayas, from Kashmir to Sikkim, at an altitude of 2800-3000m. It is a commonly used herb and often known as “the wondrous drug” because of its wide medicinal and therapeutic uses. It belongs to the Polygonaceae family, its Ayurvedic name

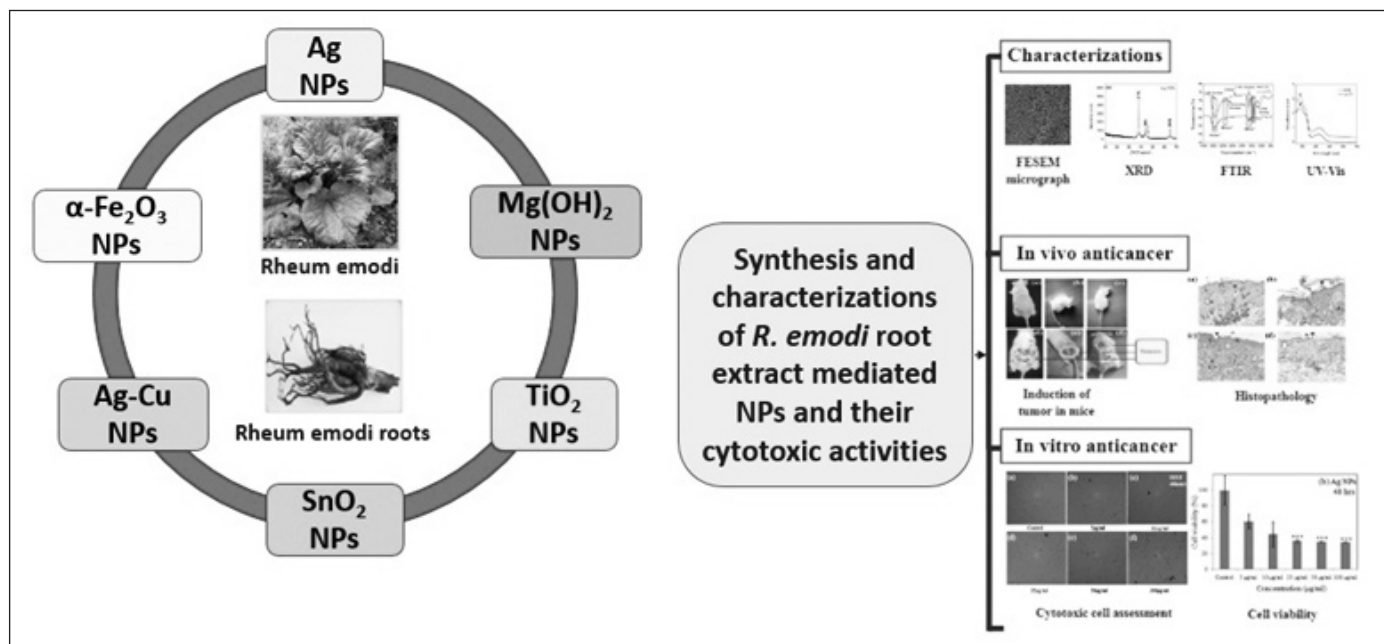


Figure: 1 Graphical Abstract

is “Amlavetasa” and popularly known under the Hindi name “Revandchini”. *Rheum emodi* is a leafy perennial herb, 1.5-3.0 m tall, with strong roots; long petioles large root leaves often 60 cm in diameter. The roots and rhizomes are the main parts used for pharmaceutical purposes and are harvested in October and November. The length of the fresh rhizome is about 15-30 cm and the color of the freshly cracked surface ranges from dull orange to yellowish brown³.

This article reports the synthesis and characterization of different metal nanoparticles using the roots of *R. emodi* roots along with its investigation on its antibacterial and cytotoxic potential (Figure: 1).

Phytochemical studies of *Rheum emodi* roots:

Rheum emodi roots contain several secondary metabolites such as oxantrone, flavonoids, phenols, stilbenes, ethers and esters, anthraquinones, phenols, anthrones, lignans, sterols, carbohydrates, and chromones etc. It acts as a mild laxative, stomachic, laxative and astringent tonic used for diarrhoea, mumps, tonsillitis, edema, ulcers and cuts. *R. emodi* is also used as an antibacterial, antioxidant, antifungal, and antitumor agent⁴.

HPLC characterization was carried out to determine the phytochemicals present in the *R. emodi* root extract used for the biosynthesis of metal nanoparticles and metal oxides in this research work. The presence of four anthraquinones, namely: emodin, aloe-emodin, physcion, chrysophanol is endorsed by HPLC investigation.

Physicochemical investigations of *Rheum emodi* roots extract (RERE) mediated NPs and their antibacterial and cytotoxic activities:

1. Ag NPs

Silver nanoparticles (AgNPs) have attracted great interest due to their distinctive properties such as chemical stability, good electrical conductivity, better catalytic, cytotoxic and antibacterial activity⁵. The environmentally friendly synthesis of AgNPs mainly involves various important steps such as: (1) selection of a reducing agent, (2) selection of a suitable solvent, and (3) selection of a non-toxic substance for Ag NP stability etc.

The biosynthesis and characterization of Ag NPs mediated by *Rheum emodi* root extract (RERE) was performed in the current study^{6,7}. The hydroxyanthraquinones (polyphenols) contained in the roots of *R. emodi* act as stabilizer. The media RERE NPs have a face-centered cubic phase structure with the special group Fm3 m, which is confirmed by the refinement of the XRD model of Rietveld. The FESEM and TEM micrographs describe the pseudospherical shape of the biosynthesized nanoparticles with an average particle size of about 30 nm. RERE and RERE-mediated Ag NPs have demonstrated substantial *in vitro* and *in vivo* cytotoxic potential versus breast cancer cell lines (MDA-MB-231) and chemically stimulated skin carcinogens in mice. The carcinogen group in mice showed higher tumor incidence, tumor yield,

tumor burden, tumor weight and cumulative tumor count compared to the RERE group. Due to properties such as high reactivity, low toxicity, small size and high surface area-to-volume ratio of treatment with RERE-mediated Ag NPs, significant reductions in tumor incidence, tumor yield, tumor weight, tumor weight and cumulative tumor count were observed. In addition, there was a substantial improvement in total protein, glutathione, catalase and superoxide dismutase levels, but showed a significant reduction in lipid peroxidation levels in both liver and skin when treated with RERE-mediated Ag NPs compared to a carcinogen-treated control group. Serious disorientation of skin histology was also noted in the carcinogen group (group IV), with corneal pellet formation, tumor nests and acanthosis, which was found to decrease after nanoparticle administration. The antitumor properties of the ligands (aloe-emodin, archin, chrysophanic acid, and parietin) were confirmed by *in silico* molecular docking with powerful anti-cancer proteins. It was noted that all ligands were successfully anchored to the CDK-4 and CDK-6 proteins. The present study suggests that chrysophanic acid is a potent anti-cancer drug with demonstrated inhibition of the CDK-4 and CDK-6 receptors⁷. The synthesised silver nanoparticles may become a candidate for anticancer drugs to combat against cancer.

2. TiO₂NPs

TiO₂NPs have various crystal structures such as tetragonal anatase, rutile, brookite and mixed phases. TiO₂NPs are widely preferred for its structural and photocatalytic properties. TiO₂ nanoscale particles have surface defects that result in surface energy useful for biological activities. Synthesis of TiO₂NPs from plant extracts provides additional biocompatibility compared to chemical synthesis. The biosynthesis of TiO₂NPs was performed using extracts from the roots of *R. emodi*. The synthesized nanoparticles were characterized using methods such as XRD, FESEM, TEM, AFM, FTIR and UV-visible spectroscopy. The cytotoxicity of TiO₂NPs was studied using HepG2 cancer cells⁸.

3. α-Fe₂O₃ NPs

Iron oxide (α-Fe₂O₃ NPs) nanoparticles have attracted the attention of researchers studying their range of applications in areas such as pharmaceutical administration, biosensors, magnetic resonance imaging, photo-electrolysis reactors, lithium-ion batteries, gas sensor, tissue- repair engineering etc.⁹. Iron oxide nanoparticles are useful due to their small size, they are able to breach through intracellular

capillaries and provoke the accumulation of the target drug, and in addition to deliver this drug to the cell using magnetic nanoparticles, cytotoxicity and alveolar inflammation were manifested¹⁰.

Antibacterial on identified bacteria and cytotoxic potential on Hela cell lines of α-Fe₂O₃ nanoparticles formed using *R. emodi* roots was studied. Substantial enhancement is noted in antimicrobial and cytotoxic potentials with α-Fe₂O₃NPs in comparison to crude extract to *R. emodi* roots¹¹. The hydroxyanthraquinones present in the roots of *R. emodi* act as a stabilizing and capping agent on α-Fe₂O₃NPs. The synthesized α-Fe₂O₃ NPs. were analysed with the help of various characterization techniques such as XRD, FESEM, TEM, AFM, FTIR and UV-Visible spectroscopy. The synthesized nanomaterials have displayed significant *in vitro* cytotoxic effect against cervical (Hela) cancer cells (IC₅₀ 41.90 µg/ml). This will be useful in studying alternative approaches to human cancer treatment. α-Fe₂O₃NPs also act as an important antibacterial agent against *E.coli* and *S. aureus* at 40 µg/ml and 80 µg/ml concentrations, respectively. These results revealed that *R. emodi* root extract mediated α-Fe₂O₃NPs have a significant medicinal application.

4. Ag-Cu NPs

Bimetallic nanoparticles (to form a single mixture of two different metals) have achieved more attention than individual metal nanoparticles because of its thermal, electrical, and excitation properties¹². As the review progresses, an eco-friendly and cost-effective method for the synthesis of Ag-Cu NPs was performed at 90 °C for 3 h. Nanoparticles can potentially represent anti-cancer and anti-bacterial applications. From the FTIR analysis, it can be understood that the hydroxyl and phenolic compounds contained in the root extract of *R. emodi* are responsible for the synthesis of NPs of Ag-Cu¹³. Synthesized green path Ag-Cu NPs show a potential anti-cancer effect against breast cancer cells (MDA-MB-231). Significant improvement in antimicrobial properties was observed against *Escherichia coli* and *Staphylococcus aureus*. In account of anticancer and antibacterial properties of Ag-Cu NPs, its further utility can be explored to have valuable discoveries in medicine and health sectors.

5. Mg(OH)₂ NPs

Due to the large surface area to volume ratio, Mg(OH)₂ NPs have been of great attention to the researchers to explore the varied spectrum of applications. *R. emodi* root extract was used to avoid the use of harmful

reducing agents for the synthesized polycrystalline Mg (OH)₂ NPs¹⁴. Physicochemical investigations of biosynthesized Mg (OH)₂ NPs were performed using XRD, FESEM, TEM, FTIR and UV-Vis spectroscopy. From the point of view of the crystallographer, the XRD studies show that the Mg (OH)₂ NPs have the hexagonal crystal structure with space group P-3m1. FTIR analysis confirms the presence of anthraquinones in *R. emodi* roots extract which perform as a reducing and stabilizing agent. The UV-Vis spectra analysis reveals the surface plasmon resonance (SPR) effect as a characteristic peak at 426nm. The microstructural analysis through the TEM characterization technique illustrates the nanometric scale formation of spherical Mg (OH)₂ NPs with an average particle diameter of ~30-50 nm. The anthraquinones present in the roots of *R. emodi* was found to be responsible for the antibacterial properties of the synthesized nanomaterials. The antimicrobial effect of Mg (OH)₂ NPs on *Escherichia coli* and *Staphylococcus aureus* was investigated along with anticancer *in vitro* cytotoxic effect on breast cancer cell lines (MDA-MB-231).

6. SnO₂ NPs

Greenway's bio-engineered nanoparticles have received special attention during medical technology for the diagnosis and treatment of cancer because of their non-toxic nature, affordability and energy effectiveness. The tin oxide nanoparticles (SnO₂ NPs) were used in a cost-effective and eco-friendly way by cascading from the roots of the *R. emodi* in the Himalayas. Structural analysis revealed that the biosynthesized SnO₂ NPs showed tetragonal crystal symmetry with the P4 / 2mm space group, as confirmed by Rietveld's sine-grained method. Using transmission electron microscopy (TEM), the mean particle diameter was estimated to be about 40 nm with a spherical shape. In addition, spectrum analysis by Fourier transform infrared spectroscopy (FTIR) revealed that the presence of metabolites (hydroxyanthraquinones) acts as a styrene, acting agent, and stabilization of SnO₂ NPs. Note that the mediated *Rheum emodi* root extraction of SnO₂ NPs revealed another magnetic role in a moving temperature magnetometer (VSM) in a magnetic characteristic environment at room temperature. It was noticed that photoluminescence spectra at room temperature showed a rich purple emission band of 419 nm. In addition, the ability of SnO₂ NPs to be violated was mediated by *Rheum emodi* root extract against different breast cancer cell lines (MDA-MB-231).

The results of this study proved to be useful, so that *R. emodi* or its nanoparticles could be used as an alternative to synthetic compounds for cancer treatment.

Conclusion:

The root of *R. emodi* is considered a miracle medicine due to a large number of medicinal properties. The root of *R. emodi* is considered a miraculous medicine due to its large number of medicinal properties. The findings of this study demonstrate the antimicrobial and cytotoxic potential of *R. emodi* and *R. emodi*-mediated nanoparticles. The presence of anthraquinones makes *R. emodi* an important candidate for cancer prevention. The variety of nanoparticles were synthesized using RERE and their physicochemical investigations support the stabilizing and reducing properties of phytochemicals present in RERE, also playing a significant role as a capping agent. The environmental benign, cost-effective, and energy-efficient preparation of metal and metal oxide nanoparticles such as Ag NPs, TiO₂ NPs, α-Fe₂O₃ NPs, Ag-Cu NPs, Mg (OH)₂ NPs, and SnO₂ NPs, using roots extract of Himalayan herb *R. emodi*, discussed in the present study paved a new way in combating various cancerous species. The results of the present report proved to be useful so that *R. emodi* or the metal and metal oxide nanoparticles synthesized using RERE, could be used as an alternative to synthetic compounds to fight against cancer. Such scientific data can project natural products in the right perspective and help a sustainable global market as an affordable agent for all for cancer prevention.

References:

1. Gan, P. P.; Li, S. F. Y., Potential of the plant as a biological factory to synthesize gold and silver nanoparticles and their applications. *Reviews in Environmental Science and Biotechnology* **2012**, *11*, 169-206.
2. Shankar, S. S.; Rai, A.; Ahmad, A.; Sastry, M., Rapid synthesis of Au, Ag, and bimetallic Au core-Ag shell nanoparticles using Neem (*Azadirachta indica*) leaf broth. *Journal of Colloid Interface Science* **2004**, *275*, 496-502.
3. Singh, A.; Hart, R.; Chandra, S.; Nautiyal, M. C.; Sayok, A. K., Traditional Herbal Knowledge among the Inhabitants: A Case Study in Urgan Valley of Chamoli Garhwal, Uttarakhand, India. *Evidence-Based Complementary and Alternative Medicine* **2019**, *5656925*, 1-21.
4. Malik, M. A.; Bhat, S. A.; Rehman, M. U.; Siddique, S.; Akhoun, Z. A.; Shrivastava, P.; Ahmad, S. B., Phytochemical analysis and antimicrobial activity of *Rheum emodi* (Rhubarb) rhizomes. *The Pharma Innovation Journal* **2018**, *7(5)*, 17-20.
5. Chaturvedi, V.; Verma, P., Fabrication of silver nanoparticles from the leaf extract of *Butea monosperma* (Flame of Forest) and their inhibitory effect on bloom-forming cyanobacteria. *Bioresources Bioprocess* **2015**, *2(18)*, 1-8.

6. Sharma, D.; Ledwani L., Bhatnagar, N., Antimicrobial and cytotoxic potential of silver nanoparticles synthesized using *Rheum emodi* roots extract. *New Frontiers in Chemistry* **2015**, *24*(2), 121-135.
7. Sharma D., Kumar N., Devki, Tiwari S., Mehrotra T., Pervaiz N., Kumar N., Cytotoxic potential of *Rheum emodi* capped silver nanoparticles and *In silico* study of human CDK-4/6 proteins with hydroxyanthraquinones. *Journal of the Indian Chemical Society* **2021**, *98*(9), 100136.
8. Sharma, D., Parveen, K., Oza, A. and Ledwani, L., Synthesis of anthraquinone-capped TiO₂ nanoparticles using *R. emodi* roots: preparation, characterization and cytotoxic potential. *Rendiconti Lincei. Scienze Fisiche e Naturali* **2018***29*(3),649-658.
9. Periyathambi, P.; Vedakumari, W. S.; Bojja, S.; Kumar, S. B.; Sastry, T. P., Green biosynthesis and characterization of fibrin functionalized iron oxide nanoparticles with MRI sensitivity and increased cellular internalization. *Materials Chemistry and Physics* **2014***148*(3), 1212-1220.
10. Parveen, K.; Banse, V.; Ledwani, L., Green synthesis of nanoparticles: Their advantages and disadvantages. In *AIP Conference Proceedings* **2015***1724*, 020048-1-020048-7.
11. Sharma, D., Ledwani, L., Mehrotra, T., Kumar, N., Pervaiz, N. and Kumar, R., Biosynthesis of hematite nanoparticles using *Rheum emodi* and their antimicrobial and anticancerous effects in vitro. *Journal of Photochemistry and Photobiology B: Biology* **2020***206*, 111841.
12. Liu, J.; Zou, S.; Xiao, L.; Fan, J., Well-dispersed bimetallic nanoparticles confined in mesoporous metal oxides and their optimized catalytic activity for nitrobenzene hydrogenation. *Catalysis Science and Technology* **2014**, *4*(2), 441-446.
13. Sharma, D., Ledwani, L., Kumar, N., Mehrotra, T., Pervaiz, N. and Kumar, R., An Investigation of Physicochemical and Biological Properties of *Rheum emodi*-Mediated Bimetallic Ag-Cu Nanoparticles. *Arabian Journal for Science and Engineering* **2021***46*, 275-285.
14. Sharma, D., Ledwani, L., Kumar, N., Pervaiz, N., Mehrotra, T. and Kumar, R., Structural and physicochemical properties of *Rheum emodi* mediated Mg(OH)₂ nanoparticles and their antibacterial and cytotoxic potential. *IET nanobiotechnology* **2020***14*(9), 858-863.
15. Sharma, D., Kumar, N., Mehrotra, T., Pervaiz, N., Agrawal, L., Tripathi, S., Jha, A., Poullikkas, T., Kumar, R. and Ledwani, L., 2021. In vitro and in silico molecular docking studies of *Rheum emodi*-derived diamagnetic SnO₂ nanoparticles and their cytotoxic effects against breast cancer. *New Journal of Chemistry* **2021***45*(3), 1695-1711.

	<p>Dr. Deepika Sharma did PhD in Nanomaterials at Manipal University Jaipur, Jaipur. Her research area includes metallic (Ag and Ag-Cu) and metal oxide [TiO₂, SnO₂, ZnO, Mg(OH)₂] etc. nanoparticles synthesized via green chemistry route and their antimicrobial applications such as antibacterial and anticancerous activities. She has published more than 10 research articles in high factor and peer-reviewed international journals and conference papers.</p>
	<p>Dr. Naveen Kumar did PhD at Punjab Engineering College (Deemed to be University), Chandigarh, India, He is recipient of national fellowship provided by Ministry of Human Resource Development (MHRD), India. He is also awarded with a national certificate of Council of Scientific & Industrial Research (CSIR), India. Presently, he is working at Chandigarh University, Mohali, India and leading the material research group. His keen research fields include advance functional materials (Multiferroics), optoelectronic nanostructures, and solid-state electrolytes. He has published more than 30 research articles in high factor and peer-reviewed international journals, conference papers and book chapters.</p>
	<p>Ms Priyanka Pareek is pursuing PhD at Manipal University Jaipur. She is recipient of prestigious Dr. Ramdas Pie Scholarship awarded by the Manipal University Jaipur. She is also working on a project funded by Department of Science and Technology, Rajasthan. She worked as a Senior Research Associate in Council of Science and Technology, Lucknow, UP from July, 2011 to January, 2012. She has joined as a Lecturer in Jayoti Vidyapeeth Women's University, Jaipur from September 2015 to August, 2018. She has presented her work in different national and international conferences organized in India.</p>
	<p>Dr. Lalita Ledwani is working as Professor of Chemistry and Dean, Faculty of Science at Manipal University Jaipur (MUJ), Rajasthan, India. Dr. Ledwani joined Manipal University Jaipur in the year 2011. Prior to joining MUJ, she was working with Pandit Deendayal Petroleum University, Gujarat as a founding faculty member in the university. Her areas of research interest are natural products, plasma surface modification polymers techniques, agriculture chemistry, green nano-materials, wastewater treatment. She is recipient of Research Grant Award 2015 from KWEF, Japan and also received financial support for various research projects from different funding agencies namely DST, Govt of India (04); DST, Govt. of Rajasthan (02); DBT, Govt of India (01) and UGC, Govt. of India (01). Dr. Ledwani has over forty-five research manuscripts published in reputed peer reviewed journals and books, two patents, delivered around three dozen invited/expert lectures besides sixty-three research papers in conferences and edited two books: i) Nanotechnology for Energy and Environmental Engineering, Springer, 2020 ii) Research Methodology in Chemical Sciences Experimental and Theoretical Approach, CRC Press, Taylor & Francis, 2016. She is guiding UG, PG, Ph.D and post-doctoral students. With over 19 years of post-PhD experience in the higher education, Dr L Ledwani has been actively engaged in academic and research activities. Dr. Ledwani is associated with various national and international professional bodies as fellow, life member, or member. Dr. Ledwani has also organized various national and international academic events in a lead role.</p>

Exploring the gravity of tin chalcogenides as potential energy materials

Gourab Karmakar^{a,b}, Adish Tyagi^{a,b*}, G. Kedarnath^{a,b}

^aChemistry Division, Bhabha Atomic Research Centre, Mumbai- 400 085

^bHomi Bhabha National Institute, Anushaktinagar, Mumbai- 400 094

Email: tyagia@barc.gov.in

Abstract

The increasing energy demands and raising environmental concerns in the present time and the time to follow has compelled us to seek environmentally clean energy resources and storage materials. Recent investigations have projected tin chalcogenides as multi-functional materials, equally suitable for photovoltaics, thermoelectric and as anode materials in lithium ion and sodium ion batteries. This article highlights the peculiar features of tin chalcogenides which makes them a versatile energy relevant material. This account will further highlight the recently adopted routes to access the tin chalcogenides with special emphasis on the single source precursor method. Furthermore, this article also discusses the recent progress made by versatile tin chalcogenides as energy materials. We believe that, this article will serve as a useful stepping stone for researchers who strive to explore tin chalcogenides and other metal chalcogenides as energy harvesting and storage materials.

Introduction

Energy needs of the world are increasing with every day and till now fossil fuels are used to meet those needs. However, excessive reliance on fossil fuels to meet our daily energy needs raises a significant concern of damage to environment- as huge amounts of carbon dioxide and sulphur dioxide are released in the combustion process. Moreover, fossil fuels being non-renewable will run out of stock considering the high consumption rate. To mitigate the remarkable surge in the global energy crisis, environmental concerns and to accomplish dreams of the fossil fuel free world- sustainable, renewable, environmentally friendly sources and energy storage devices development are required [1]. The most appreciated options to address the ever-increasing demand for green energy are:

Harnessing solar energy through photovoltaic technology: It has the potential to provide an access to the unlimited solar power irradiating earth [1]. The photon absorbing material is the most important component of the solar cell. The primary criteria for a material to be used as photon absorbing material is that the band gap of the material should be in the range of 1-1.5 eV, optimal value of solar cell performance. Furthermore, the material should have high absorption coefficient and high stability and it should be non-toxic and earth abundant [2].

Conversion of waste heat in usable form of energy: Heat can be considered as renewable energy source owing to its pervasive and inevitable nature. Through thermoelectric devices it is possible to convert waste heat into electrical

energy. The potential of thermoelectric material can be assessed in terms of thermoelectric figure of merit $zT = \sigma S^2 T / (k_{el} + K_{lat})$, where σ , S , T , k_{el} and k_{lat} are the electrical conductivity, the Seebeck coefficient, the absolute temperature, the electrical thermal conductivity and lattice thermal conductivity, respectively. Strong correlation among these parameters renders their simultaneous optimization difficult. However, the materials having intrinsically low k_{lat} owing to their complex anisotropic structure and lattice anharmonicity due to lone pairs holds strong promise for thermoelectric performance [3].

Energy storage devices: Development of reliable and environmentally friendly forms of energy storage such as lithium ion batteries (LIBs) is the need of hour to alleviate the environmental concern arises from fossil energy. However, there is urgent necessity to improve the energy densities of LIBs. Till now the widely used anode material of LIBs is graphite, owing to its low cost and reasonably high chemical stability. Only concern with graphite is its low theoretical capacity, i.e. 372 mAhg⁻¹. Consequently, massive efforts have been directed to design negative electrodes with enhanced specific capacities. Ideally, the anode material should be cost effective and environmentally friendly. It should have high theoretical capacity, high conductivity for improved rate performance and low volume changes during lithiation and de-lithiation processes [4, 5].

Recently, metal chalcogenides having graphene like structure (2-D layered structure) have attracted

significant attention of the research fraternity [6]. 2-D Metal chalcogenides, like graphene are having strong bonding within the layer and weak van der Waals interactions between neighbouring layers. Contrary to graphene, these metal chalcogenides possess band gaps which can be further adjusted over a broad range by varying the dimensions. The band gap tuning enables the 2-D layered metal chalcogenides to display a wide range of unique chemical and physical properties which have been used for diverse applications such as optoelectronic, photovoltaic devices, transistors, lithium ion battery, hydrogen generation by photocatalytic splitting of water and many more [6, 7]. Various transition metal chalcogenides such as MoS_2 , MoSe_2 etc. have been extensively explored for their relevance in energy harvesting and storage devices.

Besides transition metal chalcogenides, tin based chalcogenides are gaining momentum owing to their earth abundant, low cost and environmentally benign characteristics which significantly promote their relevance in sustainable electronic and photonic systems [8]. Tin chalcogenides, particularly sulphides and selenides have excellent semiconducting properties with tuneable narrow band gaps in the range of 0.9 to 2 eV and intense absorption across the electromagnetic spectrum making them highly suitable for photovoltaic applications.

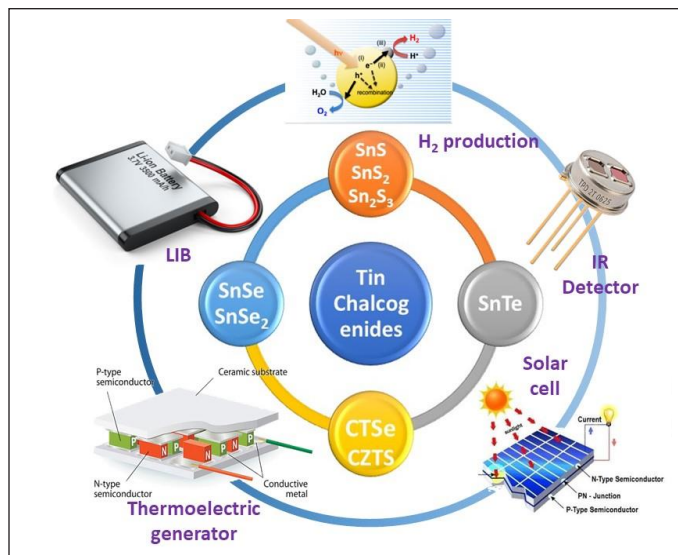


Figure 1: Schematic illustration of various tin chalcogenides and their potential applications as energy materials.

Beyond, solar energy absorbing materials, low thermal conductivity, better electronic conductivity and ionic diffusivity, swift transition between +2 and +4 oxidation states, ability to accommodate 4.4 moles of lithium per tin atoms and high theoretical capacity make tin chalcogenides an interesting and important candidate for thermoelectrics

and as anode material for LIBs [3, 8, 9]. The low thermal conductivity and better electronic conductivity exhibited by tin chalcogenides are attributed to its unique anisotropic structure (Figure 1).

Structure of tin chalcogenides

Tin chalcogenides exist in various crystal phases such as hexagonal, monoclinic, orthorhombic depending upon the oxidation state of Sn. Each phase possesses unique characteristics. SnE ($E = \text{S, Se}$) generally adopts orthorhombic phase while SnE_2 prefers to crystallize in hexagonal and monoclinic. This section will present a brief discussion about the structure of individual tin chalcogenides.

Tin sulphides are the most explored material of this family and three main compositions of the same are known namely, SnS , SnS_2 and Sn_2S_3 . The coordination environment around the central tin atom exhibits extended bonding with a coordination number ranging from 2 to 9 depending upon the valency of the Sn atom. The divalent Sn chalcogenide exhibits trigonal bipyramidal geometry around it whereas the tetravalent Sn exerts tetrahedral, trigonal bipyramidal and octahedral arrangements around the central atom [10]. SnS crystallize in a deformed NaCl structure which consists of double layer of Sn and S atoms as shown in figure 2a. Each Sn atom is coordinated to six S atoms with different Sn-S bond distances. Three long Sn-S bond with average bond distance of $\sim 3.4 \text{ \AA}$ and three short Sn-S bonds with average bond distance of $\sim 2.7 \text{ \AA}$ are observed. Another important feature of the structure is that one of the long Sn-S distances includes weak Van der Waals interaction between Sn and S from two different layers which binds the two tin sulfide layers resulting into the double-layered structure. On the otherhand, SnS_2 adopts PdI_2 type layered structure and crystallizes with hexagonal unit cell. The tetravalent Sn atoms are attached to six S atoms with average bond distance of $\sim 2.6 \text{ \AA}$. In this case, two hcp sulphur layers sandwich the Sn atom between them and the geometry around S atom is trigonal pyramidal with coordination number 3. The crystal packing features SnS_2 layers stacked on top of each other along the crystallographic c-axis which is connected together by Van der Waals forces [11]. Sn_2S_3 , a mixed valence tin sulphide material, exhibit a ribbon like structure in which the divalent and the tetravalent Sn atoms assumes trigonal pyramidal geometry and octahedral coordination geometry respectively. The average Sn-S distances in Sn_2S_3 range between $2.46\text{--}2.76 \text{ \AA}$.

Tin selenide materials are typically layered 2D material and commonly found into two compositions namely SnSe and SnSe_2 . SnSe exhibits orthorhombic crystal structure which can be regarded as a distorted NaCl-type structure

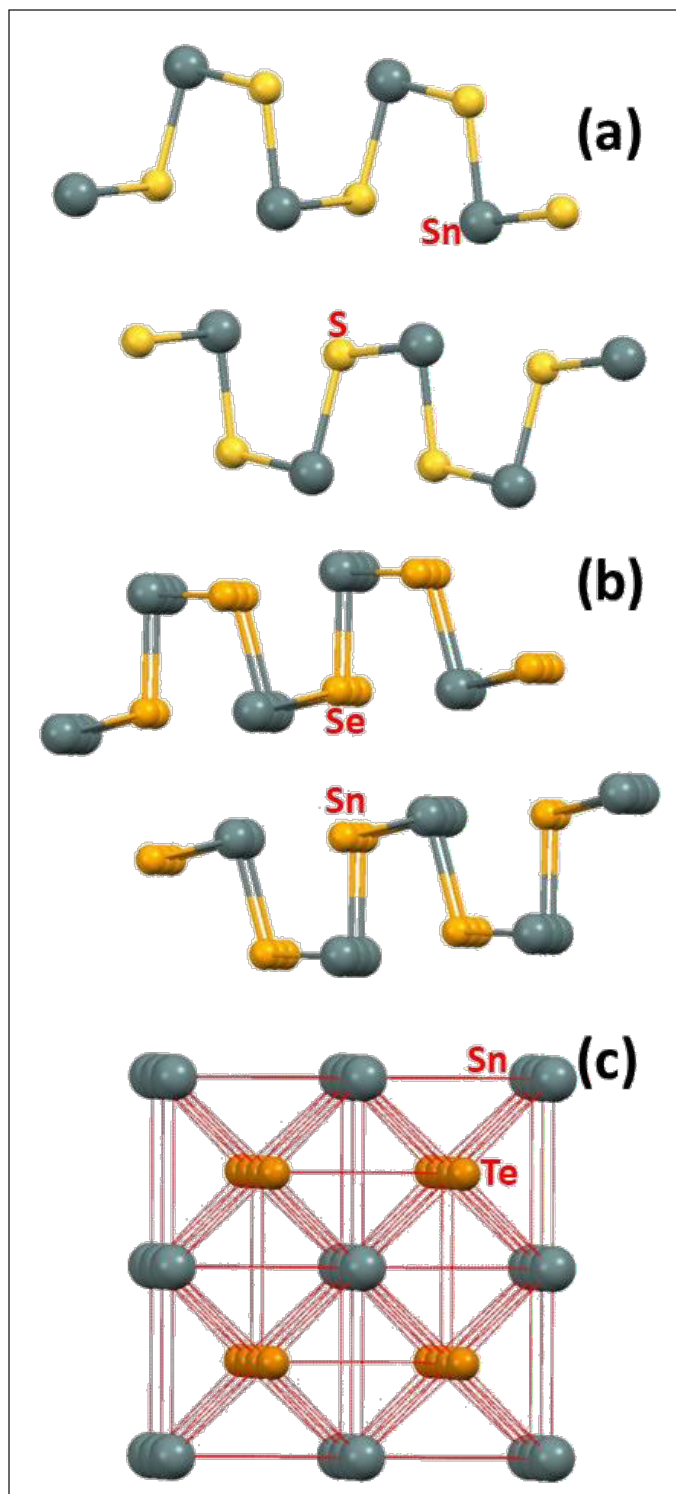


Figure 2: Structures of tin mono-chalcogenides; (a) SnS, (b) SnSe and (c) SnTe, respectively.

with space group P_{nma} (Figure 2b). The crystal packing in SnSe is achieved via nearly two atoms thick SnSe slabs with strong Sn-Se bonds along b-c plane and weaker Sn-Se bonds along a-axis. These SnSe slabs are corrugated and the perspective view along the c-axis is an armchair form

whereas the same along b-axis is a zigzag like projection [12]. This difference in perspective views along the a, b, and c axial directions leads to a highly anisotropic nature of the material. The geometry around the divalent Sn atom is a highly distorted coordination polyhedral which is defined by seven Se atoms including three short and four very long Sn-Se bonds, and a lone pair of the Sn(II) sterically placed between the four long Sn-Se bonds [13]. SnSe₂ have a hexagonal crystal structure and can be viewed as CdI₂ type crystal system with C6 lattice structure. The structure can be interpreted as strongly bonded Se-Sn-Se two dimensional layers wherein the Sn layer is sandwiched between two layers of Se atoms. Along the z-axis of this structure, these three atom thick covalently bonded Se-Sn-Se slabs are piled up together through weak Van der Waals forces [14].

Tin telluride (SnTe) crystallizes with cubic rock salt structure (Figure 2c), i.e NaCl type crystal with space group Fm3m. As a result of the cubic structure, the coordination geometry around Sn²⁺ is octahedral defined by six Se²⁻ atoms and vice versa. Chattopadhyay et al. have investigated detailed high pressure X-ray diffraction study with synchrotron radiation and reported that SnTe, interestingly undergo a pressure-induced structural phase transition from NaCl type to an intermediate orthorhombic phase at about 18 kbar. It undergoes further pressure-induced phase transition from orthorhombic to CsCl type phase at about 250 bar [15].

Synthetic routes and energy applications of tin chalcogenides

Generally, nanoparticles (NPs) of any material can be synthesized either by top-down (physical) or bottom-up (chemical/solution) approaches. The former involves the reduction of average particle size to a smaller size by crushing, grinding etc. whereas in the latter case, NPs are produced through heterogeneous/homogeneous nucleation and growth. However, the solution route provides molecular level control during synthesis which is merely absent in physical approach. In the chemical approach, a variety of synthetic routes (gas or liquid phase) have been designated depending on the nature of the precursor material which provide an extra edge over the physical route. Moreover, it has been widely accepted that the solution phase synthesis is the key to the low-cost production of both colloidal NPs and thin films [16]. Depending upon the reaction strategy, solution phase synthesis can be solvothermal, hydrothermal, hot injection, non-injection, one-pot chemical synthesis or microwave assisted synthesis while relying on the starting material, solution phase synthesis can be classified as

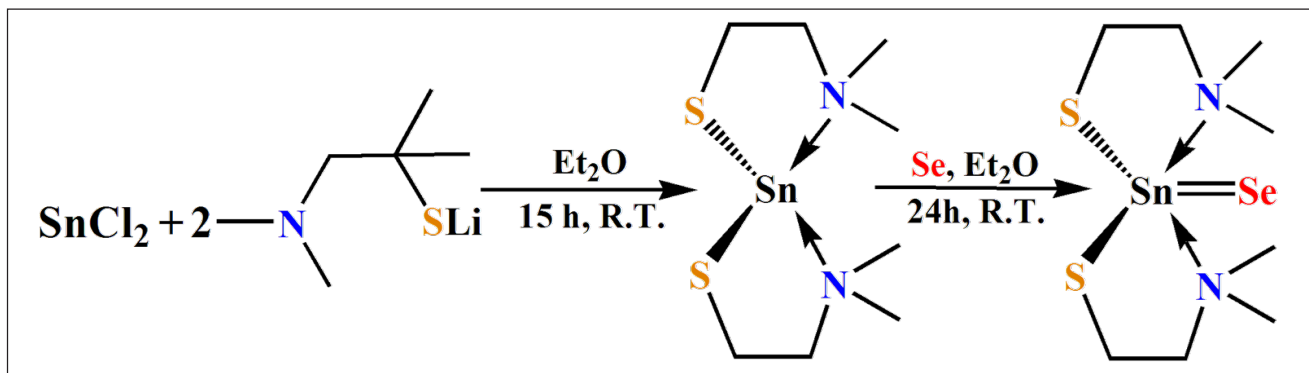
multiple source or single source molecular precursor route. In the former case, solutions of different ions and in the latter case, solution of a single molecule containing the constituent elements of the desired material in covalently bonded fashion, are subjected to controlled conditions of temperature, pressure, and solvent which lead to the formation of NPs. By controlling the nucleation and growth kinetics, temperature, time, particles of various sizes and morphologies can be produced [17].

Solution processed tin chalcogenides constitutes an important class of 2D layered semiconductor materials among group 14 metal chalcogenides. These materials have intense absorption across the electromagnetic spectrum with narrow band gaps. The result being extensive and wide array of applications of these materials in the next generation electronic, optical, optoelectronic, and flexible systems including solar cell, photocatalytic oxidation, thermoelectric generators, fuel cells, LIBs, environmental monitoring, water splitting and biofuels [18]. Wu et al. prepared SnS₂ NPs by the solvothermal route using SnCl₄·5H₂O and thioacetamide under three solvents conditions (ethylene glycol, deionized water, and ethanol). These materials exhibit good cycle retention and a high rate performance when tested as anode material in LIBs. Haque and coworkers have recently utilized SnCl₂ and thioacetamide as Sn and S source respectively with THF as a solvent to prepare mesoporous-TiO₂/SnS thin film solar cell which exhibit a conversion efficiency of 3.0% [19]. Contemporarily, colloidal tin selenide has also received attention in terms of energy conversion and storage applications. SnSe was revealed to perform as a superior thermoelectric material owing to a ZT value of 2.6 along a specific crystalline orientation (b-axis) as reported by Zhao et al. [12] whereas SnSe₂ synthesized via hydrazine assisted reduction of elemental Sn and Se by Dao and coworkers have shown a conversion efficiency (η) of 0.12% in SnSe₂-TiO₂ based solar cell [13]. Though less explored than sulphide and selenides, tin telluride have been the material of interest for scientists due to its exceptionally narrow band gap (bulk SnTe possess a direct band gap of 0.18 eV at 300 K). Narrow band gap materials have gained recognition due to their potential application in optoelectronics, mid-IR photodetectors and thermoelectric devices. Niasari et al. have reported the synthesis of SnTe NPs by reductive precipitation using an aqueous solution of 0.1 M SnCl₂·2H₂O and 0.1 M TeCl₄ containing 0.3 M 1,3-propylenediamine with KBH₄ [20]. In a recent study, Kladkaew et al. have utilized SnCl₂ and Na₂TeO₃ as dual source precursor to prepare SnTe thin film over FTO glass [21] and investigated its optical parameters and thermoelectric performance. Bhatt et al. have studied the

thermoelectric behavior of both SnTe and Mg and In codoped SnTe and reported a ZT of 1.5 at 840 K and ZT_{avg} of ~0.6 considering 300 and 840 K as cold and hot ends which make SnTe a very attractive material for thermoelectric applications [22].

Single source molecular precursor (SSP) approach, owing to their upper hand over multiple precursor routes in terms of phase purity of materials with tunable physical properties, low temperature and inexpensive nature; have also been extensively researched upon. Moreover, a SSP can be equally utilized for synthesis of NPs and deposition of thin films using aerosol assisted chemical vapor deposition (AACVD). In the nascent phase of this field, scientists have explored various tin thiolates and xanthate as molecular precursor to prepare tin sulphide thin films.

In the nascent phase of this field, scientists have explored various tin thiolates and xanthates as molecular precursor to prepare tin sulphide thin films. In some earlier work, Barone et al. have synthesized and used (PhS)₄Sn as molecular precursor for the deposition of SnS₂ thin film through AACVD [23]. The same group have also utilized some fluorinated tin thiolates, namely [CF₃(CF₂)₅CH₂CH₂S]₄Sn, [p-F-C₆H₄S]₄Sn and (SCH₂CF₃)₄Sn for the synthesis different phases tin sulphide thin films through atmospheric pressure chemical vapor deposition (APCVD) [24]. It was observed that films deposited at 450 and 500°C comprise the sesquisulfide, Sn₂S₃, whereas the films deposited at 550 or 600°C are comprised of SnS. However, the discussed precursors require the involvement of toxic H₂S gas as a co-reagent to deposit desired stoichiometric tin sulphide thin films. To encounter this shortcoming, O'Brien and co-workers have designed and synthesized benzyltinchloride-thiosemicarbazone compounds for the deposition of tin sulphide by AACVD method. They have synthesized and utilized precursors of the type Bz₃SnCl(L) (L = thiosemicarbazones of salicylaldehyde and 4-chlorobenzaldehyde, Bz = benzyl) to deposit SnS thin films in the temperature range 375-475°C [25]. It was inferred that SnS thin films were deposited irrespective of the deposition temperature. In a recent study, Park et al. have developed Sn(II) complexes with 1-(dimethylamino)-2-methylpropane-2-thiolate (dmampS) ligand of the type Sn(dmampS)₂ and Sn(dmampS)₂Se as shown in scheme 1 and established their molecular structure by single crystal XRD [26]. The former precursor was utilized for deposition of SnS thin films via MOCVD over SiO₂ substrate at varied temperatures (300 and 350°C), the latter was used to produce ternary mixed chalcogenide 2D material SnSSe. Decomposition of Sn(diethyldithiocarbamate)₂(1,10-phenanthroline) resulted into the formation



Scheme 1: Synthetic protocol for the preparation of $\text{Sn}(\text{dmampS})_2$ and $\text{Sn}(\text{dmampS})_2\text{Se}$. (Scheme is redrawn from the reference 26)

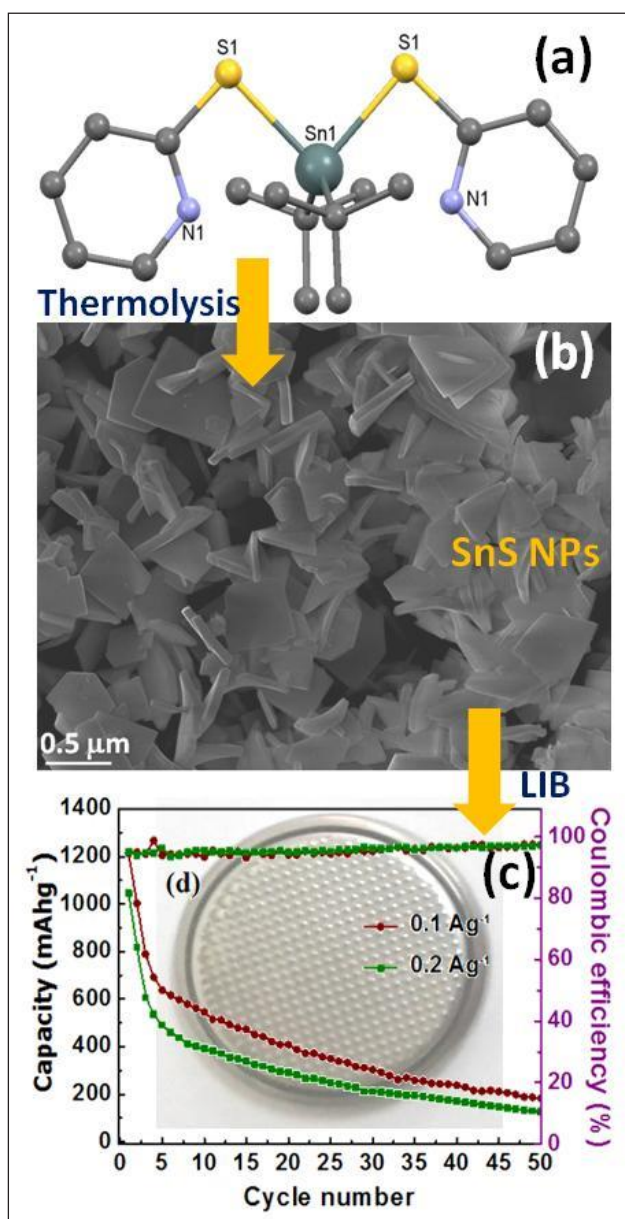


Figure 3: di-tert-butyltin dipyridyl thiolate precursor employed for the preparation of SnS nanoplatelets and their utility as an anode material in lithium ion batteries (Redrawn from reference from 28).

of large single crystals of SnS nano sheets as demonstrated by Zhang et al. [27]. The resulting SnS nanosheets showed decreasing capacity after 5 cycles when tested as an anode material in LIBs which is attributed to the ultra-thin nature of the nano materials.

An improved LIB performance was recently reported for SnS nanoplatelets obtained from the SSP di-tert-butyltin dipyridylthiolate by Tyagi and co-workers [28]. The cell demonstrated the first cycle charge and discharge capacities of 1306 mAhg⁻¹ at 50 mA g⁻¹ current density and could be run for 50 cycles with 0.1 Ag⁻¹ and 0.2 Ag⁻¹ current densities (Figure 3).

Moreover, tin sulphide nanomaterials synthesized from SSPs have also been proven worthy as absorber material in solar cell applications. Koktysh et al. have investigated the conversion of bis(diethyldithiocarbamato)tin(II) into SnS nanocrystals in oleylamine at elevated temperature [29]. The as prepared SnS displayed strong absorption in the visible and near-infrared (NIR) spectral regions making them promising candidates for solar cell energy conversion. Recently, Mbese and co-workers have developed a new SSP, bis(N-di-isopropyl-N-octyl dithiocarbamato)tin(II) which upon decomposition, yielded phase pure SnS material [30]. The optical properties of SnS nanocrystals revealed a better absorption of light in the entire visible region and the photoluminescence spectrum showed strong band edge emission peak at 460 nm assigned to tin and sulphur vacancies associated to interstitial defects. They have also observed red shifted indirect and direct energy band gaps of 1.22 and 1.35 eV respectively were observed compared to the bulk SnS due to the effect of quantum confinement which prove them to be promising materials for solar cell applications.

The SSP field for tin selenide and telluride are not quite mature yet and till date only handful of SSPs have been developed for the preparation of tin selenide and telluride nanostructures among which SSP for SnSe₂ are rather rare.

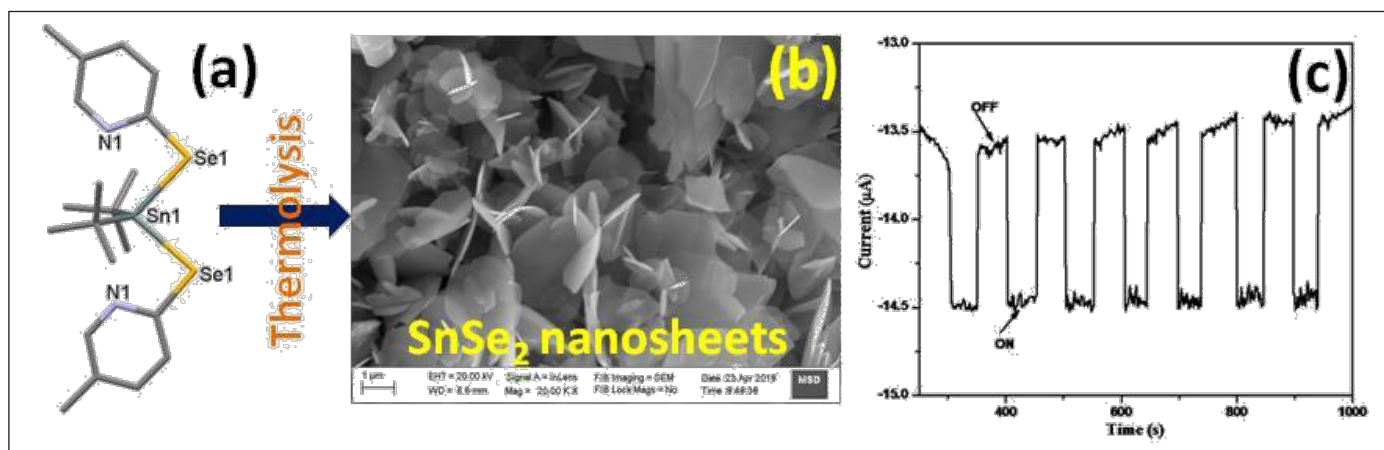
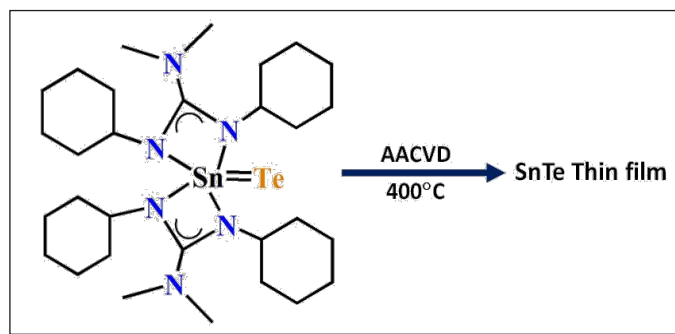


Figure 4: SnSe_2 nanosheets derived from diorganotin-5-methylpyridyl selenolate ligand and their photo-switching characteristics (redrawn from reference 35).

Some early reports include deposition of SnSe and SnTe thin films from SSP of the type $[\text{Sn}\{(\text{SiMe}_3)_2\text{CH}\}_2(\mu\text{-E})]_2$ (where E = Se or Te) by Chuprakov et al. using MOCVD technique and quality of the films were investigated by pXRD, XPS and SEM [31]. They have reported inefficient deposition of SnSe films on quartz surfaces covered with sputtered silver or gold, but have achieved good quality SnTe deposition at temperatures as low as 300 or 400°C over same substrate. Some notable research work includes deposition of SnSe/SnSe₂ through $[\text{SnCl}_4(\text{Et}_2\text{Se})_2]$ over SiO₂ substrate at 500°C [32], utilization of $[\text{SnCl}_4\{\text{nBuSe}(\text{CH}_2)_3\text{Se}^{\text{nBu}}\}]$ to deposit SnSe₂ over a variety of substrates such as Si/SiO₂/TiN at different temperatures (400-600°C) [33] and $[\text{SnCl}_4\{\text{nBuE}(\text{CH}_2)_3\text{E}^{\text{nBu}}\}]$ (E = S or Se) to deposit SnS and SnSe respectively [34]. Jain and co-workers have developed diorgano tin complexes with internally functionalized hemilabile ligands of the type $[\text{R}_2\text{Sn}\{2\text{-SeC}_5\text{H}_3(\text{Me-5})\text{N}\}_2]$ (R = Me, Et and ^tBu), established their crystal structure and utilized them as SSP for the synthesis of both SnSe and SnSe₂ NPs by varying reaction conditions [35]. They have also observed consistent switching characteristics during repeated cycles of on-off experiments under light intensity of 200 µW/cm² which demonstrate the photosensitivity of the nanostructure and prove their suitability as absorber material in solar cells (Figure 4).

Revaprasadu and co-workers have synthesized a new SSP, bis(selenobenzoato)dibutyltin(IV) which upon subjected to AACVD, produced SnSe thin film over FTO [36]. Photoelectrochemical studies demonstrated by them show the potential of the material for water splitting/hydrogen evolution reaction (HER). In a recent study, Kedarnath and co-workers have demonstrated SnSe nanosheets derived from SSP $[\text{Me}_2\text{Sn}\{2\text{-SeC}_5\text{H}_2(\text{Me-4,6})\text{N}\}_2]$ as a promising anode material for LIBs [37]. The material exhibits initial specific capacity of 1134

mAhg⁻¹ at a current density of 50 mA g⁻¹ and was found to retain a capacity of 380 mAhg⁻¹ even after 70 cycles with 100% efficiency. Though limited, some important synthetic routes towards phase pure tin telluride include the development of (Ph₃Sn)₂Te by Boudjouk et al. and its subsequent solid-state pyrolysis to obtain cubo-octahedral SnTe which were subsequently characterized by pXRD and SEM techniques [38]. They have further extended their work to prepare 2,2,4,4,6,6-Hexabenzylcyclotristannatellurane or (Bn₂SnTe)₃ and have established its molecular structure. The SSP was used under flow pyrolysis system at 200 or 275°C, for 10 h, or at 400°C for 5 h produced cubic phase pure SnTe in high yield [39]. Recently Ahmet et al. have reported telluro Sn(IV) guanidinate precursor containing Sn=Te double bond derived from the oxidative addition of telluro Sn(II) guanidinate complexes having general formula $[\{\text{RNC}(\text{NMe}_2)\text{NR}\}\text{Sn}(\text{Te})]$ (R = ⁱPr; R = Cy) and made use of 0.033 M toluene solution of the same to deposit SnTe thin films over glass and silicon substrate using AACVD technique at temperatures 300 and 400°C over 90 min deposition period and using argon at 20 psi as carrier gas [40].



Scheme 2: Utility of $[\{\text{RNC}(\text{NMe}_2)\text{NR}\}\text{Sn}(\text{Te})]$ precursor for the deposition of SnTe thin films. (Scheme is redrawn from the reference 40)

The thin films were characterized by pXRD, EDS, Raman and SEM studies. Moreover, SnTe also acts as a great precursor for some technologically important ternary thermoelectric semiconductor nanoalloys ($\text{Pb}_{1-x}\text{Sn}_x\text{Te}$, $\text{Sn}_{1-x}\text{Mg}_x\text{In}_y\text{Te}$ etc.) with size-dependent optical and electronic properties [20].

Conclusions

The wide applications of energy harvesting and energy storage materials require the discovery and development of environmentally friendly high performance earth abundant materials. Tin chalcogenides have shown promise as a photon-absorber and thermoelectric material. They have the potential to substitute the environmentally non-friendly cadmium telluride and lead chalcogenides owing to their unique structural and electronic features. Moreover, the ability of tin atom to accommodate 4.4 moles of lithium projects its chalcogenide compounds as anode materials for LIBs. However, it is realized that for actual application, synthetic methods which are simple and can be easily scaled up played an important role. Accordingly, various synthetic protocols have been summarized. Beyond, binary tin chalcogenides, ternary (Cu_2SnE_3 , Cu_2SnE_4) and quaternary ($\text{Cu}_2\text{ZnSnE}_4$) (E = S, Se) find great potential as energy harvesting and storage materials. It will imperative to explore the potential of these materials along with binary tin chalcogenides. Finally, it is believed that this article will be beneficial for the future progress of tin chalcogenides.




Acknowledgement

The authors thank Dr. A. K. Tyagi, Director, Chemistry Group for the encouragement of this work.

References:

- G. Chen, J. Seo, C. Yang and P. N. Prasad, *Chem. Soc. Rev.*, 2013, 42, 8304-8338.
- P. D. Mathew, P. D. Mcnaughtner, D. J. Lweis and P. O'brien, *Chem. Sci.*, 2017, 8, 4177-4187.
- A. Banik, S. Roychowdhury and K. Biswas, *Chem. Commun.*, 2018, 54, 6573-6590.
- Q. Tang, H. Su, Y. Cui, A. P. Baker, Y. Liu, J. Lu, X. Song, H. Zhang, J. Wu, H. Yu and D. Qu, *J. Power Source*, 2018, 379, 182-190.
- L. Zhang, L. Lu, D. Zhang, W. Hu, N. Wang, B. Xu, Y. Li and H. Zeng, *Electrochim. Acta.*, 2016, 209, 423-429.
- R. Lv, J. A. Robinson, R. E. Schaak, D. Sun, Y. Sun, T. E. Mallouk and M. Terrones, *Acc. Chem. Res.*, 2015, 48, 56-64.
- X. Duan, C. Wang, A. Pan, R. Yu and X. Duan, *Chem. Soc. Rev.* 2015, 44, 8859-8876.
- D. J. Lewis, P. Kevin, O. Bakr, C. A. Muryn, M. A. Malik and P. O'brien, *Inorg. Chem. Front.*, 2014, 1, 577-598.
- X. Liu, T. Najam, G. Yasin, M. Kumar and M. Wang, *ACS Omega*, 2021, 6, 17391-17399.
- T. Jiang and G. A. Ozin, *J. mater. chem*, 1998, 8, 1099-1108.
- B. Palosz, W. Steurer and H. Schulz, *Acta Crystallogr. Sect. B*, 1990, 46, 449-455.
- L. D. Zhao, S. H. Lo, Y. Zhang, H. Sun, G. Tan, C. Uher, C. Wolverton, V. P. Dravid and M. G. Kanatzidis, *Nature*, 2014, 508, 373-377.
- X. Yu, J. Zhu, Y. Zhang, J. Weng, L. Hu and S. Dai, *Chem. Commun.*, 2012, 48, 3324-3326.
- X. Zhou, Q. Zhang, L. Gan, H. Li, J. Xiong and T. Zhai, *Adv. Sci.* 2016, 3, 1600177.
- T. Chattopadhyay, H. G. Vonschering, W. A. Grosshans and W. B. Holzapfel, *Physica B+C*, 1986, 139, 356-360.
- W. Ahmed, M. J. Jackson, editors. *Emerging Nanotechnologies for manufacturing*. First edit. Elsevier Inc.; 2009.
- N.O. Boadi, M. A. Malik, P. O'Brien and J. A. M. Awudza, *Dalton Trans.*, 2012, 41, 10497-10506.
- M. X. Wang, G. H. Yue, Y. D. Lin, X. Wen, D. L. Peng and Z. R. Geng, *Nano-Micro Lett.*, 2013, 5, 1-6.
- D. Ding, T. Rath, L. Lanzetta, J. M. Marin-Beloqui and S. A. Haque, *ACS Appl. Energy Mater.*, 2018, 1, 3042-3047.
- M. Salavati-Niasari, M. Bazarganipour, F. Davar and A. A. Fazl, *Applied Surface Science*, 2010, 257, 781-785.
- M. Kladkaew, N. Samranlertrit, V. Vailikhit, P. Teesetsopon and A. Tubtimtae, *Ceramics International*, 2018, 44, 7186-7201.
- D. K. Bhat and S. Shenoy U, *J. Phys. Chem. C*, 2017, 121, 7123-7130.
- G. Barone, T. G. Hibbert, M. F. Mahon, K. C. Molloy, L. S. Price, I. P. Parkin, A. M. E. Hardy and M. N. Field, *J. Mater. Chem.*, 2001, 11, 464-468.
- T. G. Hibbert, M. F. Mahon, K. C. Molloy, L. S. Price and I. P. Parkin, *J. Mater. Chem.*, 2001, 11, 469-473.
- B. P. Bade, S. S. Garje, Y. S. Niwate, M. Afzaal and P. O'Brien, *Chem. Vap. Deposition*, 2008, 14, 292-295.
- J. -H. Park, S. G. Kang, Y. K. Lee, T. -M. Chung, B. K. Park and C. G. Kim, *Inorg. Chem.*, 2020, 59, 3513-3517.
- Y. Zhang, J. Lu, S. Shen, H. Xu and Q. Wang, *Chem. Commun.*, 2011, 47, 5226-5228.
- A. Tyagi, G. Karmakar, B. P. Mandal, D. D. Pathak, A. Wadawale, G. Kedarnath, A. P. Srivastava and V. K. Jain, *Dalton Trans.*, advance article, 2021 (DOI: 10.1039/d1dt01142a)
- D. S. Koktysh, J. R. McBride and S. J. Rosenthal, *Nanoscale Res. Lett.*, 2007, 2, 144-148.
- E. L. Meyer, J. Z. Mbese, M. A. Agoro and R. Taziwa, *Optical and Quantum Electronics*, 2020, 52, 90.
- I. S. Chuprakov, K. H. Dahmen, J. J. Schneider and J. Hagen, *Chem. Mater.*, 1998, 10, 3467-3470.
- S. D. Reid, A. L. Hector, W. Levason, G. Reid, B. J. Waller and M. Webster, *Dalton Trans.*, 2007, 4769-4777.
- C. D. Groot, C. Gurnani, A. L. Hector, R. Huang, M. Jura, W. Levason and G. Reid, *Chem. Mater.*, 2012, 24, 4442-4449.
- C. Gurnani, S. L. Hawken, A. L. Hector, R. Huang, M. Jura, W. Levason, J. Perkins, G. Reid and G. B. Stenning, *Dalton Trans.*, 2018, 47, 2628-2637.

35. A. Tyagi, G. Karmakar, A. Wadawale, A. Y. Shah, G. Kedarnath, A. P. Srivastava, V. Singh and V. K. Jain, *Journal of Organomet. Chem.*, 2018, 873, 15-21.
36. M. D. Khan, M. Aamir, M. Sohail, M. Sher, N. Baig, J. Akhtar, M. A. Malik and N. Revaprasadu, *Dalton Trans.*, 2018, 47, 5465-5473.
37. G. Karmakar, K. K. Halankar, A. Tyagi, B. P. Mandal, A. P. Wadawale, G. Kedarnath, A. P. Srivastava and V. Singh (unpublished result)
38. P. Boudjouk, D. J. Seidler, S. R. Bahr and G. J. McCarthy, *Chem. Mater.*, 1994, 6, 2108-2112.
39. P. Boudjouk, M. P. Remington, D. G. Grier, W. Triebold and B. R. Jarabek, *Organometallics*, 1999, 18, 4534-4537.
40. I. Y. Ahmet, M. S. Hill, P. R. Raithby and A. L. Johnson, *Dalton trans.*, 2018, 47, 5031-5048.

	<p>Mr. Gourab Karmakar received his M.Sc. degree in Chemistry from IIT Roorkee. He joined Chemistry Division, BARC as a Scientific Officer (C) in the year 2016. Since then, he is actively involved in the design and development of efficient single source molecular precursor for metal chalcogenide nanomaterials and thin films. Currently he is pursuing Ph.D. from HBNI. He has published several research papers and conference papers as well as presented his research work at various scientific platforms.</p>
	<p>Dr. Adish Tyagi did his post-graduation in Chemistry from Delhi University, Delhi in 2010 and joined BARC in 2011 after successful completion of one year orientation course from BARC Training School. He obtained his Ph.D. degree in Chemistry from HBNI in 2018. Currently, he is working as Scientific Officer-E in Chemistry Division of BARC. His research interests include synthesis of organometallic molecular precursors for technologically important nanomaterials, development of efficient phosphor for white light emission and purification of strategic materials. He has several international papers and two book chapters to his credit.</p>
	<p>Dr. G. Kedarnath, Scientific Officer (G), joined BARC in the year 2000 after graduating from BARC training school. He has been working on designing and development of single source molecular precursors for metal chalcogenide nanomaterials and thin films. He was awarded Ph. D. (Chemistry) in 2010 by University of Mumbai. He pursued his post-doctoral research at Virginia Commonwealth University, Richmond, USA. He has published more than 50 papers in peer-reviewed journals. He is also a reviewer of ACS, RSC and Elsevier publishers. He is a recognized Ph. D. (Chemistry) guide of HBNI and is a recipient of Scientific and Technical Excellence Award of DAE in 2013.</p>

Electrochemical Techniques in Evaluation of Processes for Energy and Sensing Applications

S. Manna^{1,2§}, Abhishek Sharma^{1,2§}, Srikant Sahoo¹ and A.K. Satpati^{1,2*}

¹Analytical Chemistry Division, Bhabha Atomic Research Centre, Trombay, Mumbai-400085, India

²Homi Bhabha National Institute, Anushaktinagar, Mumbai 400094, India

*Corresponding author email: asatpati@barc.gov.in

§Equal contribution from both the authors

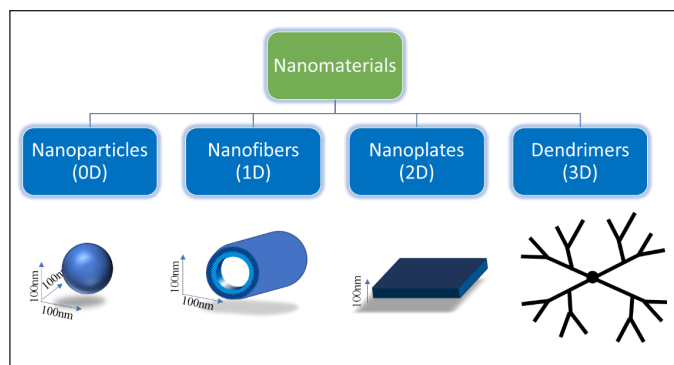
Abstract

Present article has been focused on the applications of the electrochemical techniques in the evaluation of the chemical processes generated from different materials and molecules. The nanophase-based materials behaves differently compared to their bulk form. In view of this the evaluation of the characteristics of properties generated from the nano phase materials are interesting to investigate by electrochemical measurements. Basic introductions about the conventional electrochemical techniques and the important parameters that could be evaluated from such techniques are discussed. In addition to the conventional techniques, electrochemical impedance spectroscopy has been discussed due to its usefulness in evaluating the electrochemical interface. The hyphenated techniques like, spectroelectrochemistry has been used in the evaluation of mechanism of electrochemical process with the support from both electrochemical and the spectroscopic evaluation. The utilisation of the techniques have been discussed taking some of the relevant examples related to the evaluation of the mechanism of the process, analytical determination and the material characterisation.

1. Introduction

Nanomaterials are the class of material which are having at least one internal or external dimension measures in 1-100nm range. These are having same composition as bulk but are having different physio-chemical properties. When reduced to nanoscale material shows different properties compared to what they show at macroscale, for instance insulator becomes conductor i.e. silicon, inert becomes catalyst i.e. platinum used in several catalysis processes. There is various classification of nanomaterial, one is based on number of dimensions out of nanoscale range. On the basis of this classification nanomaterials are classified as;

- (i) **Zero dimensional nanomaterials:** Materials in which all the dimensions are in nanoscale range e.g. Nanoparticles, quantum dots.
- (ii) **One dimensional nanomaterials:** Materials in which two of the dimensions are in nanoscale range and one in macroscale e.g. Nanotubes
- (iii) **Two dimensional nanomaterials:** Materials in which one dimension is in nanoscale range and other two in macroscale e.g. Nanoplates
- (iv) **Three dimensional nanomaterials:** Materials in which none of the dimension is in nanoscale range e.g. Dendrimers, polycrystalline



Scheme 1. The schematic presentation of the classifications of different nano materials

There are several methods to form various nanomaterials classified as 'top-down' and 'bottom-up.' Nanomaterials constructed from top-down techniques produce tiny structures from larger pieces of material, for example, synthesis of Graphene oxide from graphite by Hummers method. These can also be constructed by bottom-up techniques where self-assembly of atom by atom or molecule by molecule arranged into a structure, for example, chemical vapor deposition of semiconductors.

Nanomaterials plays crucial role in developing novel energy generation and storage devices. The unusual quantum impact at nanoscale benefits the electron transport and band designing in nanomaterials, resulting in excellent device performance. Nanomaterials found their

application in photovoltaics, batteries, supercapacitors, electrocatalysts, and photoelectrochemical catalysts. Wide-bandgap nanomaterials are prepared from II-VI and III-V elements in photovoltaics. These are drawing significant attention for their potential applications in energy generation. Nanomaterial based solar cells, i.e., Organic solar cells with nano-crystalline films, polymer thin films with inorganic nanostructures, nanostructured dye sensitive solar cells, and perovskite solar cells, have improved electron-hole pair creation probability due to increase of the photon path inside nanostructures. For instance, BiFeO₃ nanostructures were used as additive for organic halide perovskite CH₃NH₃PbI₃, it results in increased charge carrier mobility and electron diffusion length which lead to the increase of the short circuit current of Perovskite solar cell[1]. The use of nanomaterials in batteries increases surface area for electrode and electrolyte materials, and nanoparticles could enhance the conductivity, allowing charge to flow more freely, resulting in higher capacity and shorter charge/discharge cycle. Several nanomaterials have been investigated, which would enable higher storage densities of lithium than standard graphite or metal electrodes, i.e., LiMn₂O₄[2] or LiCo₂O₄[3] nanoparticles, carbon-coated silicon nanowires, Phosphorene-graphene hybrid material. The addition of Al₂O₃, SiO₂, or ZrO₂ nanoparticles to solid polymer gel could significantly boost the conductivity and storage capacity of the electrolyte. 2D MoS₂ acts as an efficient protective layer for Li metal anodes in high-performance Li-S batteries[4].

Nanostructuring strongly influences the performances of supercapacitors. Carbon nanomaterials i.e. graphene and carbon nanotubes[5] and nanostructured metal oxide i.e. MnO₂[6], owing to their large surface area, high mesoporosity and electrolyte accessibility, and good electrical properties make them promising candidates to replace the electrode materials in high-performance supercapacitors.

Nanomaterials also have wide application in energy storage in chemical form such as storing of hydrogen. Nano catalysts for electrocatalytic and photoelectrocatalytic applications are utilized for hydrogen generation. Electrocatalysts i.e. MoS₂, NiS, FeP and photoelectrocatalysts i.e. BiVO₄, Fe₂O₃, WO₃ greatly reduces the activation energy and overpotential leading to improved catalytic activity.

Properties of a good sensors are better sensitivity and higher resolution. Many nanomaterials have been used for sensing application for (i) Improved sensitivity due to higher active surface area for oxidation or reduction of the analyte. This in turn allows ultrasensitive low

concentration detection (ii) Sharper and well separated peaks due to enhanced conductivity and better electron transfer allows simultaneous detection of many analyte. Different nanomaterials and their application in sensing will be discussed in details in the later part of the article.

Electrochemistry and related processes build upon interrelation of electrical and chemical effects and spans broad and interdisciplinary areas of research and development. It encompasses an array of different phenomena (e.g., electrophoresis and corrosion), devices (electrochromic displays, electroanalytical sensors, batteries, supercapacitors, catalysts, and fuel cells etc.), and technologies (the electroplating of metals and the large-scale production of aluminum and chlorine). Electrochemical methods are sensitive, low cost, simple, easily reproducible with a plenty of scope for improvisation at the same time they are known for their robustness, fast response, miniature size. Most of the techniques require very small quantity of samples or almost no requirements of sample preparation or pretreatment making it popular technique.

Even though electrochemistry is accurate and reliable but its application in characterization of nanomaterials involves some interesting challenges. Challenges arise from the very nature of the nanomaterials and the sensitivity of the available analytical methods[7, 8]. Due to active nature of nanomaterials, their physicochemical properties tend to change depending upon physical environment or processing history i.e. change in structure and switching of oxidation state. Since, electrochemical behavior is a surface phenomenon, complications arise because of dynamic surfaces and interfaces of the nanomaterials due to surface contamination, agglomeration or impurities. Complications increases with interaction of the nanomaterial with solution. In spite of the complications, one can choose apt electrochemical techniques for the purpose of characterization of the nanomaterials depending upon the application of interest. Prominent techniques being, cyclic voltammetry (CV), differential pulse voltammetry (DPV), electrochemical impedance spectroscopy (EIS), spectroelectrochemistry. Desired potential is applied on the working electrode (WE) and basic analyte signals in terms of current (i), potential (E), charge, and resistance(R), and impedance generated via electro or chemocatalysis processes are measured and correlated to various properties of the nanomaterials.

Application of electrochemical techniques for nanomaterial characterization and their application has broader aspect. Under the scope of this article discussions will be confined to the basics of various electrochemical

techniques e.g. CV, DPV, EIS and spectroelectrochemistry and among various applications of various nanomaterials, electrochemical characterization for sensors spanning sensing and quantitative detection of biological indicator like hydrogen peroxide and dopamine, drugs, hazardous heavy metal ions, pollutants like nitrate ions will be discussed using some relevant examples.

2. Techniques used for electrochemical characterization of materials and processes

2.1 Cyclic voltammetry (CV)

Cyclic voltammetry is an important electrochemical technique used to measure a redox-active analyte's current response to a triangular voltage waveform, such as that shown in Fig. 1(1). The voltage at which reversal takes place is called switching voltage. The range of switching voltage is chosen such that diffusion-controlled oxidation or reduction of one or more analytes occurs in that voltage range. The direction of the scan can be positive or negative, depending on the sample composition. The measured current response is dependent on the concentration of redox species and described by combining Faraday's law and Fick's first law of diffusion

$$i_d = nFAD_0 \left(\frac{\partial C_0}{\partial x} \right)_0$$

Where i_d is the diffusion-limited current, A is the electrode area, D_0 is the diffusion coefficient of the analyte and $(\partial C / \partial x)$ is concentration gradient at the electrode surface. The duck-shaped plot generated by cyclic voltammetry is called a cyclic voltammogram. Fig. (1) shows the cyclic voltammogram of 6mM $K_3Fe(CN)_6$ in 1M KNO_3 solution. Initially, at +0.8V, some anodic current is observed, which soon becomes zero as the scan continues; it arises due to oxidation of water to oxygen, which is essentially the background current. No current is observed up to +0.4V as no reducible and oxidizable species are present in this potential range. When potential becomes more cathodic to +0.4V, the current increases exponentially as the analyte is oxidized at the working electrode surface. The process is under electrochemical control, and the current linearly increases with increasing potential with a constant concentration gradient of the analyte species near the electrode surface within the double layer. Soon the current decreases from linearity because the analyte is depleted, and the double layer grows in size. The current reaches peak maximum at point D (cathodic peak current (i_{pc})) for reduction at the cathodic peak potential (E_{pc}). Now the process is under mixed control, i.e., more negative potentials cause an increase in current, which is offset by

a decreased analyte flux at the electrode surface. From this point, the mass transport of the analyte species from the bulk to the double layer will limit the current, which is slow on the electrochemical timescale. It results in the decrease of current to point F. However, when the scan is reversed, the current continues to be cathodic because the potentials are still negative enough to cause a reduction of $Fe(CN)_6^{3-}$. As the potential sweeps in the positive direction, eventually, potential reaches the value where the reduced analyte accumulated at the electrode surface gets re-oxidized. The process for oxidation mirrors that for the reduction, only with an opposite scan direction and an anodic peak (i_{pa}) at the anodic peak potential (E_{pa}). Anodic and cathodic peak currents are approximately equal magnitude for a reversible electrode reaction but are of opposite signs. The difference in peak potentials, ΔE_p , for a reversible electrode reaction at 25°C is expected to be

$$\Delta E_p = |E_{pa} - E_{pc}| = \frac{0.0592}{n}$$

where n is the number of electrons involved in the half-reaction. For irreversible reaction, electron transfer kinetics are slow, so ΔE_p exceeds to the expected value. At slower scan rate, an irreversible reaction may appear to be reversible, but with increasing the scan rate, increase the value of ΔE_p shows sign of irreversibility. Quantitative information can be determined from the cyclic voltammetry measurements using the Randles-Sevcik equation, which at 25°C is

$$i_p = 2.686 \times 10^5 n^{3/2} A c D^{1/2} v^{1/2}$$

where i_p is the peak current in amperes, A is the electrode area in cm^2 , D is the diffusion coefficient in cm^2/s , c is the concentration in mol/cm^3 , and v is the scan rate in V/s . Hence, with known value of scan rate, area of electrode and concentration, it is possible to determine value of diffusion coefficient using CV. As an example, consider the cyclic voltammogram for PBNCs/ SnO_2 QDs/RGO and PBNCs/ SnO_2 QDs nanocomposite in Fig. (2). Sahoo et al.[9] determined the diffusion coefficients for the PBNCs/ SnO_2 QDs/RGO and PBNCs/ SnO_2 QDs nanocomposite modified electrodes and found that PBNCs/ SnO_2 QDs/RGO nanocomposite has larger diffusion coefficient for ion transport than PBNCs/ SnO_2 QDs nanocomposite.

Applications of CV

CV is a valuable method for quickly determining information about the thermodynamics of redox processes, the kinetics of electronic-transfer reactions, and the energy

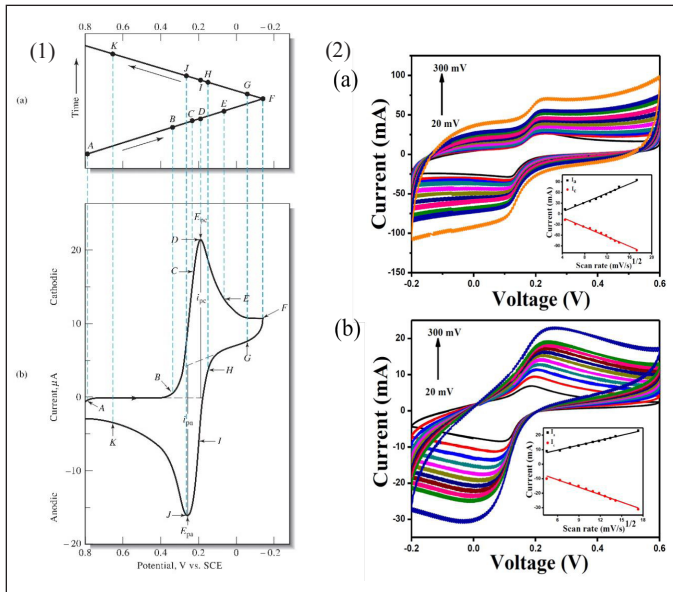


Fig. 1 (a) Potential versus time waveform. (b) Cyclic voltammogram for a solution that is 6.0 mM in $K_3Fe(CN)_6$ and 1.0 M in KNO_3 [10] (2) (a) & (b) Cyclic voltammograms of PBNCs/SnO₂ QDs/RGO and PBNCs/SnO₂ QDsnanocomposites at different scan rates (20-300 mVs^{-1}) in 0.1 M PBS (pH 7.4, 0.1 M KCl). Inset (a) & (b): peak currents (I_a & I_c) vs. square root of the scan rate ($v^{1/2}$)[9].

levels of the analyte. The energy level of HOMO and LUMO can be determined using CV. Shafiee et al.[11] determined the energy levels of HOMO and LUMO using E_{on} (onset) defined from the CV for the measurements in film (P3OT) and solution (PCBE) shown in Fig. 2. The empirical equation used was

$$E_{LUMO} = [(E_{red} - E_{1/2}(ferrocene)) + 4.8] eV$$

$$E_{HOMO} = [(E_{ox} - E_{1/2}(ferrocene)) + 4.8] eV$$

Ferrocene was used as an external standard that shows two peaks at 0.37 and 0.44 V; hence, the $E_{1/2}$ (ferrocene) is equal to 0.41 V.

Based on the theory of Matsuda and Ayabe[12] and Nicholson and Shain[13], the electron transfer rate constant can be straightforwardly determined from the CV. They introduced the dimensionless parameter Λ , which represent the relation between the standard rate constant k_0 and mass transport m_{trans} i.e.

Where n is no of electron transferred, D is the diffusion coefficient in cm^2/s , v is the scan rate in V/s . Matsuda and Ayabe followed by Nicholson and Shain have devised correlation between ΔE_p and Λ , and using the value of

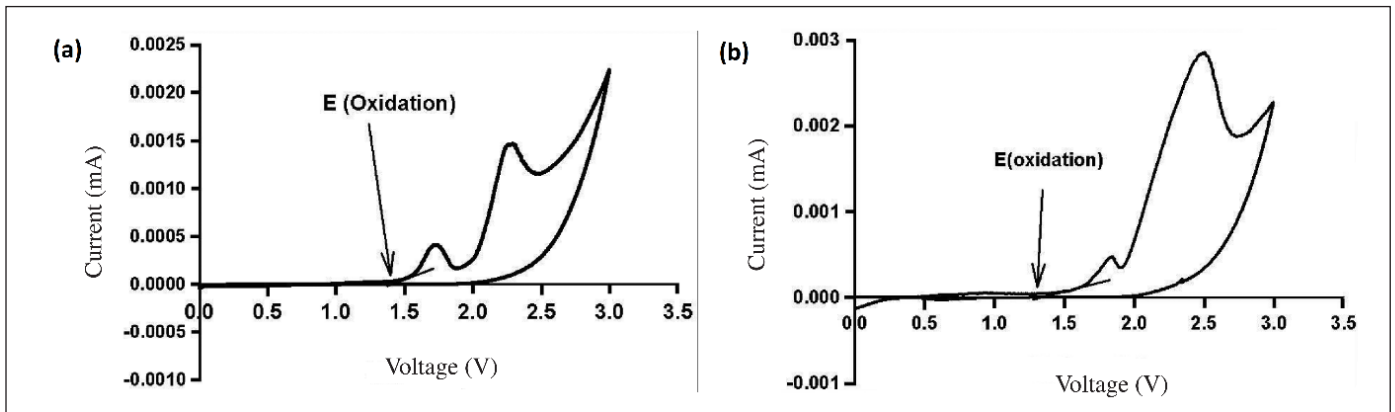


Fig 2. (a) & (b) Current -voltage curve for PCBE&P3OT[11]

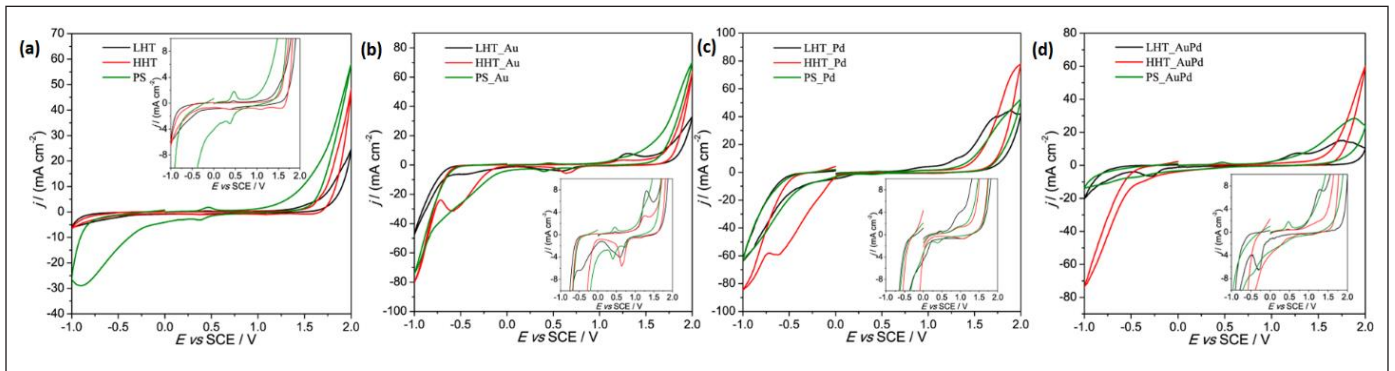


Fig 3. Cyclic voltammetry (CV) of PS, LHT, and HHT unmodified (a) and modified with AuNPs (b), PdNPs(c) & AuPdNPs (c) recorded in H_2SO_4 0.1 M at $100 mVs^{-1}$ [15].

Λ , electron transfer rate constant can be determined. Correlation between Nicholson parameter and k_0 to determine the electron transfer mechanism is given in table 1 [14]

Table 1. The typical standard rate constant values indicating the reversible quasi-reversible and irreversible processes.

Reversible	$\Lambda > 10$	$k_0 > 0.35 \cdot v^{1/2}$
Quasi-reversible	$10 > \Lambda > 10^{-2}$	$0.35 \cdot v^{1/2} > k_0 > 3.5 \cdot 10^{-4} \cdot v^{1/2}$
Irreversible	$\Lambda < 10^{-2}$	$k_0 < 3.5 \cdot 10^{-4} \cdot v^{1/2}$

Cyclic voltammogram also provides clue to determine whether reaction mechanism is reversible or irreversible. It can be carried out using three methods. Firstly, criteria is, the peak current for cathodic and anodic reaction to be the same i.e. $I_p(\text{oxd})/I_p(\text{red}) = 1$. Secondly, the peak current is directly proportional to square root of scan rate for reversible reaction as given by Randles-Sevcik equation. Third point is, for reversible reaction difference between oxidation and reduction potential remains same at all the scan rates.

CV can also be used to characterize morphology and particle size of nanoparticles. Testolin et al. shows electrochemical characterization of Au, Pd, and AuPd Nanoparticles Supported on Different Carbon Nanofibers using CV [15] shown in Fig. 3. Karami et al. [16] studied the effect of particle size of nanostructured lead oxide on CV parameter and found good linear relationship between anodic potential and particle size. Smaller particle increases the cathodic and anodic current and decrease the oxidation

potential for lead oxide formation, it was so because decreasing of particle size makes increased active surface area to take part in electrode reaction.

2.2 Differential Pulse Voltammetry

In differential pulse voltammetry (DPV) potential pulses are applied on a linear potential ramp. Typically, a small pulse of 50 mV is applied during the time period of around 50-100 ms, the excitation signal as shown in Fig. 4. The base potential value in DPV is chosen such that there is no faradaic reaction and it is increased between pulses with equal increments. Current measurements are made alternately at two points: one at S_1 , and other at S_2 at the end of the pulse. The difference between them is recorded as a function of the linearly increasing excitation potential. A DPV curve results as a peak and the height of peak is directly proportional to concentration. In DPV, the peak potential, E_p , can be approximately identified with $E_{1/2}$. With increasing irreversibility of reaction, E_p deviates from $E_{1/2}$ as the base of the peak widens and its height decreases. DPV is often used with a Dropping Mercury Electrode (DME) or a Static Mercury Drop Electrode (SMDE). When dropping mercury electrode is used, the technique is called as Differential Pulse Polarography (DPP).

Applications of DPV

DPV offers advantages compared to other electrochemical techniques when used as an analytical tool. DPV is very sensitive and allows direct analysis at the ppb (parts per billion) level. The ppt (parts per trillion) analyses are also possible when DPV is used in a stripping mode. The sensitivity of DPV is attributed to relatively short pulse time and its differential nature

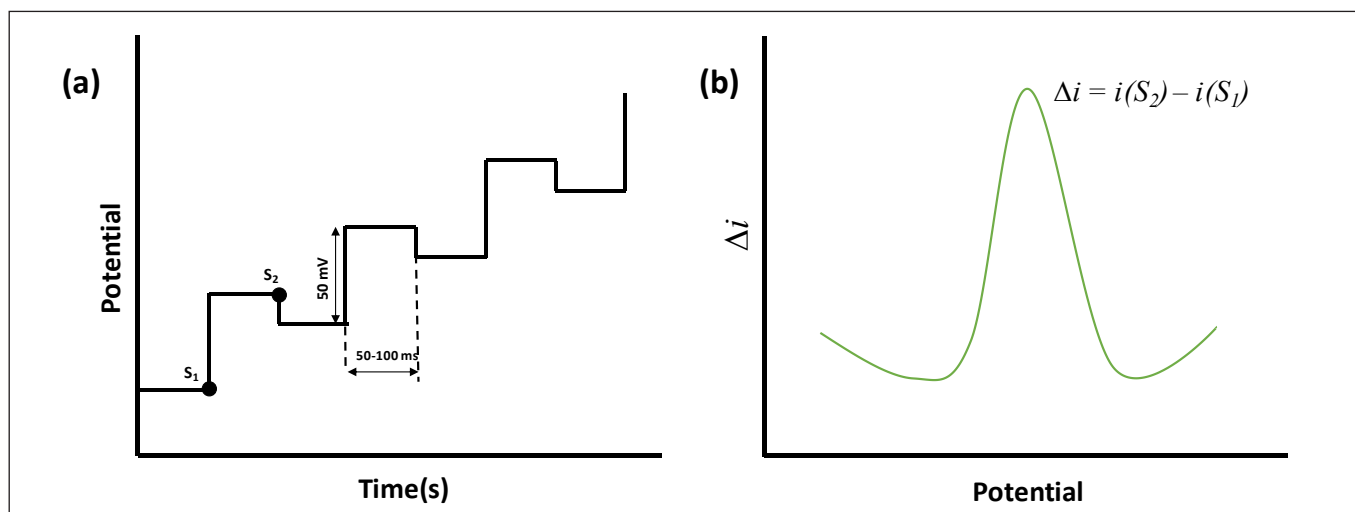


Fig. 4: (a) Diagram of the application of pulses in the differential pulse voltammetry (DPV) technique (b) Typical response of a differential pulse voltammogram

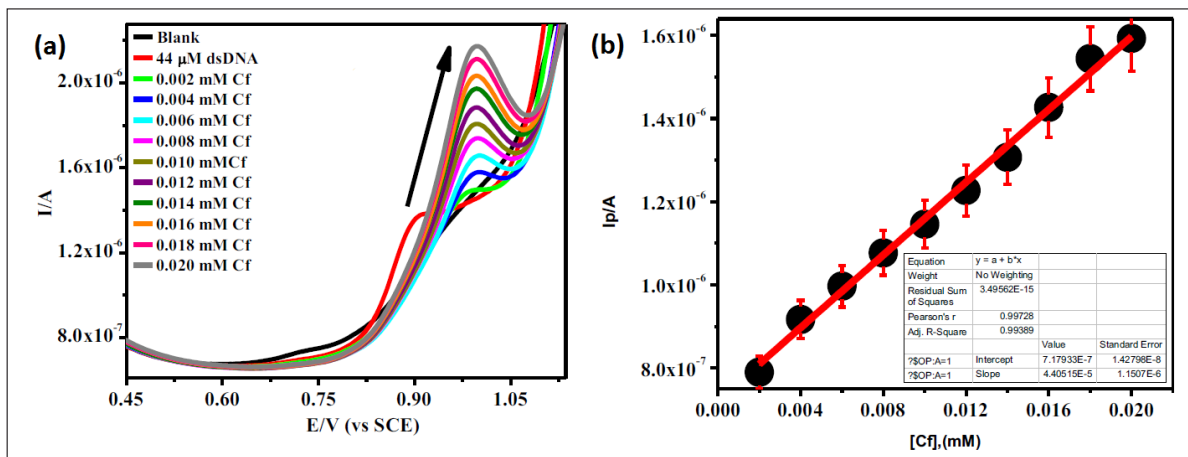


Fig. 5: (a) DPV plot of variable concentration of Cf in the presence of 44 µM dsDNA (b) Corresponding peak current vs. concentration of Cf.[17]

which causes an enhancement of the faradaic current and decrease in the non-faradaic charging current. DPV is used for quantitative chemical analysis and to study chemical reactions' mechanism, kinetics of electron transfer process and for the investigations of thermodynamics. For instance, DPV was developed to study the interaction of ciprofloxacin with dsDNA[17]. The experimental results show increase in oxidation current in the presence of dsDNA which indicates the ciprofloxacin molecule interacts with dsDNA.

Sahoo et al.[18] demonstrated the use of gold NPs and rGO composite modified carbon paste electrode for the ultra-trace detection of Arsenic (III) and DPV was used for analytical measurements. The authors obtained linear dynamic range in the concentration range of 1mgL⁻¹ to 20 mgL⁻¹ and the limit of detection(LOD) in the standard solution was found to be 0.13 mgL⁻¹.

2.3 Electrochemical Impedance Spectroscopy

Electrochemical impedance spectroscopy (EIS) is an important electrochemical technique based on the analysis of electrochemical processes occur at electrode/ electrolyte interface. This technique determines the frequency dependent resistance called impedance by applying sinusoidal potential excitation and measure the current through the cell. Electrochemical impedance is normally measured using small excitation signal as to obtain pseudolinear response of cell. The current response to a sinusoidal potential excitation will be sinusoidal at the same frequency but shifted in phase for a linear or pseudo-linear system.

The impedance is represented as a complex number:

$$Z_{\omega} = \frac{E}{I} = \frac{E_0 e^{j\omega t}}{I_0 e^{j(\omega t + \phi)}} = Z_0 e^{j\phi} = Z_0 (\cos\phi + j\sin\phi)$$

Where $Z_0 \cos\phi$ is real impedance and $Z_0 j\sin\phi$ is imaginary impedance. Impedance measurement produces numerical results, usually as real Z' and imaginary Z'' or modulus $|Z|$ & phase angle ϕ as a function of frequency. Graphical inspection of the obtained results makes it possible to identify electrical equivalent circuits. There are two fundamental types of graphical representation are done using impedance data:

Complex Plane plots If the negative of the imaginary part of Z_{ω} is plotted versus the real part, we get a "Nyquist Plot" which is also called as the Argand diagram, the typical nature of Nyquist plots is shown in Fig.6a.

Bode Plots

The impedance is plotted with log frequency on the X-axis and both the absolute values of the impedance ($|Z|$) and the phase-shift on the Y-axis.

Electrochemical Impedance spectroscopy provides valuable information on study of films deposited on electrodes as it can distinguish the different conductivity processes i.e. resistance of the electrolyte between a working and reference electrode, interfacial charge transfer resistance on WE due to adsorbed species, charge transfer resistance due to Faradaic processes, diffusion processes and adsorption of the reactant/product on the interface. This technique provides mechanistic and kinetic information about surfaces and for the characterization of various coatings, corrosion processes, semiconducting electrodes and nanomaterials. For instance, Yoon et al.[19] demonstrated the electrochemical characterization of graphene oxide (GO) solution using EIS and showed that the highly resistive GO became very conductive in the deionized water. EIS is also prove to be important technique in characterisation of sensors. A non-

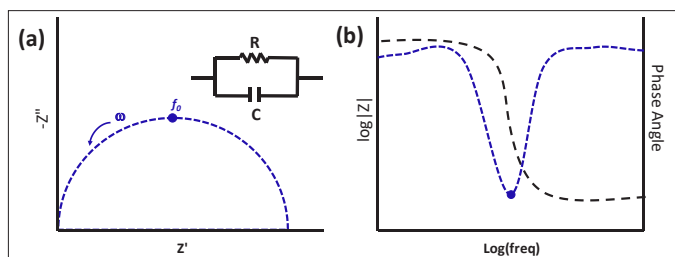


Fig. 6: (a) Nyquist Plot for parallel RC circuit (b) Bode Plot for Parallel RC circuit

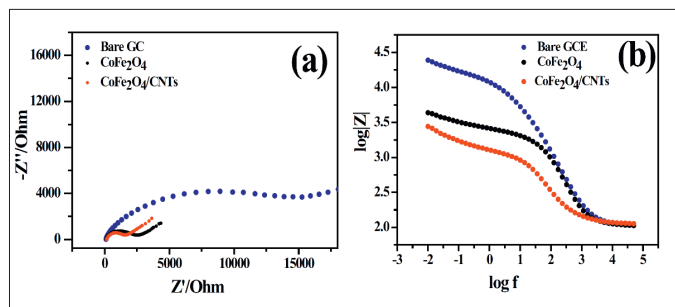


Fig. 7: (a) Nyquist plot of different modified electrodes in 1mM $K_4[Fe(CN)_6]$ solution (b) corresponding Bode plot is shown[20]

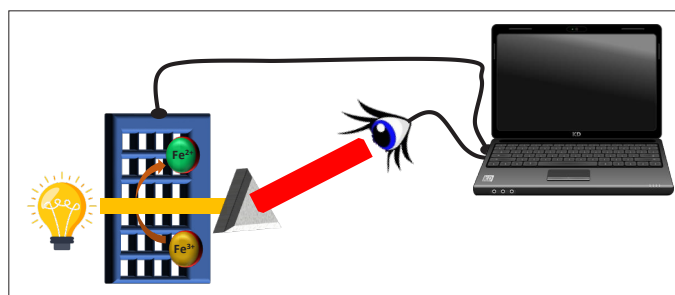


Fig. 8: Schematics for Spectroelectrochemistry

enzymatic hydrogen peroxide sensor was developed by Sahoo et al.[20] and characterized using EIS shown in Fig. 7. The author reported the decrease in the charge transfer resistance of $CoFe_2O_4/CNTs$ nanocomposite indicated facilitated electron transfer process and material could be suitable for the non-enzymatic sensing of H_2O_2 .

2.4 Spectroelectrochemistry

Spectroelectrochemistry (SEC) refers to the branch of analytical techniques that combines electrochemistry which allows us to correlate the electrical current produced during an electrochemical reaction with the concentration of a substance, and simultaneously record the spectral change in the matter. When these two techniques are combined, spectral measurements are made on molecules resulting from oxidation or reduction of the analyte at the electrode. Thus, it records both signals arising from electrochemical and spectrochemical changes

simultaneously. Undergoing electrochemical reaction characterized spectroscopically allowed us to establish relationship between reaction mechanisms and their structures. The structural information unavailable from the electrochemical response is complemented by optical monitoring.

Blanco et al. [21] uses spectroelectrochemistry for monitoring the electrosynthesis of silver nanoparticle modified electrodes. In this study, spectroelectrochemistry provide the information about electrosynthesis process as well as the type of nanoparticle deposited on the electrode surface. Technique also yield useful information to understand the voltammetric signal obtained during the H_2O_2 reduction on silver modified electrodes. Spectroelectrochemistry is also useful technique to study the interaction of drug with biomolecules. For instance, Ipte et al.[17] investigated the interaction of Ciprofloxacin with dsDNA using spectroelectrochemical measurement. The author reported decrease in absorbance in the spectroelectrochemical study due to oxidation of Cf in Cf-dsDNA complex while no significant change in the absorption spectra is observed without Cf, thus indicating the interaction between the Cf and dsDNA.

3. Application of Nanomaterials as Sensors

3.1 Composite metal oxides

Various molecules originate from specific cells of human body which acts as indicator of physiological balance of living cells. High H_2O_2 level is indicative of higher level of free radical in the cells while molecules like dopamine acts as neurotransmitter. Electrochemistry provides rapid, low cost, simple and selective detection of these molecules if proper catalyst is chosen. Cobalt ferrite ($CoFe_2O_4$), which is an inverse spinel compound, has peroxidase mimetic properties. In spite of low cost, reasonably good electrical conductivity, low toxicity, good biocompatibility, high adsorption ability and easy preparation, it becomes inapt for sensing due to agglomeration problem. Carbon nanotubes (CNTs) are known to improve electrochemical response by improving electrical conductivity and reducing overpotential for redox reactions. $CoFe_2O_4/CNTs$ [20] nanocomposite was synthesized through a facile one-pot hydrothermal method. Working electrode was prepared by modifying glassy carbon electrode (GCE) with nanocomposite ink. Materials has been characterized by conventional techniques like X-ray diffraction (XRD), Raman spectroscopy, XPS, SEM etc. Physical characterizations show successful synthesis of nanocomposite material where spherical $CoFe_2O_4$ nanoparticle of size 7-30nm are uniformly distributed over the surface of CNTs as seen in Fig.9.

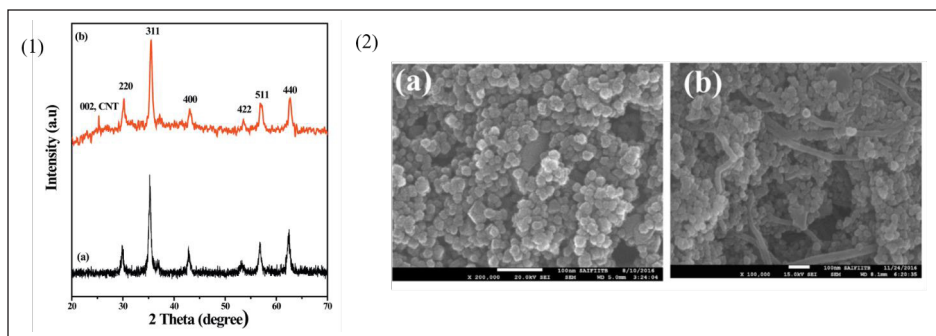


Fig. 9: (1) XRD pattern of (a) CoFe_2O_4 and (b) $\text{CoFe}_2\text{O}_4/\text{CNTs}$ nanocomposites. (2) SEM image of (a) bare CoFe_2O_4 and (b) $\text{CoFe}_2\text{O}_4/\text{CNTs}$ [20]

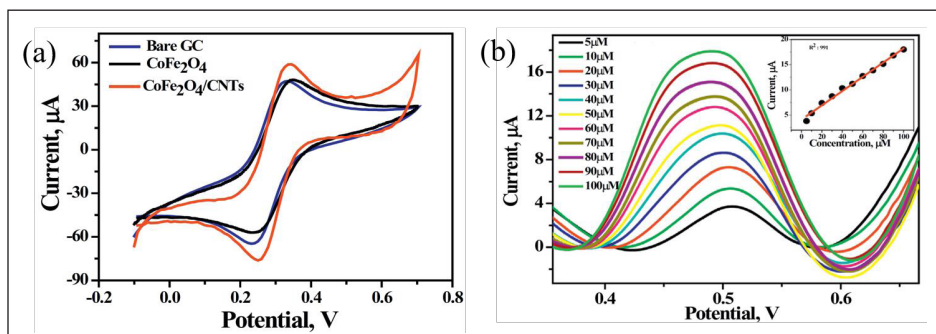


Fig. 10: (a) CV plot of different modified electrodes in 1 mM $\text{K}_4[\text{Fe}(\text{CN})_6]$ solution using different electrodes. (b) Square wave voltammetry plot of H_2O_2 with successive addition of H_2O_2 in 0.1M phosphate buffer medium at pH 7. Applied potential and accumulation time was kept as 0.3 V and 30 s respectively. (Inset: shows the linear calibration plot) [20]

The composite has also been characterized using electrochemical methods like CV and EIS before being tested for sensing ability for H_2O_2 . In CV measurements, potassium ferrocyanide ($\text{K}_4[\text{Fe}(\text{CN})_6]$) was used as standard redox probe to investigate electron transfer properties. Sharper increase in current compared to bare GCE or CoFe_2O_4 itself is indicative of enhanced charge transfer property. Cause of this enhanced current density was investigated using EIS and it was found from the Nyquist plot that charge transfer resistance of $\text{CoFe}_2\text{O}_4/\text{CNTs}$ nanocomposite is lower compared to the CoFe_2O_4 owing to better conductivity of CNTs. The nanocomposite was applied successfully for quantitative detection of H_2O_2 using anodic stripping voltammetry technique. The corresponding results are shown in Fig. 10.

Optimum pH for the voltammetry study was found to be pH 7. Stripping voltammetry generally involves preconcentration or accumulation step. Response was found to be best for accumulation potential 0.3V, while there was no significant increase in current after 100s of accumulation due to saturation effect of the surface. Analyte accumulation at 0.3V for 30s generated good analytical signal. Highly sensitive detection is possible with the modified $\text{CoFe}_2\text{O}_4/\text{CNTs}/\text{GCE}$, with sensitivity of $1.41 \times$

$10^{-7} \text{ A}/\mu\text{M}$ and the detection limit of $0.02 \mu\text{M}$ (S/N=3) and linear dynamic range of 5–100 μM . Selectivity is reflected from interference free detection even in the presence of common biological molecules such as urea, cysteine, glucose, dopamine, uric acid and ascorbic acid

Similar kind of material has been used by the same group for sensing of NO_2^- , which is a major soil and water pollutant. Manganese ferrite (MnFe_2O_4) grown on reduced graphene oxide was combined with polyaniline to increase to conductivity by taking the advantage of pi-pi interaction between rGO and PANI. Also, preconcentration of nitrate ions is possible owing to favorable surface charge of PANI. MnFe_2O_4 was synthesized by solvent less thermolysis technique using oleic acid as stabilizer and long chain oleyl amine as reducing agent, while chemical oxidative polymerization was adapted for synthesis of PANI.

The schematic representation of the synthesis process is shown in Fig.11.

CV and EIS was carried out to characterize the composites electrochemically. Higher current and sharper peak indicates better electron transfer property. Effective working surface area obtained from Randle Sevcik's plot for composite is 8.14 cm^2 and bare GCE is 0.07 cm^2 . Charge transfer resistance obtained from Nyquist plot indicates better electron transfer in case of composite. Hence, higher current is synergistic effect of both high surface area as well as better electron transfer due to elevated conductivity. DPV was used as analytical method. The nanocomposite detects NO_2^- by oxidizing it to NO_3^- . Under applied positive potential Mn(II) oxidizes to Mn(III) and due to directed electric field hole generated in valence band of MnFe_2O_4 migrates to PANI and it finally oxidizes nitrite to nitrate and Mn(III) returns back to Mn(II). This facilitated oxidation can also be inferred from standard rate constant obtained from Laviron equation by analyzing CV data at various scan rate.

Where, E_p is the peak potential, E^0 is the formal potential, R is the universal gas constant ($8.314 \text{ J/mol} \cdot \text{K}$), T is the absolute temperature, a is the electron transfer coefficient, n is electron transfer number, F is Faraday's

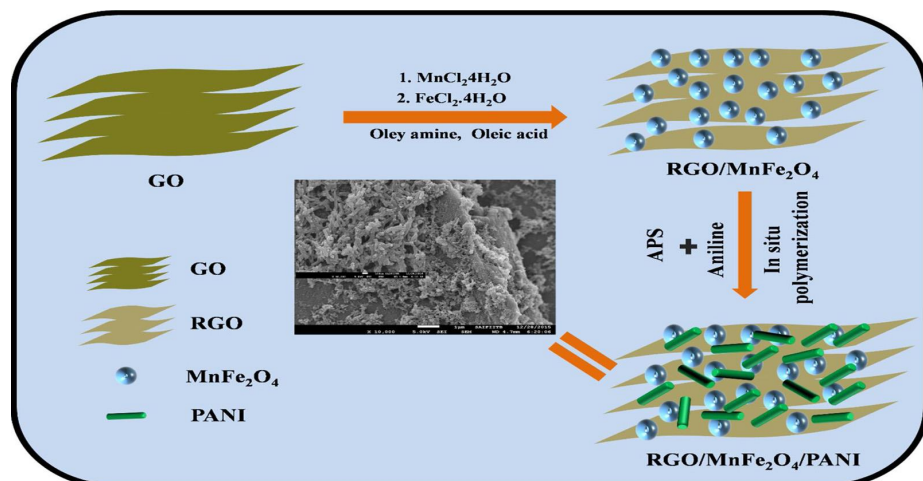


Fig. 11: The synthesis procedure adopted to synthesize the nano composite material[22].

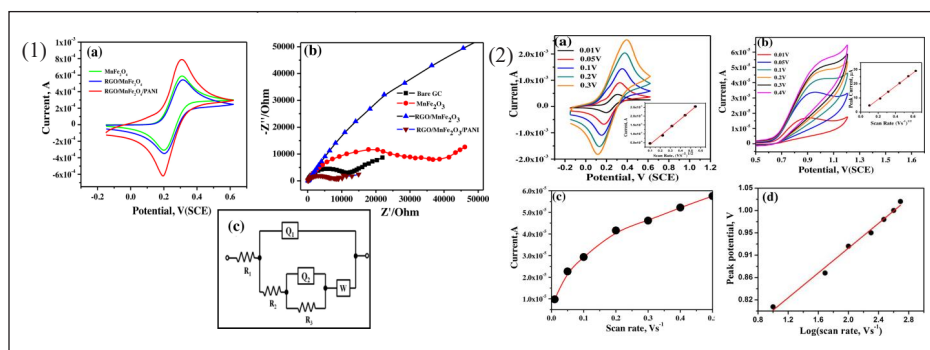


Fig. 12:(1) (a) Cyclic Voltammetric plot of Ferrocyanide using electrodes modified with different modifier in 0.1M phosphate buffer of pH 7 (b) Nyquist plot recorded at the excitation potential of 0.3 V using electrodes modified with different modifier in 0.1M phosphate buffer of pH 7 (c) Equivalent circuit used for the fitting of the Impedance plot[22] (2) (a) CV of Ferrocyanide at different scan rates on Inset: Corresponding peak current vs. square root of scan rate plot (b) CV of Nitrite ions at various scan rates Inset: Corresponding peak current vs. square root of scan rate plot (c) Peak current vs. Scan rate plot from the CV measurements of plot (B), (d) Peak current vs. log of scan rate plot from the CV measurements of plot (B); experiments are carried out in 0.1M phosphate buffer of pH 7[22]

constant 96485 Cmol^{-1} , k_s is standard rate constant of the reaction, v is scan rate (V/s). The (an) value is obtained using the correlation. E^0 of NO_2^- is obtained from the intercept of the correlation between peak potential with respect to the scan rate of the measurements (plot is not shown). The value of E^0 obtained in this way is 0.81 V. From the slope and intercept of the plot in Fig. 12, the (an) and the k_s values are obtained as 0.22 and 14.2 s^{-1} respectively. The electron transfer rate constant obtained using the Laviron analysis procedure is reasonably fast, indicating enhanced electron transfer process on the ternary composite modified electrode surface due synergistic effect of both rGO and PANI. RGO/MnFe₂O₄/PANI fibrous nanocomposite modified GCE has a large linear dynamic range from 0.05 to 12000 μM with a limit of detection 0.015 μM ($S/N=3$).

3.2 Metal Nanocomposites

In addition to the metal oxide nanocomposites, metal nanoparticles with uniform distribution over conductive reduced graphene oxide sheets can also be used for sensitive detection up to as low as ppb level. Bismuth nanoparticles anchored onto reduced graphene oxide (rGO) has been applied for developing analytical method for the ultrasensitive detection of Cd^{2+} , Pb^{2+} , Zn^{2+} and Cu^{2+} using stripping voltammetry technique. Due to appearance of the peaks at different potentials it is possible to detect all these metal ions simultaneously, but for enhanced sensitivity they may also be detected individually, especially Zn^{2+} ion. The detection limits obtained were 2.8, 0.55, 17, 26 $\mu\text{g/L}$ respectively for Cd^{2+} , Pb^{2+} , Zn^{2+} and Cu^{2+} .

In a similar fashion gold nanoparticle grown hydrothermally onto rGO surface has been applied for the successful detection of Hg metal, which is very toxic. Simple Gold electrode is not suitable for use due to formation of amalgamation with Hg. Hence, the analytical method developed relies on use of carbon paste electrode which offers renewability of the electrode surface. Hg is preconcentrated by cathodic bias and it is analysed by oxidation i.e. anodic stripping. Preconcentration enhances the sensitivity allowing the method to detect in ppb level. Limit of detection obtained was 0.25 $\mu\text{g/L}$ [23].

3.3 Carbon Nanospheres

Dopamine (DA) and uric acid (UA) are important biological molecules and simultaneous detection of the duo is impossible over GCE due to overlapping peak potentials. Functionalized carbon nanosphere synthesized by chemically functionalizing Vulcan carbon provides a way out due to peak potential shift, thereby separation of peaks becomes possible over modified electrode. Linear dynamic range of DA and UA were obtained as $4.93 \times 10^{-8} \text{ M}$ to $3.98 \times 10^{-6} \text{ M}$ and $5 \times 10^{-7} \text{ M}$ to $9 \times 10^{-6} \text{ M}$ respectively. The detection limits in the case of DA and

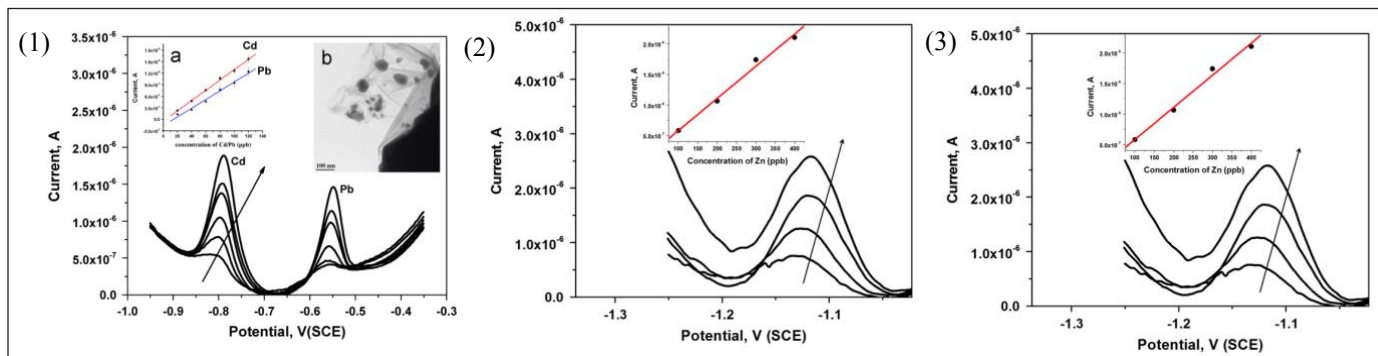


Fig. 13: (1)DPV of Cd^{2+} and Pb^{2+} in 0.1 M acetate buffer at pH 5.5 as the supporting electrolyte medium using RGO/Bi composite modified carbon paste electrode. Inset (a) shows corresponding calibration plot with linear correlation and inset (b) is the TEM image of RGO/Bi nanocomposite (2) DPV of Zn^{2+} in 0.1 M acetate buffer at pH 6.5 as the supporting electrolyte medium using RGO/Bi composite modified carbon paste electrode. Inset (a) shows corresponding calibration plot with linear correlation (3) Differential pulse anodic stripping voltammetry of Cu^{2+} in 0.1 M acetate buffer at pH 5.5 as the supporting electrolyte medium using RGO/Bi composite modified carbon paste electrode. Inset (a) shows corresponding calibration plot with linear correlation[23].

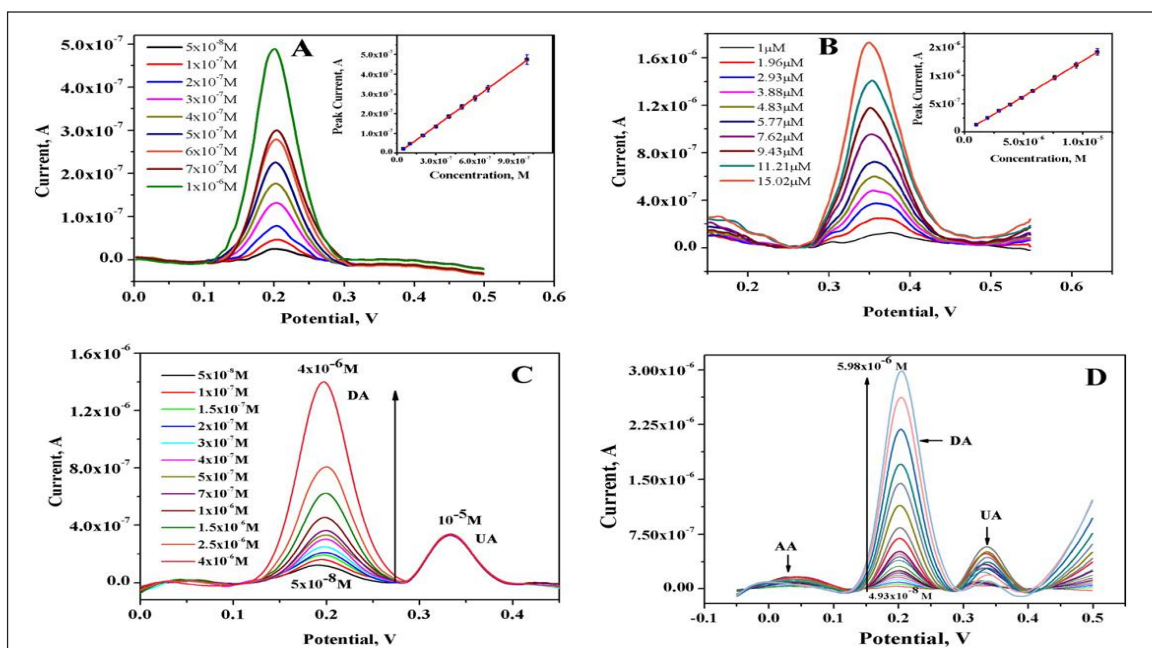


Fig. 14(A) Voltammogram of DA at different concentration Inset: corresponding calibration plot of peak current vs. concentration (B) Voltammogram of UA at different concentration Inset: corresponding calibration plot of peak current vs. concentration (C) Voltammogram of DA at different concentration with fixed concentration of UA (D) Voltammogram of DA, UA and AA at varying concentration. AA was varied at 100 times higher and UA was varied at 10 times higher in concentration than DA. Experiments were carried out at pH7 (PBS) accumulations at, 0 V for 600 s.[24]

UA were obtained as 10 nM and 42 nM respectively[24]. Hence, method developed is very sensitive.

Carbon nanospheres (CNSs) with a completely different synthesis route has been utilized for sensing of antibacterial drug ciprofloxacin (Cf) by the same group. CNSs of uniform size were synthesized by electrochemical route from high purity graphite rods and applying cyclic voltammetry technique. Cf was detected using DPV through monitoring oxidation current of Cf and detection limit was found to be 0.15 μM [25]

4. Conclusion

Application of electrochemical methods for characterization of nanomaterials and inherent challenges has been discussed in the article. Application of various techniques for sensing application using different types of nanomaterial has been discussed using some of the related examples emphasising on the properties of the nanomaterials such as active surface area, electron transfer rate, charge transfer resistance etc. revealed by the respective techniques applied. The electrochemical

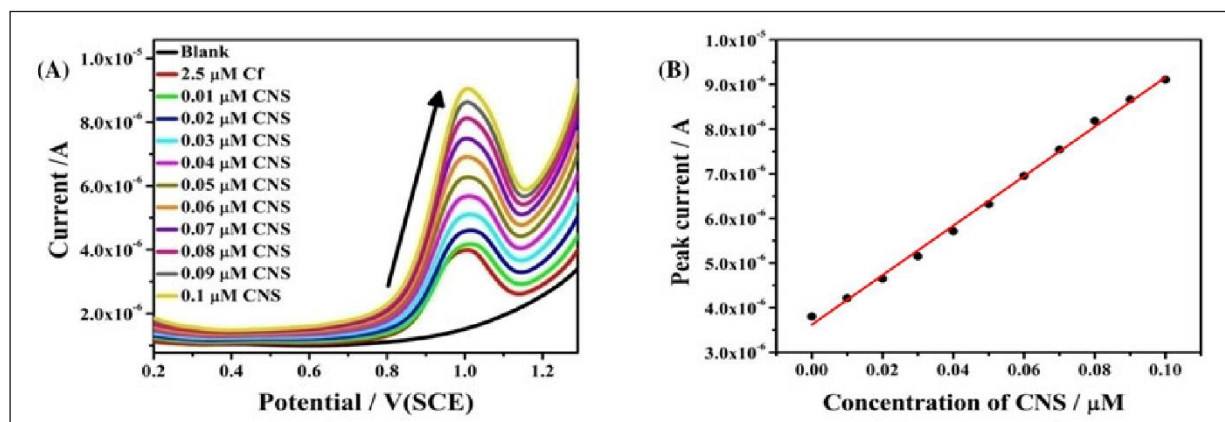





Fig. 15:(A) DPV plot showing interaction of 2.51M Cf with varied concentrations of CNSs at pH 7 every time fresh experiments are carried out (B) Corresponding peak current vs concentrations of CNSs[25]

quantities have been linked to inherent characteristics of the materials such as conductivity, higher surface to volume ratio, stability etc. Thus, electrochemistry provides useful, relevant information about the nanomaterials making it crucial, critical and indispensable tool for the evaluation of nano composite materials and their use in energy and sensing application. It may also be emphasised that there is not a single best electrochemical technique for characterization due to limitations related to instrumentation. There are bunch of electrochemical techniques available for all round understanding of the underlying processes associated with the chemical system under application for energy harvesting/storage, sensor, biological applications and so on.

5. References

- H. Xu, H. Zhang, Y. Ma, M. Jiang, Y. Zhang, Y. Wu, H. Zhang, R. Xia, Q. Niu, X.a. Li, Morphology control of organic halide perovskites by adding BiFeO₃ nanostructures for efficient solar cell, *Scientific Reports* 9(1) (2019) 1-8.
- M.-J. Lee, S. Lee, P. Oh, Y. Kim, J. Cho, High performance LiMn₂O₄ cathode materials grown with epitaxial layered nanostructure for Li-ion batteries, *Nano letters* 14(2) (2014) 993-999.
- S. Choi, A. Manthiram, Synthesis and electrochemical properties of spinel LiCo₂O₄ cathodes, *Materials for Electrochemical Energy Conversion and Storage* 127 (2006) 215-224.
- E. Cha, M.D. Patel, J. Park, J. Hwang, V. Prasad, K. Cho, W. Choi, Publisher Correction: 2D MoS₂ as an efficient protective layer for lithium metal anodes in high-performance Li-S batteries, *Nature Nanotechnology* 13(6) (2018) 521-521.
- A.K. Geim, K.S. Novoselov, The rise of graphene, *Nature Materials* 6(3) (2007) 183-191.
- T. Zhai, X. Lu, F. Wang, H. Xia, Y. Tong, MnO₂ nanomaterials for flexible supercapacitors: performance enhancement via intrinsic and extrinsic modification, *Nanoscale Horizons* 1(2) (2016) 109-124.
- D.R. Baer, J.E. Amonette, M.H. Engelhard, D.J. Gaspar, A.S. Karakoti, S. Kuchibhatla, P. Nachimuthu, J. Nurmi, Y. Qiang, V. Sarathy, Characterization challenges for nanomaterials, *Surface and Interface Analysis: An International Journal devoted to the development and application of techniques for the analysis of surfaces, interfaces and thin films* 40(3-4) (2008) 529-537.
- D.R. Baer, M.H. Engelhard, G.E. Johnson, J. Laskin, J. Lai, K. Mueller, P. Munusamy, S. Thevuthasan, H. Wang, N. Washton, Surface characterization of nanomaterials and nanoparticles: Important needs and challenging opportunities, *Journal of Vacuum Science & Technology A: Vacuum, Surfaces, and Films* 31(5) (2013) 050820.
- S. Chauhan, S. Sahoo, A.K. Satpati, C. Sharma, P.K. Sahoo, Prussian Blue Nanocubes-SnO₂ Quantum Dots-Reduced Graphene Oxide Ternary Nanocomposite: An Efficient Non-noble-metal Electrocatalyst for Non-enzymatic Detection of H₂O₂, *Electroanalysis* 32(8) (2020) 1763-1771.
- P.T. Kissinger, W.R. Heineman, Cyclic voltammetry, *Journal of Chemical Education* 60(9) (1983) 702.
- A. Shafiee, M.M. Salleh, M. Yahaya, Determination of HOMO and LUMO of [6, 6]-phenyl C₆₁-butyric acid 3-ethylthiophene ester and poly (3-octyl-thiophene-2, 5-diyl) through voltammetry characterization, *Sains Malaysiana* 40(2) (2011) 173-176.
- H. Matsuda, Y. Ayabe, The theory of the cathode-ray polarography of Randles-Sevcik, *Zeitschrift fuer Elektrochemie and Angewandte Physikalische Chemie* 59 (1955) 494-503.
- R.S. Nicholson, I. Shain, Theory of Stationary Electrode Polarography. Single Scan and Cyclic Methods Applied to Reversible, Irreversible, and Kinetic Systems, *Analytical Chemistry* 36(4) (1964) 706-723.
- J. Heinze, Cyclovoltammetrie – die "Spektroskopie" des Elektrochemikers, *Angewandte Chemie* 96(11) (1984) 823-840.
- A. Testolin, S. Cattaneo, W. Wang, D. Wang, V. Pifferi, L. Prati, L. Falciola, A. Villa, Cyclic voltammetry characterization of Au, Pd, and AuPd nanoparticles supported on different carbon nanofibers, *Surfaces* 2(1) (2019) 205-215.
- H. Karami, M. Alipour, Synthesis of lead dioxide nanoparticles

- by the pulsed current electrochemical method, *Int. J. Electrochem. Sci* 4 (2009) 1511-1527.
17. P. Ipte, A. Sharma, H. Pal, A. Satpati, Probing the interaction of ciprofloxacin with dsDNA: Electrochemical, spectro-electrochemical and AFM investigation, *Journal of Electroanalytical Chemistry* 885 (2021) 115098.
 18. S. Sahoo, P.K. Sahoo, A.K. Satpati, Gold nano particle and reduced graphene oxide composite modified carbon paste electrode for the ultra trace detection of arsenic (III), *Electroanalysis* 29(5) (2017) 1400-1409.
 19. Y. Yoon, J. Jo, S. Kim, I.G. Lee, B.J. Cho, M. Shin, W.S. Hwang, Impedance spectroscopy analysis and equivalent circuit modeling of graphene oxide solutions, *Nanomaterials* 7(12) (2017) 446.
 20. S. Sahoo, P. Sahoo, S. Manna, A. Satpati, A novel low cost nonenzymatic hydrogen peroxide sensor based on CoFe₂O₄/CNTs nanocomposite modified electrode, *Journal of Electroanalytical Chemistry* 876 (2020) 114504.
 21. C. Fernández-Blanco, Á. Colina, A. Heras, UV/Vis spectroelectrochemistry as a tool for monitoring the fabrication of sensors based on silver nanoparticle modified electrodes, *Sensors* 13(5) (2013) 5700-5711.
 22. S. Sahoo, P. Sahoo, A. Sharma, A. Satpati, Interfacial polymerized RGO/MnFe₂O₄/polyaniline fibrous nanocomposite supported glassy carbon electrode for selective and ultrasensitive detection of nitrite, *Sensors and Actuators B: Chemical* 309 (2020) 127763.
 23. P. Sahoo, B. Panigrahy, S. Sahoo, A.K. Satpati, D. Li, D. Bahadur, In situ synthesis and properties of reduced graphene oxide/Bi nanocomposites: as an electroactive material for analysis of heavy metals, *Biosensors and Bioelectronics* 43 (2013) 293-296.
 24. M.K. Dey, A.K. Satpati, Functionalised carbon nano spheres modified electrode for simultaneous determination of dopamine and uric acid, *Journal of Electroanalytical Chemistry* 787 (2017) 95-102.

	<p>Ms. Sudipa Manna is currently working as Scientific Officer at Analytical Chemistry Division, BARC. She completed M.Sc. in Chemistry from Visva-Bharati University, West Bengal. Her research interest includes synthesis of nanomaterials and their application for electrochemical sensing of various drugs and biomolecules and electrochemical and photoelectrochemical catalysis.</p>
	<p>Mr. Abhishek Sharma is Senior Research Fellow at Analytical Chemistry Division, BARC. He obtained M.Sc. in Chemistry from Kurukshetra University, Haryana. His research interests are synthesis of catalysts from earth abundant materials for electrochemical and photoelectrochemical water splitting and study of drug-biomolecule interaction using various electrochemical techniques.</p>
	<p>Dr. A. K. Satpati is presently working as Scientific Officer-G and Head, Electrochemical Methods Section, Analytical Chemistry Division, Bhabha Atomic Research Centre, Mumbai. His research interest includes electrochemical investigation of thin films, biomolecules and semiconductor interfaces, fabrication of ultramicro electrodes for scanning electrochemical microscopy (SECM). He has been working on the development of composite materials for efficient supercapacitors and electrochemical investigation of materials for supercapacitors. He has investigated electron Transfer (ET) reactions in homogeneous and micro-heterogeneous media using photochemical techniques. Dr. Satpati has developed composite cathode and anode catalysts for the electrochemical and photoelectrochemical (PEC) generation of hydrogen from water, investigated the electrochemical interfacial processes during PEC splitting of water using SECM. He has significant contribution on development of analytical methods using voltammetry and developed many electro analytical methods and used them for the determination of metal ions at trace and ultra-trace levels. Developed modified electrode based on carbon paste and carbon nano-tube, thio-compound and DNA modified electrodes for sensing and interaction studies. He is teaching electrochemistry and analytical chemistry in the post graduate level since 2004. Dr. A.K. Satpati is recipient of the following awards and recognition; "Young Scientist Award-2008" from Department of Atomic Energy, Government of India, Fulbright fellowship to carry out research work in University of Texas Austin, USA during 2011 to 2012, Young associate of Maharashtra Academy of Sciences 2015, Member of National Academy of Sciences India (NASI) in 2018, Fellow of the Maharashtra Academy of Sciences 2020.</p>

Quantum Cutting Nanomaterials via Ionic Liquids

Pushpal Ghosh*

School of Chemical Sciences and Technology, Department of Chemistry, Dr. Hari Singh Gour University (A Central University), Sagar-470003, M.P. India,

Email Id: pushpalghosh27@gmail.com; pghosh@dhsu.edu.in

Abstract

Energy-saving and environmentally benign lighting (devoid of Hg) is the need of the hour. Similarly, increasing efficiency of conventional solar cells has drawn a tremendous interest in both the scientific community as well as in society. Interestingly for both lighting and solar cells, quantum cutting (down converted) nanomaterials can play a significant role. Currently green synthesis for important materials specially by using Ionic Liquids (ILs) have generated a huge interest. The unique properties of ILs like tunability, negligible vapour pressure, non-flammability etc; enable ILs to be called as "green" and "designer" solvents. This perspective highlights about the recent advancements in the ionic liquid assisted synthesis of quantum cutting (QC) nanomaterials and their subsequent applications in environmentally benign and energy efficient lighting, solar cells, plasma display panel etc. Finally, various useful properties of ILs like their use as solvent, templating agent and reaction partner ("three in one") in quantum cutting nanomaterials synthesis are demonstrated.

Keywords: Nanophosphors, Quantum Cutting, Ionic liquid, Rare-earth, Photonic

Introduction

Creation of sufficient "clean" energy is very important, both for energy perspective as well as for environment. Approximately one-fifth of the earth's energy is utilised for lighting purposes and yesteryear's incandescent lamps are replaced by light emitting diodes (LEDs), and compact fluorescent Lamps (CFLs), etc. as they need lesser energy compared to the incandescent lamps. But, in CFLs also, mercury is used as a sensitizer and that is not environmentally benign and highly toxic. Thereby, it is the need of the hour to develop environmentally benign, highly energy efficient and specially Hg-free sensitizing nanomaterials.¹⁻¹¹

As the population explosion is continuing through last decade, consumption of conventional energy resources gradually increasing; resulting the release of greenhouse gases like CO₂ and others, which cause hazardous effect on the flora and fauna. Therefore, un-conventional source of energy like wind, geo-thermal, hydro and solar energies draw a huge attention. Amongst these, solar energy is most promising and India is very blessed with Sun as it receives a significant time of sunlight throughout the day, in any season. Recently, devices as a 'spectral converter' are substantially used for absorbing the solar energy and then convert it into electrical energy. Normally a solar cell device should absorb over a wider range of wavelength: from

near infrared to visible wavelength (~950 nm to 350 nm) for the effective transformation of the incident light to charges. Then the charges are accumulated at a high voltage with necessary current for the desired work.¹² So rightly, solar energy harvesting and to convert it into electrical energy by using solar cell device have drawn tremendous attention.¹³⁻¹⁴

From these point of view, quantum cutting down-converting (QC) nanomaterials with doping of rare-earth ion (Gd³⁺, Eu³⁺/Tb³⁺) maybe a potential replacement of Hg-free light emitting sources as well as spectral converter for increasing solar cell efficiency.⁵⁻¹¹ These QC nanomaterials are non-toxic and can increase the efficiency of energy by transforming a single photon of high energy into two visible photons with lower energy via a down-conversion photophysical process. Thereby, theoretical prediction indicates that nearly 200% (maximum) quantum cutting efficiency (QCE) of nanomaterials can be achieved.¹² A high QCE of 194% in BaF₂:Gd³⁺/Eu³⁺ have been found some time back.⁸ QCE of 187% (NaGdF₄:Eu³⁺ nanorods) and 154% (NaGdF₄:Eu³⁺ nanocrystals) have been obtained by Ghosh et al.^{1,10-11} For GdF₃:Eu³⁺ nanoparticles, 145% quantum cutting efficiency is observed.⁴

On the other hand, for designing materials at nanoscale, room temperature ionic liquids (RTILs) mediated synthesis protocols have drawn a huge attention due to their safer environmental aspects.^{1,4-6,10-11} RTILs usually have some interesting physical and chemical properties such as very low vapour pressure, non-flammable in nature, wide

electrochemical window (in some cases it can be spanned up to 6V), large liquidus range and having tunable band gap under ambient conditions. By judicious tuning of side alkylchains attached to the ring, proper choice of cation/anion combination and ionic liquid concentration etc., physicochemical properties of IL can be effectively tuned.⁶ Thus, ILs can be termed as 'green and designer' solvents.⁶ It is also observed that ionic liquids can be used as a solvent, templating agent and often as a reaction partner too.^{4,6} For designing nanomaterials, recently 'green' synthesis draws tremendous attention, especially for the less energy consuming and environmentally benign lighting purposes.

In this perspective, very basic of quantum cutting nanomaterials and how they can be synthesized using ionic liquid based 'green' synthesis are discussed. In addition, the potential application of quantum cutting materials in energy efficient and environmentally lighting, increasing efficiency of solar cells etc. are highlighted.

Fundamentals of quantum cutting nanomaterials

Normally, RE³⁺ ions exhibit a general electronic configuration [Xe] 4fⁿ. This generates a high number of (excited) electronic states. It is interesting to note that filled 5s² 5p⁶ sub-shells shield the 4f orbitals effectively and as a result, the electronic level's energy are not significantly affected by the chemical surroundings in which the rare-earth ions are located. This phenomenon results in observation of sharp inner-shell *f-f* transitions from specific energy levels.¹ The origin of photoluminescence property in RE³⁺ ion is predominated by intraconfigurational *f-f* electronic transitions and their number of allowed excited states could be determined by the equation $14!/(14-n)!n!$, (number of electrons situated in the *f*-orbitals in III oxidation state is designated as *n*).^{1,6} By judicious choice of a combination of trivalent RE³⁺ ions, various photophysical processes such as normal direct excitation, charge and energy transfer, upconversion and quantum cutting (downconversion) can be observed.^{1,6} Quantum cutting downconversion may be visualized as the reverse of a photophysical affair generally known as upconversion.

This is basically concerned to the conversion of single photon of higher energy to lower energy photons (more than one) by quantum cutting materials. Here, sensitizer normally has one or more metastable state as shown in **Figure 1**.⁶ During this photophysical process, sensitizer absorbs the high energy ultraviolet photon and is getting excited. Then, two conditions may arise. Firstly, as the excited electron comes back to metastable state, energy is released and that is transferred to the upper excited state of the activator via an energy transfer operation. After that,

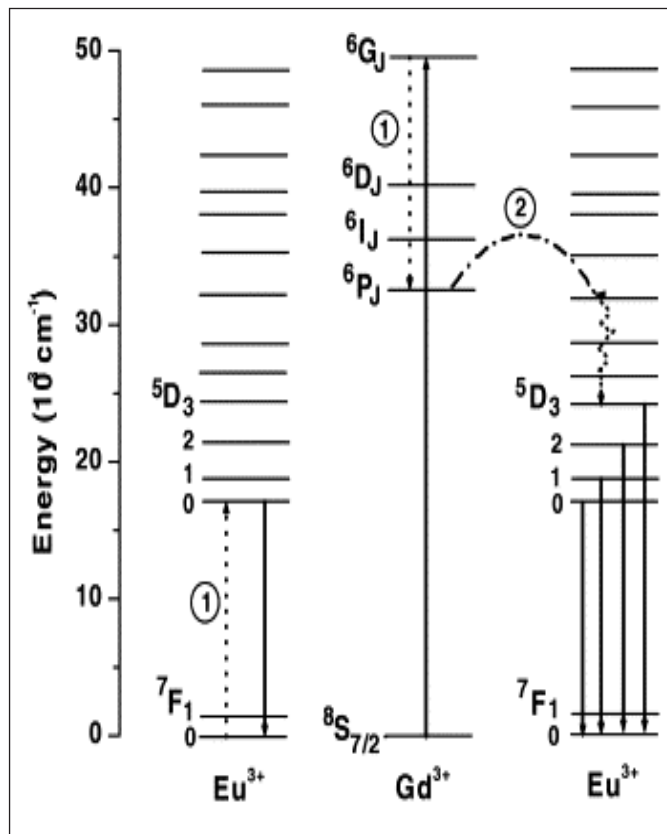


Figure 1: Energy level diagram of Gd³⁺-Eu³⁺ system depicting transitions and energy transfers.¹⁰

through a non-radiative process, electron may descend to the lower excited state of the activator followed by its relaxation to the ground state. This relaxation affair occurs through a radiative emission with one lower energy photon (**Figure 1**).¹⁰⁻¹¹

Another possibility comes, when liberated energy is immediately taken up by another activator rare-earth ion and get excited to its upper energy level, followed by its relaxation to its ground state by emitting second lower energy photon. Finally by this process, two lower energy photons can be obtained after absorbing single photon with higher energy. This kind of photophysical process often occurs in binary and ternary fluorides nanocrystals doped with Eu³⁺ ions like GdF₃:Eu³⁺, NaGdF₄:Eu³⁺ or BaGdF₅:Eu³⁺ etc.. Here, Gd³⁺ ion is exploited as sensitizer and Eu³⁺ is as an activator ion.^{4,5} For instances, NaGdF₄:Eu³⁺ nanomaterials absorb ultraviolet (UV) light and visible light in the red region is emitted.¹⁰ However, green emitting quantum cutting is noticed, for Er³⁺ and Tb³⁺ doped NaGdF₄ materials.⁴

To determine the quantum cutting, (⁸S_{7/2}-⁶G_J) and (⁸S_{7/2}-⁶I_J) transitions are extremely necessary as per the following equation:^{7,9}

$$\frac{P_{CR}}{P_{CR} + P_{DT}} = \frac{R(^5D_0 / ^5D_{1,2,3})_{^6G_J} - R(^5D_0 / ^5D_{1,2,3})_{^6I_J}}{R(^5D_0 / ^5D_{1,2,3})_{^6I_J} + 1} \quad (1)$$

where the probabilities of direct energy transfer (from Gd^{3+} to Eu^{3+}) and cross-relaxation are mentioned by the term P_{DT} and P_{CR} respectively. $R(^5D_0 / ^5D_{1,2,3})$ is the ratio of the emission intensity of 5D_0 and $^5D_{1,2,3}$; 6G_J and 6I_J are the excitation states from which emission occurs. Downconversion happens when ratio of P_{CR} and $P_{CR} + P_{DT}$ is a positive integer. This indicates that the emission intensity of $R(^5D_0 / ^5D_{1,2,3})$ which generates after excitation into 6G_J level should be more than the emission intensity of $R(^5D_0 / ^5D_{1,2,3})$ that is happening after excitation into 6I_J level. Thereby, QCE is calculated using equation (1). Quantum cutting efficiency for the $NaGdF_4:Eu^{3+}$ ion was first calculated by the method developed by Wegh et al.⁹ First the intensity ratio of $^5D_0 / ^5D_{1,2,3}$ was determined both for the 6G_J and 6I_J levels excitation and these values are 16.67 and 8.44 respectively. Now from these intensity ratios, cross relaxation efficiency can be determined according to equation 1 and it is seen that the ratio $P_{CR} / (P_{CR} + P_{DT})$ is 0.87. This means that 8.7 of 10 Gd^{3+} ion in the 6G_J excited levels comes back through a two step energy transfer to Eu^{3+} and results in two visible photons. Whereas, 1.3 of 10 Gd^{3+} ions in the excited 6G_J states transfers all its energy to a high energy levels of Eu^{3+} ion and results the emission of one visible photon. Thereby, a visible QCE of 187% is obtained which is very close to the maximum possible limit of 200%.⁹

Fundamentals of ionic liquids in nanomaterials synthesis

Recently, ionic liquids (ILs) are used in several reactions alternative to organic solvents and surfactants to avoid harmful effects on *flora* and *fauna*. Basically, ionic liquids (ILs) are composed of discrete cation and anion and exist in liquid state at ambient conditions (Figure 2).^{5-6,15-17}

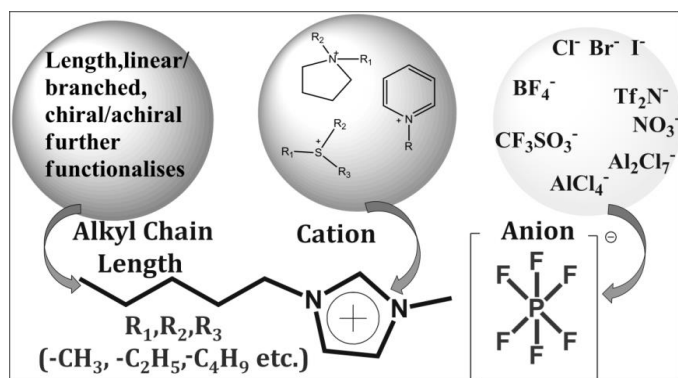


Figure 2. Schematic representation of tunable ILs using cation-anion combination and alkyl chain length.

Cation part mostly consists of the nitrogen containing heterocycles such as dialkylimidazolium, N-alkylpyridinium, phosphonium and alkylammonium etc.; amongst them dialkylimidazolium cation based ionic liquid are popular because imidazolium cation is stable in both *i.e.* oxidative and reductive condition, and show low viscosity. Also the synthesis procedure of imidazolium based ILs are comparatively easy.¹⁸⁻¹⁹ In addition, tunability of these ILs can be achieved as N-atom of imidazole can be attached to different alkyl chain length and anions can be replaced as required. For example, counter ions or anions may be halide for e.g. chloride, bromide, iodide etc., BF_4^- , PF_6^- for fabricating fluorides; and $[SeO_2(OCH_3)]^-$ as source of selenide (Se^{2-}) and phosphate based ILs $[H_2PO_4]^-$ for phosphate ion (PO_4^{3-}) respectively etc.²⁰⁻²⁸ The physical and chemical properties of ionic liquid show pivotal impact due to the flexibility of anions and symmetry of cation. In addition, other factors also influenced such as charge delocalized anions, bulky cation, high entropy and thermodynamically high thermal stability etc. which do not permit them to be crystallized in ambient condition.²⁹ Most of the ionic liquids are liquid in nature. Why ionic liquids are liquid? These are also explained on the basis of lattice and solvation energy.²⁹ H. Weingärtner and his group have estimated the Gibbs free energy ($\Delta_{fus}G^T$) of fusion of ionic liquids which is dependent on the lattice Gibbs energy ($\Delta_{latt}G^T$) and solvation Gibbs energies ($\Delta_{solv}G^T$). They have exploited the Born-Fajans-Haber cycles for the calculation. A negative value of $\Delta_{fus}G$ is obtained for ionic liquids, which is the main reason for ILs to exist in liquid state.^{6,29} Ionic liquids have numerous physical and chemical properties like high thermal stability, nonflammability in nature (normally), large liquidus range, wide electrochemical window (in some cases it can be spanned upto 6V), and negligible vapour pressure. These properties can be tuned by judicious combination of anion-cation, concentration of ionic liquid and on changing the alkyl chain length.^{11,15-17,29-33} Task specific ionic liquids are also used in the potential application of catalysis, energy application, batteries, reaction partner in materials synthesis at nanoscale etc.^{15-17,29-33} However, protic based ILs are used in fuel cell; zwitterionic ILs are used in IL based membrane and aprotic types ILs are applicable in supercapacitors and lithium ion batteries.³⁴

Preparative methods for quantum cutting nanomaterials using ionic liquids

There are various synthesis protocols for the rare earth-based nanomaterials. Recently, IL-assisted synthesis approaches draw a huge interest in the preparation of RE-based nanomaterials specially quantum cutting

nanomaterials. This protocol not only assist in the formation of targeted nanoparticles but also can tune the crystal phase, size and shape of the nanoparticle. In this perspective, we have discussed state of the art synthesis protocols, like ionic liquid assisted hydrothermal/solvothermal, microwave and sonochemical techniques etc.

Ionic Liquids (ILs)-Assisted Solvothermal/Hydrothermal Method

Currently, solvothermal/hydrothermal technique is a frequently used technique for the synthesis of materials at nanoscale with desired properties such as controlled size, crystal phase, morphology and so on.^{1,5-6,10} In a compact closed container when water is used as solvent and heated above its boiling point (at 100 °C), then it exerts tremendous amount of pressure in reaction container and the process is named as hydrothermal process. But, if other solvent besides water is utilized, then it is named as solvothermal process. In this synthesis technique, reaction mixture is put into the teflon lined container which is further wrapped with stainless steel jacket. After that, the container is placed at a particular temperature which results high pressure inside the reaction container that aids in accelerating the reaction and targeted materials are obtained. Ionic liquids are frequently used so far for the preparation of various lanthanide doped fluorides (both binary and ternary), phosphate, oxides nanomaterials etc. as ILs having high thermal and chemical stability.^{1,5-6}

An 1-Ethyl-3-methylimidazolium bromide [C_2mim] Br IL assisted solvothermal technique was exploited to synthesize a single phase, oxygen free, hexagonal doped $NaGdF_4:Eu^{3+}$ nanorods with a high visible quantum cutting efficiency (QCE) of 187%.¹⁰ Quantum efficiency decreases significantly (127%) in case of mixed phase containing cubic and hexagonal $NaGdF_4:Eu^{3+}$. Here, [C_2mim] cation plays an important role as templating agent, thus influencing

both the crystal phase and morphology. It is observed that the cation of IL controls the generation of hexagonal $NaGdF_4:Eu^{3+}$. Similarly, an increasing concentration of fluorides (Gd : F = 1 : 8) and higher reaction temperatures (200 °C) also stabilizes hexagonal phase formation. Very recently Chouryal et al. reported 1% Eu^{3+} -doped $BaGdF_5$ nanophosphors which are prepared using IL-assisted solvothermal/hydrothermal method. In addition, this group studied the temperature dependent quantum cutting and found 160% QCE in the presence of ionic liquid, however QCE is significantly decreased (123%) when no IL is used for the materials synthesis.⁵

(b) Microwave-assisted ionic liquid method:

Microwave assisted synthesis is one of the latest techniques to prepare nanoparticles. In the context of microwave science, ILs can play a significant role as it contains large ions with high polarizability and conductivity. Thereby, ILs are effective media for absorbing microwaves. This eventually generates high heating rates of the reaction mixture and results in a high formation rate of nuclei which facilitate completion of the reaction with very short span of time, even in the range from seconds to a few hours at maximum are expected. This provides ILs an additional advantage over other organic solvents for the preparation of nanomaterials.³⁵

IL assisted microwave synthesis protocol has also been used for synthesizing various Ln^{3+} -doped nanomaterials, even for quantum cutting nanomaterials. Lorbeer et al. developed a microwave assisted synthesis to develop $GdF_3:Eu^{3+}$ nanoparticles of nanoparticles with 145% quantum efficiency using [C_4mim]BF₄ IL as solvent and reaction partner.³⁶ The similar group have developed a microwave assisted route to quantum cutting $NaGdF_4:Ln$ nanoparticles producing two photons.⁴ Other binary and ternary quantum cutting nanofluorides are

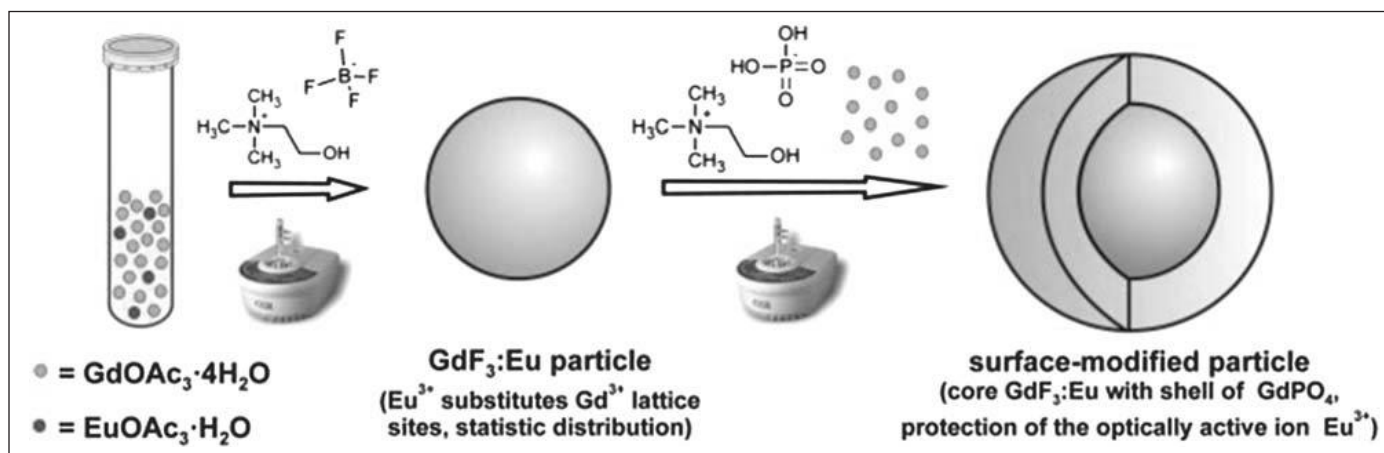


Figure 3. Scheme represents the microwave-assisted IL method for synthesis of $GdF_3:Eu^{3+}@GdPO_4$.⁴¹

also reported. For example, Lorbeer et al. synthesized various lanthanide doped binary and ternary fluorides by exploiting different types of ILs via microwave-assisted techniques.^{4,36,38-40}

Using the similar method, [Choline][BF₄] IL is used to prepare fluoride nanophosphors such as GdF₃:Eu³⁺. Then this nanoparticle GdF₃:Eu³⁺ is coated with GdPO₄ and for that [Choline][H₂PO₄] IL (Choline = 2-hydroxyethyl trimethylammonium) is used as a source of phosphate ion. As a result, oxygen free, core-shell GdF₃:Eu³⁺@GdPO₄ is formed.⁴¹ Microwave assisted synthesis is also exploited to prepare LaPO₄:Ce,Tb; LaPO₄:Eu nanophosphors by employing the tributylmethylammonium triflylimide ([MeBu₃N][SO₂CF₃)₂N] ionic liquid as a solvent.⁴²

(c) Other methods: Ionic liquid-assisted sonochemical method and ionic liquid assisted microemulsion method are other potential methods to induce the chemical reaction and are frequently used in nanomaterials synthesis. Also, physio-chemical parameters of the synthesized nanoparticles can be controlled by employing these methods.⁴³⁻⁴⁴ For example, using sonochemistry, high energy bubbles generate, that preserve significant quantity of energy in them. When these high energy bubbles are destroyed, a high temperature (~5000K) and high pressure (~1000 bar) is developed for very short time. This high temperature and pressure are sufficient to enhance the reactions significantly.⁴⁴ Along with ionic liquid, sonochemical process is frequently considered as environmentally benign process for nanomaterials synthesis. This method has been used for designing various lanthanide based nanoparticles to date. Hexagonal LaF₃:Tb³⁺ phosphors have been prepared using this sonochemical technique and by using [C₄mim][BF₄] IL where IL is used as co-solvent, templating agent and reaction partner (source of fluoride ions).⁴⁴ Along with the previously discussed methods, there are additional methods like ionic liquid assisted microemulsion method which are also reported to prepare the lanthanide ion doped nanoparticles and can be employed to prepare quantum cutting nanomaterials. For example, LaPO₄:Eu and CePO₄:Tb nanocrystals have been prepared by ionic liquid assisted microemulsion method. By judicious mixing of tributylphosphate, 1-octyl-3-methyl-imidazolium chloride, and water in a microemulsion, TBP/[C₈mim]Cl/H₂O can be prepared, which can be used to tune the nucleation and growth of the nanocrystals.⁴⁵

The important properties of ionic liquids useful for nanomaterials synthesis

Several researchers have already established that, ILs are not only used as reaction medium, but can be employed as reaction partner and templating agent specially in the case

of lanthanide doped nanophosphors.^{4,6,10-11,16-17,24,30-33} Various tunable and adjustable parameters of ILs like cation-anion combination, high thermal stability, low vapour pressure, large liquidus range can influence the crystal phase, size, shape etc. of the host which can control the optical properties of rare-earth dopant ions.⁶

Ionic liquid for tuning crystal phase of quantum cutting nanomaterials:

Ionic liquid as a templating agent can significantly tune the crystal phase of nanomaterials during synthesis. For example, tuning of alkyl chain length, interaction between crystal facet and IL via H-bonding and IL's concentration have a significant effect on the crystal phase of quantum cutting NaGdF₄:Eu³⁺ nanoparticles.¹¹ In absence of IL, only cubic phase forms with less crystallinity, but in the presence of [C₂mim]Br IL under the identical reaction condition, hexagonal phase is created. Tetramethyl ammonium bromide (TMAB), [C₂mim][Cl] and [C₂dmim][Br] ILs were used to elucidate the effect of hydrogen bonding, π-π interaction and counter ions on the crystal phase respectively. From this work, it has been found that there is no effect of hydrogen bonding and counter anion of ionic liquid on the nanoparticles, as only hexagonal phase of Eu³⁺ doped NaGdF₄ nanoparticles was obtained.¹¹ However, only cubic phase was observed, in the case of TMAB. TMAB is used to elucidate the importance of non-aromatic cation of ionic liquid on the crystal phase. In addition, [C₄mim][Br], [C₈mim][Br] or [C₂dmim][Br] IL were used to receive more information about the effect of, hydrogen-bonding, higher alkyl chain length on the crystal phase of nanoparticles. It is observed that due to steric hinderance developed by long alkyl chain length of ILs, unlike [C₂mim][Br] IL, only cubic phase of Eu³⁺ doped NaGdF₄ nanoparticles were found.¹¹

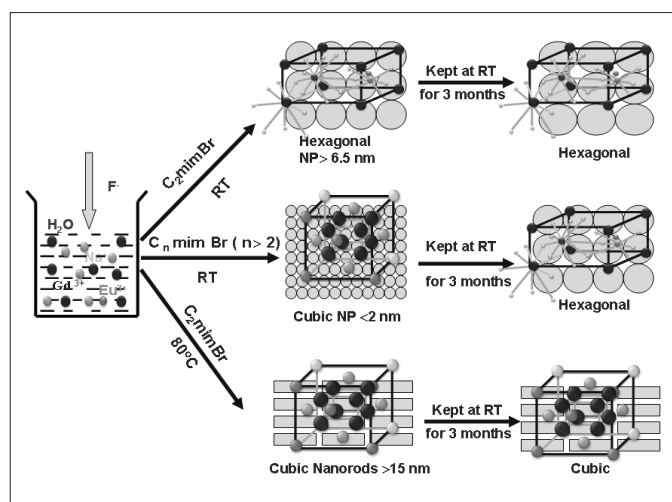


Figure 4. Quantum cutting NaGdF₄:Eu³⁺ nanophosphors and the spontaneous room temperature phase transformation.¹¹

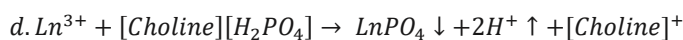
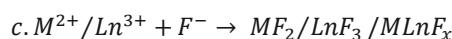
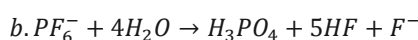
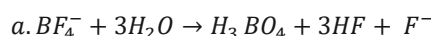
Ionic liquid for controlling shape of the nanocrystals

In addition with tuning the crystal phase, ILs can also be extensively used to control morphology as well as size as they have tunable cations, hydrogen bonding and $\pi-\pi$ stacking ability. Concentration of ionic liquids used also have significant effect on the size and morphology of nanocrystals.¹¹ Relative reactivity of IL can play a major role in morphology control.⁶ For example, ILs can also be used as precursor for the preparation of lanthanide doped binary and ternary fluoride nanoparticles. But the release of fluoride ions by ionic liquids in the reaction is slow and depends on the type of the counter anions. It is observed that thermal degradation of ILs consisting PF_6^- ions as counter ion is easier compared to the BF_4^- ions as bond strength of P-F is weaker compared to the B-F bond strength.⁶ Likewise, hydrogen bonding and $\pi-\pi$ stacking can play an important role in shape tuning. The cationic part of ionic liquids like $[C_n\text{mim}]^+$ consist hydrogen atom at C2 position of imidazolium ring and this may create H-bonding with the primary nuclei of nanoparticles which may control the shape or the phase of the nanoparticles. As a consequence, ionic liquids can attach at the active site of developing nanocrystals which leads to controlled growth.⁴⁶ In addition, adsorption at nucleation site by ionic liquid counterpart can play an important role in tuning of morphology.

Ionic liquid as reaction partner

ILs can be used as reaction partner or precursor and this property of ionic liquids enables them better than other conventional solvents. Specially, by changing the anion part of ionic liquids, various reaction partners may be tailored as per the targeted product.^{4,6,24,27,36-41}

For example, for the preparation of rare-earth doped binary and ternary fluorides and phosphate-based host materials; BF_4^- , PF_6^- ions and $H_2PO_4^-$ containing ILs have been extensively exploited.^{4,6,24,27,36-41} On heating or hydrolysis at particular temperature, the counter ions of ILs release the fluoride or phosphate ions in reaction medium and generate fluoride and phosphate-based nanomaterials.^{6,36-41} Mechanism related to the release of F^-/PO_4^{3-} ion during the synthesis of nanomaterials is given below.



Similarly, anomaly can be drawn for the RE^{3+} ions doped phosphate based $LnPO_4$ nanomaterials.^{6,41} Earlier $LnPO_4$ nanoparticles have been synthesized by using H_3PO_4 , $(NH_4)_3PO_4$, etc along with ILs (templating or reaction medium). However, phosphate containing ILs have been used for the preparation of various $LnPO_4$ such as Choline dihydrogenphosphate ($[Choline][H_2PO_4]$) and butylammonium dihydrogenphosphate. For example, Eu doped YPO_4 , $LaPO_4$ and $GdPO_4$ etc. have been synthesized by using the $[Cholin][H_2PO_4]$ IL.^{6,41}

Quantum cutting materials and their application

This section is typically focussed on how quantum cutting materials can be used for environmentally benign and energy efficient lighting, increasing efficiency in solar cells etc.

Environmentally and energy efficient lighting

Environmentally benign and energy efficient nanophosphors which can emit white light, generates tremendous attention for reducing the energy consumptions. Currently, normal incandescent lamps is almost replaced by LEDs and CFLs or as both of them consume less energy compared to the conventional incandescent lamps. But mercury is used as a discharge medium in CFLs, and contains serious toxicity issues. Currently two approaches are exploited for obtaining the white light. One is by combining three coloured LEDs (blue, green and red) and the other is phosphor converted LEDs. The latter shows high resemblance to the compact fluorescent lamps.¹ However, LEDs and CFLs are also facing several issues for their complex constructing protocols. Additionally, high purity

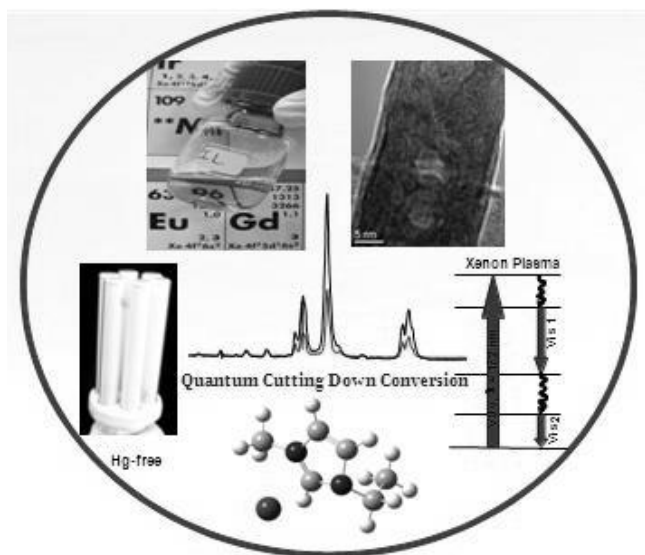


Figure 5: Quantum cutting materials via ionic liquids and their application in Hg free lighting.¹¹

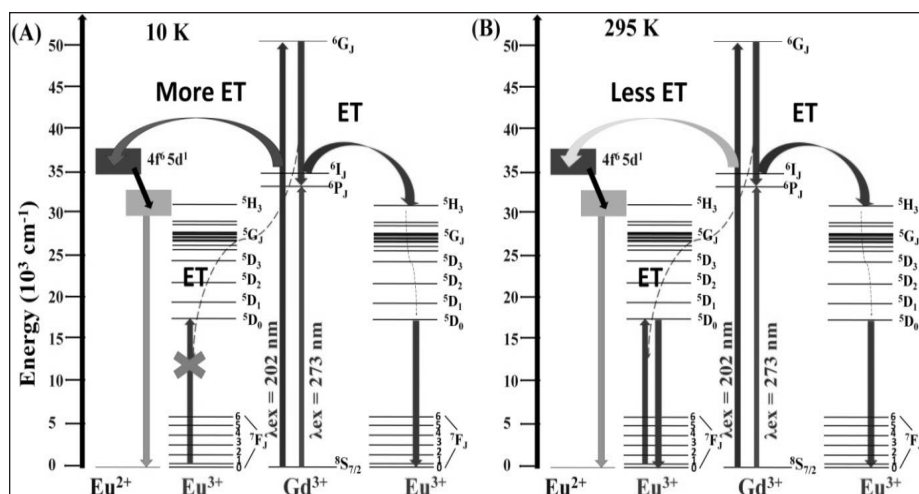


Figure 6. Schematic diagram of visible quantum cutting down conversion in BaGdF₅:Eu³⁺ (1%) : (A) at 10 K and (B) 295 K.⁵

is prerequisite for phosphors and dimming decreases their applications significantly.¹

Recently, mercury based CFLs are used in lieu of conventional incandescent lamp to save energy in a significant extent, however several issues like delayed start-up time, environmental hazardous effect at the end is a major concern. Recently, it is conceptualized that non-toxic, noble gas Xenon (Xe) can be a replacement in CFLs as discharge medium in place of Hg. But Xe also has own limitation like lesser discharge efficiency than mercury etc. In order to overcome these issues, Ln³⁺ doped down converted nanomaterials can be used which can transform the ultraviolet (UV) or vacuum ultraviolet (VUV) light into visible light and explained earlier.^{4-6,10,11} It is already shown that, QCE can be targeted maximum up to 200% which is the highest possible theoretical limit for any quantum cutting nanomaterials.^{10,11} Crystal phase-dependent QCE for Eu³⁺ doped NaGdF₄ nanomaterials like 154% and 107% for hexagonal and cubic phases, are reported, respectively.¹⁰

Temperature Dependent Quantum cutting

In another interesting work, Ghosh et al. reported efficient quantum cutting BaGdF₅:Eu³⁺ nanophosphors useful for energy efficient lighting as well as in nanothermometry. Here ionic liquid exerts a formidable effect on the QCE of BaGdF₅:Eu³⁺ nanophosphors. At room temperature, 160% QCE are noticed for BaGdF₅:Eu³⁺ synthesized with IL. But in absence of IL, efficiency decreases to 123%. However, quantum cutting is not observed at low temperature (10 K). At RT, energy transfer occurs from Gd³⁺ to Eu³⁺ causing quantum cutting, however at low temperature energy transfer is mainly occurring from Gd³⁺ to Eu²⁺. The inherent presence of

Eu²⁺ ions are important cause for not having any quantum cutting effect at 10 K. A non-radiative depopulation of ⁶I₁ levels of Gd³⁺ causes to lower energy transfer between Gd³⁺ and Eu³⁺. This phenomenon is also established using temperature dependent X-ray excited luminescence measurements (Figure 6).

Applications in Photovoltaic Cells

Creation of sufficient "clean" energy is very important, both for energy perspective as well as for environment. As the population explosion is continuing through last

decade, consumption of conventional energy resources gradually increasing; resulting the release of greenhouse gases like CO₂ and others, which cause hazardous effect on the flora and fauna. Therefore, un-conventional source of energy like wind, geo-thermal, hydro and solar energies draw a huge attention. Amongst these, solar energy is most promising and India is very blessed with Sun as it receives a significant time of sunlight throughout the day, in any season. Recently, devices as a 'spectral converter' are substantially used for absorbing the solar energy and then convert it into electrical energy. An efficient solar cell should absorb a wide spectral range, from near infrared (NIR) to visible wavelength (~950 nm to 350 nm), and transform the incident light into charges. Then the charges are collected at a high voltage with suitable current for doing necessary work.¹² So rightly, solar energy harvesting and to convert it into electrical energy by using solar cell device have drawn tremendous attention.¹³⁻¹⁴

However, limiting band gap is the major issue of this device. The incident energy is lost when it is less than the band gap of solar cell device and known as sub-band gap losses.^{6,47} This sub-band gap loss is varied for various materials exploited in solar cell applications. Sub-band gap loss can be compensated by using the upconverting (UPC) materials. UPC materials can be attached with the above mentioned solar cell devices to absorb the sub-band gap lost energy. It is established that UPC nanomaterials absorb NIR region of light and get excited. By the process of up conversion, two sub-band gap photons can be transformed into one photon of the optimum energy and may help to enhance the efficiency of solar cells. Such UPC phosphor can absorb the transmitted sub-band-gap photons by sequential ground state absorption/excited state absorption as shown in Figure 7.

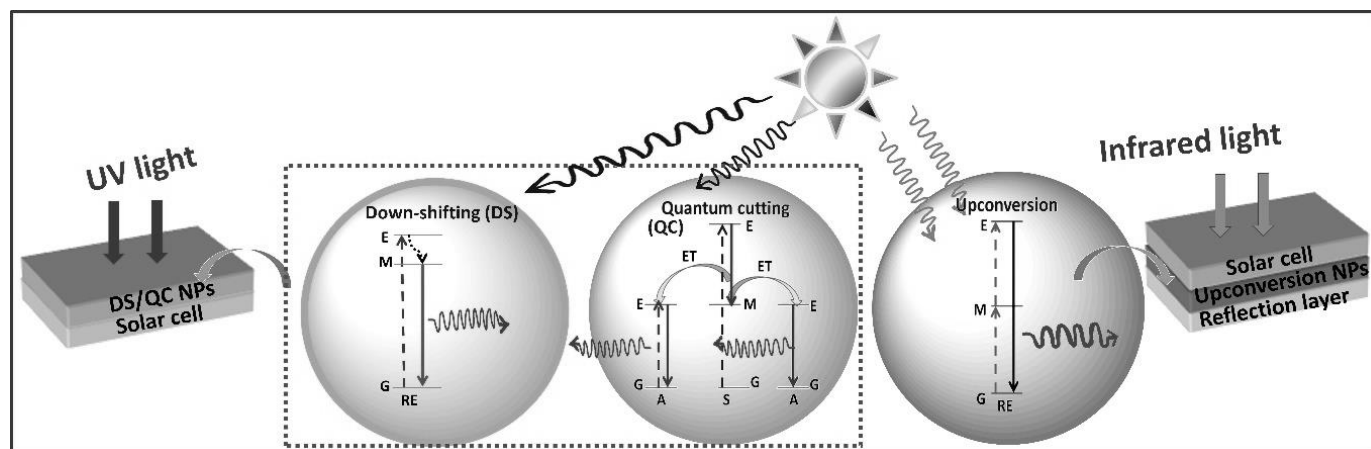


Figure 7: Schematic diagram of down shifting, quantum cutting (down converting) and upconversion nanoparticles in a solar cell device.⁶

As a result, an excited state is created in the UPC phosphor from which photons are emitted and then can be absorbed in the solar cell to create electron-hole pairs. It is predicted from theoretically, that Shockley-Queisser efficiency can be enhanced up to ~40% from ~30% by combining with UPC materials under nonconcentrated air mass (AM) 1.5 solar irradiation.⁴⁸⁻⁴⁹ $\text{NaYF}_4:\text{Er}^{3+}$ upconverted phosphor are used for enhancing NIR solar cell response in a bifacial buried silicon solar cell.⁵⁰ An UPC layer was attached on the rear of the silicon solar cell and increased solar cell response in the NIR region was verified.

The so called “down converted” or quantum cutting materials are able to absorb photons (from VUV or UV/VIS) and then convert it to two visible or infrared photons, and have a quantum yield larger than 100%. As already discussed, quantum cutting materials have huge potential applications in Hg free energy efficient and environmentally benign lighting. Apart from mercury-free fluorescent lamps, down-conversion phosphors can find possible applications in plasma display panels and in improving the efficiency of the semiconductor solar cells. In 1961, Shockley and Queisser calculated theoretically the efficiency limit of a semiconductor solar cell to be 30%. The main loss is due to the mismatch of the solar spectrum and the semiconductor absorption edge, which means that a large part of the sun’s light is not efficiently converted to electric energy. With down-conversion phosphors, current doubling is possible for the high energy part of the solar spectrum ($\lambda < 500$ nm) and the efficiency of solar cell can be increased by 25%. For example, to enhance the efficiency of solar cell with band gap about 1.1 eV, luminescence down-converter materials with intermediate or interband transition can play an important role.⁵⁴ For example, by using a luminescence converter with one intermediate band, 39.63% efficiency can be achieved for a cell with

bandgap $E_g = 1.05$ eV. In addition, on applying the down-converter on the front surface, solar cell efficiency of 38.6% for $E_g = 1.1$ eV was obtained over conventional solar cell with 30.9% efficiency.⁵¹

Conclusion

In conclusion, quantum cutting nano materials are very important in terms of environmentally benign and energy efficient luminescent materials useful for lighting applications. Also these have a great promise to be used in increasing the solar cell efficiency. On the other hand, IL based synthesis has tremendous potential in materials synthesis due to their superior properties compared to normal organic solvent and templating agents like long chain amines etc. As there exists 10^{18} possible cation/anion combination for ILs, ILs can be tuned in such a way that not only twelve basic principles of “green chemistry” will be followed but also these can work as “designer” solvents for the preparation of nanoparticles, even for quantum cutting nanomaterials.

Acknowledgement

PG acknowledges Science and Engineering Research Board (SERB), Govt of India (Core Research Grant) India for funding.

References

1. R. K. Sharma, A. V. Mudring, P. Ghosh, *J. Lumin.*, **2017**, 189, 44.
2. A. Ivaturi, H. Upadhyaya, *A. Compr. Guid. to Sol. Energy Syst.*, **2018**, 279.
3. X. Liu, X. Hu, H. Miao, G. Zhang, J. Mu, T. Han, D. Zhang, *Sol. Energy*, **2016**, 134, 45.
4. C. Lorbeer, A. V. Mudring, *Chem. Commun.*, **2014**, 50, 13282.
5. Y. N. Chouryal, R. K. Sharma, K. Lvanovskikh, A. Ishchenko, Q. Shi, V. Lvanov, S. Nigam, A. Pandey, P. Ghosh. *New J. Chem.* **2021**, 45, 1463.

6. R. K. Sharma, P. Ghosh, *Front. Chem*, **2021**, 9:715531.
7. R. T. Wegh, H. Donker, K. D. Oskam, A. Meijerink, *J. Lumin.*, **1999**, 82, 93.
8. B. Liu, Y. Chen, C. Shi, H. Tang, Y. Tao, *J. Lumin.*, **2003**, 101, 155.
9. R. T. Wegh, H. Donker, K. D. Oskam, A. Meijerink, *Science*, **1999**, 283, 663.
10. P. Ghosh, S. Tang, A. V. Mudring, *J. Mater. Chem.*, **2011**, 21, 8640.
11. P. Ghosh, A. V. Mudring, *Nanoscale*, **2016**, 8, 8160.
12. M. M. Lee, J. Teuscher, T. Miyasaka, T.N. Murakami, H. J. Snaith, *Science*, **2012**, 338, 643.
13. B O'Regan, M. Grätzel, *Nature*, **1991**, 353, 737.
14. F. Bella, C. Gerbaldi, C. Barolo, M. Grätzel, *Chem. Soc. Rev.*, **2015**, 44, 3431.
15. T. Welton, *Chem. Rev.*, **1999**, 99, 2071.
16. Y. N. Chouryal, S. Nema, R. K. Shrama, H. Kewat, A. Pandey, P. Ghosh, Y. Bhargava, *Biomater. Sci.* **2020**, 8, 6730.
17. R. K. Sharma, Y. N. Chouryal, S. Chaudhari, J. Saravanakumar, S. R. Dey, P. Ghosh, *ACS Appl. Mater. Interfaces*, **2017**, 9, 11651.
18. R. A. Olofson, W. R. Thompson, J. S. Michelman, *J. Am. Chem. Soc.* **1964**, 86, 1865.
19. S. Sowmiah, V. Srinivasadesikan, M.-C. Tseng, Y.-H. Chu, *Molecules*, **2009**, 14.
20. J. S. Wilkes, M. J. Zaworotko, *J. Chem. Soc., Chem. Commun.*, **1992**, 13, 965.
21. M. J. Earle, P. B. McCormac, K. R. Seddon, *Green Chem.* **1999**, 1, 23.
22. A. Wang, X. Deng, J. Wang, S. Wang, X. Niu, F. Hao and L. Ding, *Nano energy*, **2021**, 81, 105631.
23. X. Duan, J. Ma, J. Lian, W. Zheng, *CrystEngComm*, **2014**, 16, 2550.
24. P. S. Campbell, C. Lorbeer, J. Cybinska, A.-V. Mudring, *Adv. Funct. Mater.* **2013**, 23, 2924.
25. X. Liu, J. Ma, P. Peng, W. Meng, *Langmuir*, **2010**, 26, 9968.
26. X. Duan, X. Liu, Q. Chen, H. Li, J. Li, X. Hu, Y. Li, J. Ma, W. Zheng, *Dalton Trans.*, **2011**, 40, 1924.
27. J. Cybinska, C. Lorbeer, E. Zych, A.-V. Mudring, *ChemSusChem*, **2011**, 4, 595.
28. J. Xia, S. Yin, H. Li, H. Xu, Y. Yan, Q. Zhang, *Langmuir*, **2011**, 27, 1200.
29. I. Krossing, J. M. Slattery, C. Daguene, P. J. Dyson, A. Oleinikova, H. Weingärtner, *J. Am. Chem. Soc.*, **2006**, 128, 13427.
30. R. K. Sharma, S. Nigam, Y. N. Chouryal, S. Nema, S. P. Bera, Y. Bhargava, P. Ghosh., *ACS Appl. Nano. Mater.*, **2019**, 2, 927.
31. R. K. Sharma, Y. N. Chouryal, S. Nema, S. Nigam, S. P. Bera, Y. Bhargava, P. Ghosh., *ChemistrySelect*, **2020**, 5, 9105.
32. R. K. Sharma, Y. N. Chouryal, S. Nigam, J. Saravanakumar, S. Barik, P. Ghosh., *ChemistrySelect*, **2018**, 3, 8171.
33. Y. N. Chouryal, R. K. Sharma, D. Acharjee, T. Ganguly, A. Pandey, P. Ghosh. *J. Chem. Sci.* **2019**, 131, 93.
34. M. Armand, F. Sndres, D. R. MacFarlane, H. Ohno, B. Scrosati, *Nature Mater.* **2009**, 8, 621.
35. Y. Wang, Q. Hou, M. Ju, W. Li, *Nanomaterials* **2019**, 9, 1.
36. C. Lorbeer, J. Cybinska, A.-V. Mudring, *Chem. Commun.*, **2010**, 46, 571
37. C. Lorbeer, A. V. Mudring, *ChemSusChem* **2013**, 6 (12), 2382.
38. Q. Ju, A. V. Mudring, *RSC Adv.* **2013**, 3, 8172.
39. C. Lorbeer, J. Cybińska, A. V. Mudring, *Cryst. Growth Des.* **2011**, 11 (4), 1040.
40. C. Lorbeer, A.V. Mudring, *J. Phys. Chem. C* **2013**, 117 (23), 12229.
41. J. Cybińska, C. Lorbeer, A. V. Mudring, *J. Mater. Chem.* **2012**, 22, 9505.
42. G. Bühler, C. Feldmann, *Angew. Chemie - Int. Ed.* **2006**, 45 (29), 4864.
43. Z. Li, J. Dong, H. Zhang, Y. Zhang, H. Wang, X. Cui, Z. Wang, *Nanoscale Adv.* **2021**, 3(1), 41-72.
44. L. Zhu, S. Liu, Y. Hui, B. Zou, X. Cao, *Nano* **2014**, 9 (7), 1-9.
45. C. Zhang, J. Chen, X. Zhu, Y. Zhou, D. Li, *Chem. Mater.* **2009**, 21 (15), 3570-3575.
46. Y. Sun, W. Zheng, *Dalt. Trans.* **2010**, 39 (30), 7098-7103.
47. J. C. Goldschmidt, S. Fischer, *Adv. Opt. Mater.* **2015**, 3, 510.
48. G. Chen, H. Ågren, T. Y. Ohulchanskyy, P. N. Prasad *Chem. Soc. Rev.* **2015**, 44, 1680;
49. T. Trupke, A. Shalav, B. S. Richards, P. Würfel, M. A. Green. *Sol. Energy Mater. Sol. Cells* **2006**, 90, 3327
50. K. Inagaki, T. Toshima, S. Tanda, K. Yamaya *Appl. Phys. Lett.* **2005**, 86, 013505.
51. T. Trupke, M. A. Green, P. Würfel, *J. Appl. Phys.* **2002**, 92 (3), 1668.



Dr. Pushpal Ghosh joined Department of Chemistry, Dr. H.S. Gour Central University, Sagar, Madhya Pradesh in October, 2013. He has earned his Ph.D degree from Indian Association for the Cultivation of Science (IACS), Kolkata (Degree given by Jadavpur University), under the supervision of Prof. Amitava Patra [FRSC] in 2009. Then he moved to Germany with prestigious **Alexander von Humboldt Fellowship (AvH)** and worked in Ruhr University Bochum, Germany from December 2009 to October 2013 under mentorship of Prof Anja-Verena Mudring [FRSC]. Despite AvH, he also worked in **European Research Council(ERC)** Project in Germany. His Alma mater are also Presidency College (Presently Presidency University), Kolkata (MSc) and Ramkrishna Mission Residential College Narendrapur, Kolkata (B.Sc with Honours in Chemistry). He is a recipient of several awards and recognitions. A few to name are prestigious **AvH Fellowship, Inventor Award for the year 2012 at Ruhr University Bochum, Germany, International Travel Grant by SERB, Best Poster Prizes in the several National/ International conferences, "The Governor of West Bengal's Award"** as an all-round student of the school in an academic year etc. Owing to his contribution in his field, recently he is inducted as **Editorial Board** member in prestigious journal **Green Chemistry Letters and Reviews** (Taylor & Francis Journal with impact factor **4.99**)

Currently he is leading a research group funded by 6 research projects (5 as PI): UGC Start-Up grant, SERB (Young Scientist and Core-Research Grant Scheme), BRNS and IUCR, New Delhi. He has supervised two students for PhD, five M.Sc. projects and currently guiding two students for PhD, four students for MSc projects and one project student. His interest is to synthesis new generation optoelectronic nanomaterials using green synthesis. He has published more than 35 highly cited research articles (**h index: 22, i-10 index: 25**) in high impact factor international journals, book chapters including one German and one Indian patent (applied and published).

Development of Surface Functionalized Nanoparticles for Cancer Therapy

S. B. Shelar^a, K. C. Barick^{a,b,*}, P. A. Hassan^{a,b,*}

^aChemistry Division, Bhabha Atomic Research Centre, Mumbai – 400085, India

^bHomi Bhabha National Institute, Anushaktinagar, Mumbai – 400085, India

*Corresponding Authors: kbarick@barc.gov.in (K. C. Barick), hassan@barc.gov.in (P. A. Hassan)

Abstract

Surface chemistry plays a vital role in developing nanoparticles (NPs) for various biomedical applications. Among the others, iron oxide nanoparticles (IONPs) and gold nanoparticles (GNPs) have emerged as attractive materials and their surface modification with desired functional groups is considered as a prerequisite for biomedical applications. This article summarizes some of our recent developments in the area of surface functionalization of IONPs and GNPs. Further, the biomedical applications of these NPs in drug delivery, hyperthermia treatment of cancer as well as combination therapy involving hyperthermia and chemotherapy are discussed. Specifically, short chain organic molecules, polymers, biomolecules, peptides and receptors were introduced on the surface of NPs to make them amenable for various biomedical applications. In particular, the presence of stimuli responsive amino acids or peptide shells on the surface of these particles makes them attractive materials for healthcare applications.

Keywords: Nanoparticles, Fe₃O₄, Au, Drug delivery, Cancer therapy

1. Introduction

In recent years, IONPs and GNPs have received great deal of attention due to their unique physio-chemical properties and potential applications in various biomedical fields [1,2]. The biomedical applications of NPs require narrow size distribution of particles and their long term colloidal stability in aqueous and physiological medium. Further, significant challenges lie in evading unwanted uptake of NPs by reticulo-endothelial system (RES) as well as their site-specific targeting. NPs introduced into the blood flow undergo a complex pathway before reaching a target site. They extensively interact with various components of blood such as proteins and antibodies during circulation, which also affects their clearance from the body. Further, NPs have to escape from the spleen and kidney, where filtration process occurs. Therefore, NPs should have large circulation time in blood vasculature and have the efficacy to pass through the fine capillary systems.

The other most important criteria for biomedical applications of NPs are biocompatibility and toxicity. The size and shape of NPs affects their biocompatibility and toxicity. The NPs of Fe₃O₄, γ-Fe₂O₃ and Au are widely used for biomedical applications due to their good biocompatibility and chemical stability under physiological conditions. These NPs are generally composed of an inorganic core functionalized with a biocompatible shell [1]. The coating materials not only shield NPs from the external environment but also provide sites for further conjugation. The common strategy involved in surface functionalization is coating of short chain organic molecules, polymers and

inorganic materials (gold, silica) [3]. Specifically, the NPs used for biological applications should be chemically and colloidal stable, biocompatible, efficient and rapidly internalized into the specific target cells. Thus, this article mainly summarizes some of our recent developments in the area of surface functionalization of IONPs and GNPs with various biocompatible molecules, and discussed their therapeutic and diagnostic applications.

2. Surface functionalization of nanoparticles

The surface charge and surface chemistry primarily play crucial role in colloidal stabilization (either by electrostatic or steric stabilization) of NPs. The biocompatible surface passivating agents used for stabilizing NPs can be adsorbed or end grafted on the surface of particles by *in-situ* or post-synthesis processes. The *in-situ* surface modification is usually attained in a single step using passivating agents during synthesis process, whereas post-synthesis surface modification can be achieved through ligand exchange, ligand addition and encapsulation processes (Figure 1) [3]. We have used various passivating agents such polymers, organic molecules and biomolecules for surface functionalization of NPs.

One of the most promising surface passivating agent, polyethylene glycol (PEG) a water soluble, biocompatible and biodegradable polymer. Recently, we have prepared 10 nm carboxyl PEGylated Fe₃O₄ nanoparticles (CPMN) by co-precipitation of Fe²⁺ and Fe³⁺ ions in basic medium followed by *in-situ* coating of bifunctional PEG-diacid molecule [4]. These CPMN were further used as a core

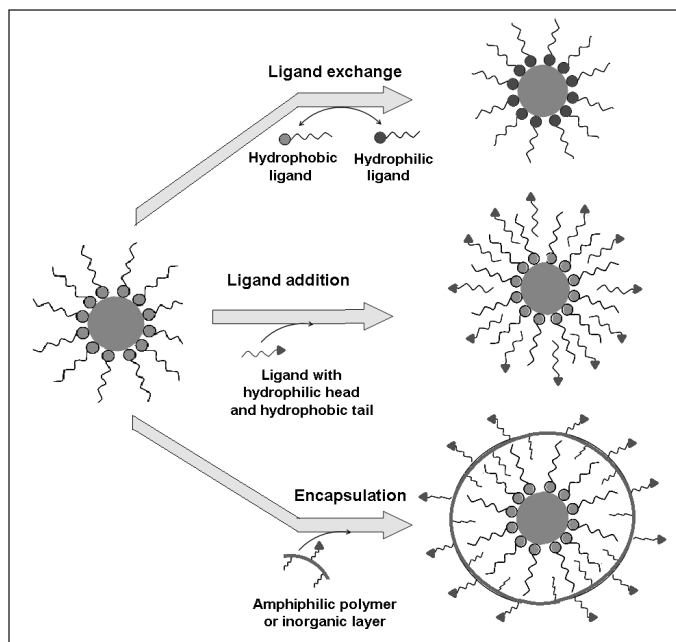


Figure 1. Schematic illustrations of surface functionalization of NPs.

material for preparation of polyaniline shell cross-linked Fe_3O_4 nanoparticles because of their good water dispersibility and high negative surface charge [5]. This type of composite structure of PEG and polyaniline could be advantageous for the effective transport of heat from Fe_3O_4 core to surrounding medium during hyperthermia treatment. Further, a novel pluronic stabilized Fe_3O_4 magnetic nanoparticles (PSMNP) were developed by introducing PEG based block co-polymer, Pluronic P123 onto surface of 7 nm hydrophobic magnetic nanoparticles (HMNPs) by ligand addition method and investigated their efficacy for delivery of hydrophobic anticancer drugs (Figure 2a) [6]. The polymeric shell not only provides colloidal stability but also allows the encapsulation of drugs. Moreover, these PEG coated NPs are protein resistant in nature.

Recently, the use of small organic molecules as passivating agent has been described as an alternative strategy for surface functionalization of NPs. Small chain organic molecules having functional head groups such as carboxyl, amine, thiol and phosphate were used as stabilizer for preparation of water-dispersible, biocompatible Fe_3O_4 nanoparticles [7-10]. For instance, phosphate anchored nanocarriers were prepared by *in-situ* functionalization of Fe_3O_4 particles using sodium hexametaphosphate and sodium tripolyphosphate. The phosphate molecules conjugated to the surface of particles via chemisorption of some of its phosphate groups [9,10], while remaining free phosphate groups provide aqueous stability to particles by forming hydrogen bonding with water. In addition, these free surface functional groups create sufficient surface charge on particles and hence, make them hydrophilic. The organosulfur compound, 2,3-dimercaptosuccinic acid (DMSA) was also used for stabilizing hydrophobic Fe_3O_4 nanoparticles by ligand exchange method [8]. Bifunctional Fe_3O_4 MNPs (carboxyl for drug binding and amine for receptor tagging) are also prepared by introducing bioactive cysteine molecules onto the surface of undecenoic acid coated Fe_3O_4 magnetic nanoparticles via thiol-ene click reaction [11]. The use of these small molecules is predominantly attractive because of their easy preparation process and simple conjugation chemistry.

We have also reported that amino acid such as glycine would be an attractive molecule for surface passivation of SPIONs due to the strong binding affinity of its carboxylate groups towards Fe_3O_4 [12]. These glycine functionalized magnetic nanoparticles (GMNPs) were chosen as the core material for further fabrication of peptide mimic shell cross-linked Fe_3O_4 magnetic nanocarriers (PMNCs) because of their good aqueous stability and biocompatibility [1]. PMNCs (Figure 2b) were prepared by reaction between

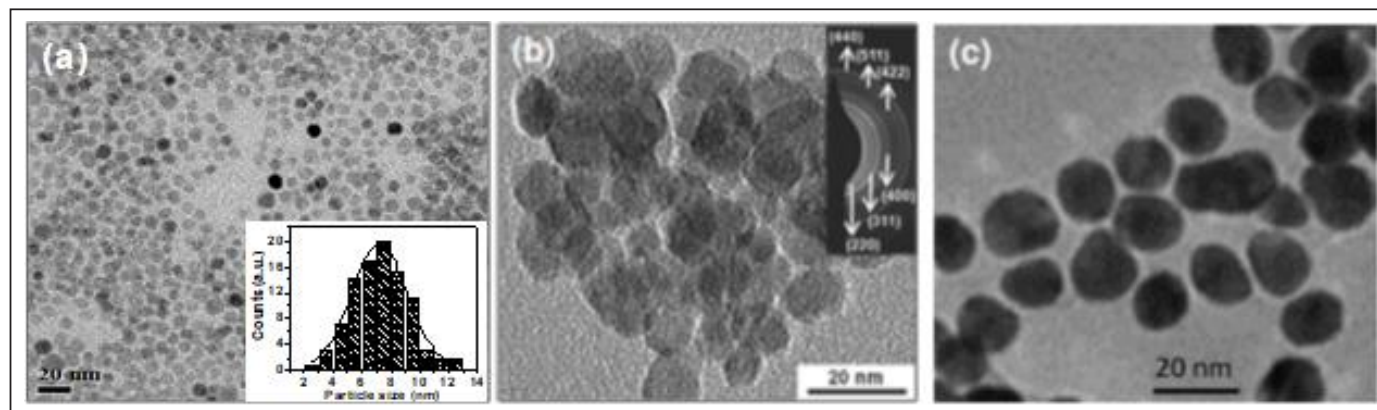


Figure 2. TEM micrographs of (a) PSMNPs (inset: particle size distribution), (b) PMNCs (inset: SAED pattern showing high crystallinity of PMNCs) and (c) lanreotide peptide-decorated GNPs [1,6]. Fig. 2 (a) and (b) are reproduced from Ref.6 (Copyright © 2016) and 1 (Copyright © 2012) with permission from the Royal Society of Chemistry and WILEY-VCH Verlag GmbH & Co., respectively.

the free amine group of GMNPs and double bond of methyl methacrylate. Subsequently, the ester moieties were reacted with ethylenediamine and arginine molecules to achieve the peptide mimic shell cross-linked Fe_3O_4 magnetic nanocarriers with multifunctionality. The organic shell grown on GMNPs by Michael addition/amidation reaction composed of many amide linkages involving two amino acids (glycine and arginine) similar to peptides. The terminal amino acid on the shell of PMNCs allows us to create functionalized exteriors with high densities of organic moieties (both amine and carboxyl) for conjugation of drug molecules and biolabelling.

In recent years, there has been an increasing interest in targeted therapy and diagnostics of cancer using natural or synthetic analogues of ligands that are specific to the surface receptors expressed on cancer cells. Therefore, in another study, a lanreotide peptide (LP) decorated gold nanoparticles (GNPs) system (Figure 2c) has been developed for targeting GNP to somatostatin receptor 2 (SSTR2) expressing cancer cells (Ref.). In this study, citrate stabilized gold nanoparticles (GNPs) were prepared using a citrate reduction method where gold salt is reduced to form ~10-15 nm sized GNP and *in situ* coating of negatively charged citrate ions imparts colloidal stability via a phenomenon of electrostatic repulsion [13]. Furthermore, these GNPs were coated with LP (a synthetic structural analogue of naturally occurring hormone “somatostatin-14”) in a pH-dependent manner [15]. In between pH 7.0-8.0, the electrostatic interaction between positively charged LP and negatively charged GNPs forms a colloidally stable GNP-LP complexes. The cellular uptake studies performed by flow cytometry and laser scanning confocal microscopy has demonstrated selective delivery of GNP-LP complexes in high (AR42J cells) vs low (CHO cells) SSTR2 expressing cancer cells.

3. Therapeutic and diagnostic applications of nanoparticles

IONPs are extensively used as heating source for heat activated killing (hyperthermia therapy) of cancer cells at 5-7 °C above the human body temperature under AC magnetic field (AMF) [1]. The hyperthermia therapy is a non-invasive methodology and it allows the heating to be limited to the tumour area (localized heating). Cancer cells are more sensitive to heat damage compared to normal cells. The functional molecules used in stabilization of IONPs significantly affect the heating efficacy of nanoparticles, which is expressed in terms of the specific absorption rate (SAR). The heating ability of IONPs is mainly associated with the combined effect of Néel and Brownian relaxation

loss processes [12]. These NPs are also used as a contrast agent in magnetic resonance imaging (MRI).

Recently, we have explored the heating ability of carboxyl decorated iron oxide nanoparticles (CIONs) and MR contrast properties were investigated [14]. CIONs exhibit superparamagnetic behavior with maximum magnetization of 58 emu/g at 20 kOe and blocking temperature (T_B) of around 200 K (Figure 3a). Our inductive heating experiments show that a magnetic field of 0.251 kOe at fixed frequency of 265 kHz is able to produce energy enough for raising the temperature of the magnetic suspension of 1 mg/ml to 42-43°C (hyperthermia temperature) within 20 min (Figure 3b). The SAR values of CIONs were found to be 58.5, 131.7 and 204.0 W/g of Fe with an applied field of 0.251, 0.335 and 0.419 kOe, respectively (at a fixed frequency of 265 kHz). The observed high SAR values can be attributed to the combined effects of good colloidal dispersion, strong magnetic responsivity and narrow size distribution of particles. Further, their infrared thermal imaging confirmed the localized heating of CIONs under AMF (inset of Figure 3b). This is highly advantageous for the *in-vitro* hyperthermia therapy of cancer cells. These aqueous suspensions of CIONs also

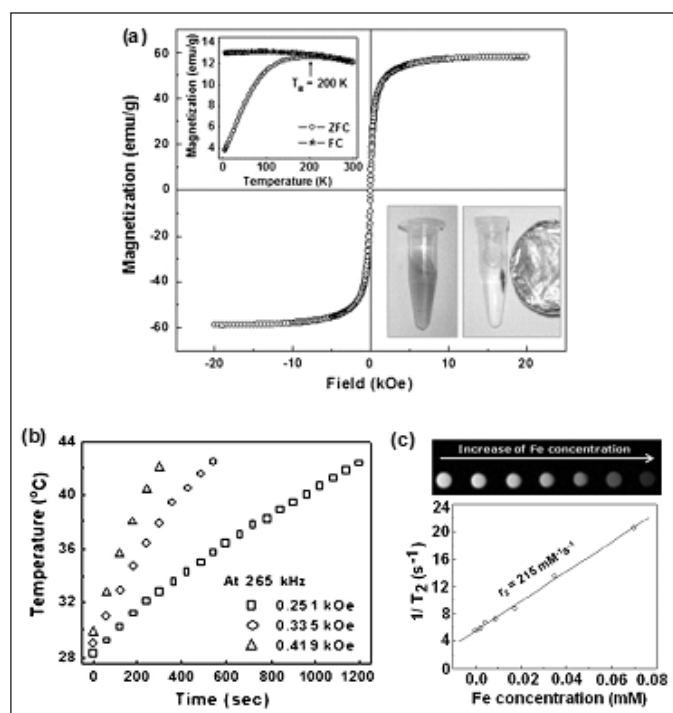


Figure 3. (a) Magnetization vs. field plot of CIONs at 300 K (top inset: ZFC-FC plot, bottom inset: photographs of CIONs suspension in presence and absence of a table-top magnet), (b) temperature vs. time plot of aqueous suspension of CIONs under AMF and (c) T_2 -weighted MR images of CIONs for different concentrations of Fe along with $1/T_2$ vs. Fe concentration plot at 1.5 T. Reprinted from Ref. 14 (Copyright © 2013) with permission from Elsevier.

shows excellent contrast properties in MRI. Even at a low concentration, these CIONs suspension still have a strong T_2 signal intensity. The signal intensity of T_2 images changes significantly with an increasing amount of Fe concentration (Figure 3c), indicating that these magnetic samples generate MR contrast on transverse proton relaxations-times weighted sequences due to the dipolar interaction of magnetic moment of the particles and proton in the water. The transverse relaxivity (r_2) value was found to be $215 \text{ mM}^{-1}\text{s}^{-1}$. The good colloidal stability and high r_2 value make these CIONs as promising candidate for high-efficiency T_2 contrast agent in MRI diagnosis even at lower dose.

We have also explored the *in-vitro* hyperthermia on cancer cells (WEHI-164) in presence of carboxyl PEGylated Fe_3O_4 magnetic nanoparticles (CPMN) and polyaniline shell cross-linked Fe_3O_4 nanoparticles (PSMN) under AMF of 0.335 kOe for 10 min [4,5]. It has been observed that the control cells (untreated) and treated cells with particles only (-hyperthermia) did not show significant change in the percentage cell viability. However, PSMN under AMF (+ hyperthermia) showed about 22.5% decrease in viability of WEHI-164 cells for 1 mg of PSMN as compared to the marginal (~8%) decrease with CPMN under similar condition. At hyperthermia temperature, various cellular damaging mechanisms such as apoptosis, protein denaturation and DNA cross-linking may occur to kill the cancer cells.

IONPs with suitable surface functionality are taken up by cells more easily than larger molecules. Thus, they can be successfully used as delivery tools for currently available bioactive compounds. In these systems, the drugs may be adsorbed or bound on the surface (covalent or electrostatically) of functionalized IONPs or encapsulated in their core-shell structure. Various surface functionalized SPIONs were developed for entrapping drug molecules [1,4-7,9]. The positively charged anticancer drug, doxorubicin hydrochloride (DOX) used to loaded onto the surface of negatively charged citrate, phosphate and cysteine functionalized iron oxide nanoparticles through electrostatic interactions. This drug loaded particle can be targeted to cancer cells by active or passive targeting mechanisms.

Pluronic stabilized Fe_3O_4 magnetic nanoparticles (PSMNPs) were developed for passive targeting of hydrophobic anticancer drug, curcumin (CUR) to breast cancer cell lines. It has been observed that curcumin was encapsulated into the hydrophobic interface between hydrophobic MNPs (HMNPs) and Pluronic layer without any changes in chemical composition [6]. The drug loading efficiency of about 98 % was observed at drug to

particles ratio of 1:2 and curcumin loaded PSMNPs (CUR-PSMNPs) showed pH dependent release behaviour. The CUR and CUR-PSMNPs showed significant reduction in proliferation of MCF-7 cells with half maximal inhibitory concentration (IC_{50}) values of be 25.1 and 18.4 μM , respectively. The higher toxicity of CUR-PSMNPs was further confirmed by cellular uptake and cellular imaging studies. These results suggested that our CUR-PSMNPs formulation is superior than pure curcumin in causing tumor cytotoxicity, which is possibly due to the increase in the bioavailability of drug to the targeted site. Similarly, surfactant stabilized Fe_3O_4 nanocarriers (SMNCs) were also developed for simultaneous delivery of both hydrophilic and hydrophobic anticancer agents such as doxorubicin hydrochloride (DOX) and curcumin (CUR), respectively. DOX was electrostatically conjugated onto the surface of nanocarriers, whereas CUR was engulfed into the hydrophobic interlayer between oleic acid and sodium dodecyl sulphate through hydrophobic interaction (Figure 4) [15]. It has been reported that the CUR and DOX loaded SMNCs (CUR-DOX-SMNCs) exhibit slow and sustained release of drug molecules and inhibit the growth of mouse skin fibrosarcoma cells (WEHI-164) in dose dependent manner. In addition, anticancer drug such DOX was also conjugated to nanocarriers by covalent bridging involving acid cleavable amide or carbamate bonds [16]. We have also addressed the receptor mediated drug targeting using folic acid conjugated magnetic nanocarriers (FMNCs) [11]. It has been observed that use of FMNCs as a drug delivery vehicle significantly enhance the accumulation of DOX (as observed from DOX fluorescence intensity) in folate receptors over expressed cancer cells (KB cells) as compared to magnetic nanocarriers (MNCs) without folate labeling. Further, drug targeting by external magnetic field is also accepted as a platform technology for site-specific drug delivery.

Magnetic hyperthermia in association with drug not only increases the concentration of drug at the tumor site but also enhances the drug toxicity in certain cancer cells. Therefore, the combination therapy involving hyperthermia and chemotherapy is recently evolving as an attractive strategy to cancer therapy, as it often results in synergistic effects. Our pH responsive peptide mimic shell cross-linked magnetic nanocarriers (PMNCs) PMNCs showed excellent self-heating ability under AMF, high affinity towards anticancer drug (DOX) and their substantial cellular internalization in conjugation with DOX [1]. Specifically, the release studies under reservoir-sink conditions (Figure 5a) showed pH dependent release behaviour of DOX. The pH triggered release of DOX could be attributed to the weakening of the electrostatic

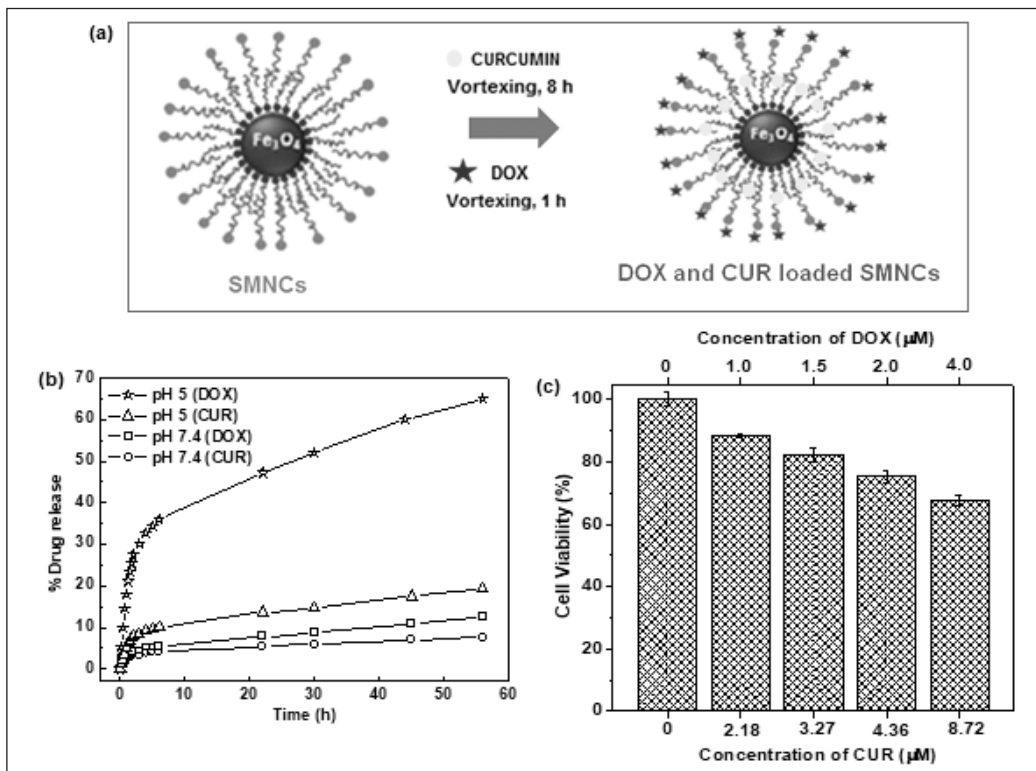


Figure 4. (a) Schematic representation of simultaneous loading of DOX and CUR onto the SMNCs, (b) release profile of drugs from CUR-DOX-SMNCs under different reservoir pH at 37°C and (c) viability of WEHI-164 cells in presence of CUR-DOX-SMNCs at 48 h in culture conditions. Reproduced from Ref. 15 (Copyright © 2017) with permission from Elsevier.

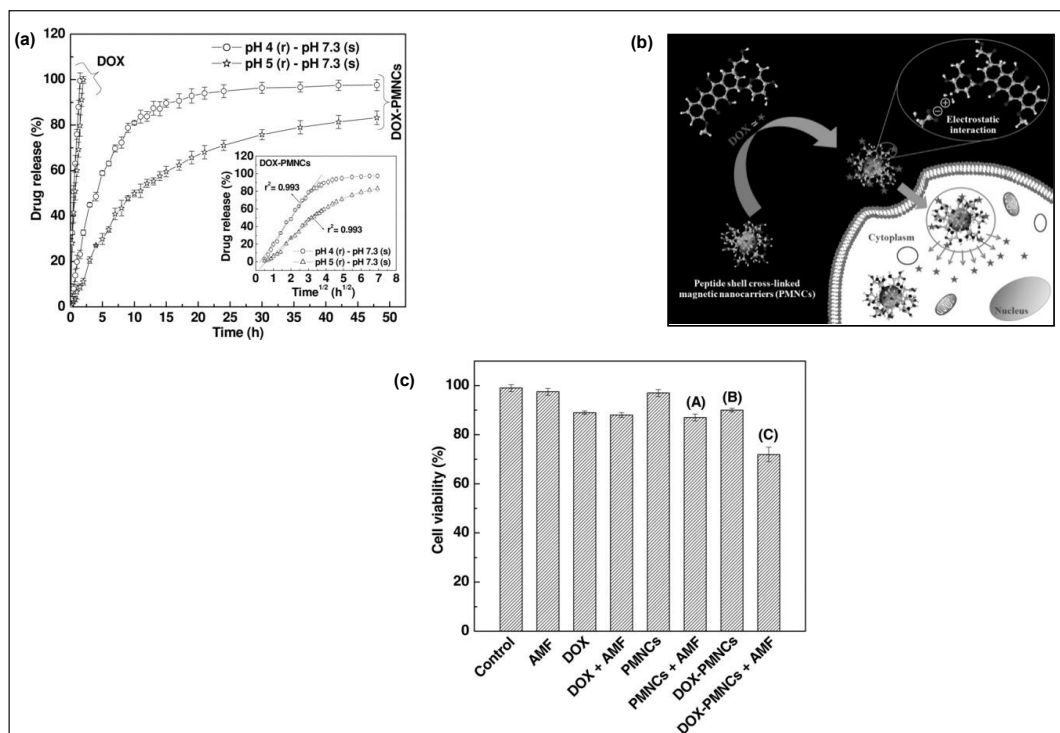


Figure 5. (a) pH dependent drug release profile of pure DOX and DOX-PMNCs in cell mimicking environment (reservoir (r): pH 5/pH 4 and sink (s): pH 7.3) at 37°C (inset: Higuchi drug release model of DOX-PMNCs), (b) proposed mechanism for drug release and (c) viability of HeLa cells during combination therapy using DOX-PMNCs with a DOX concentration of 8 μM along with various control groups [synergistic effect: (C) < {(A)×(B)}/100]. Reproduced from Ref. 1 (Copyright © 2012) with permission from WILEY-VCH Verlag GmbH & Co.

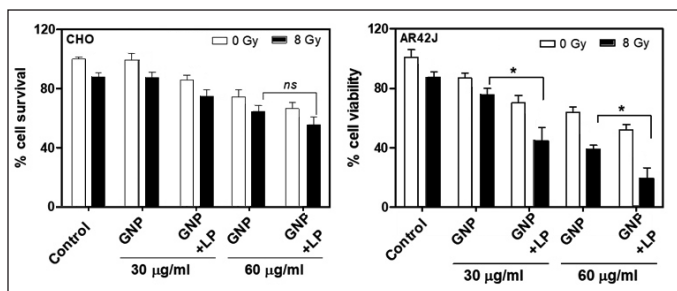


Figure 6. Cell viability of (A) CHO and (B) AR42J cells treated with GNP and GNP-LP for 4-5 hrs and then exposed with gamma radiation. Cell viability was evaluated 72 hr after gamma radiation by MTT assay.

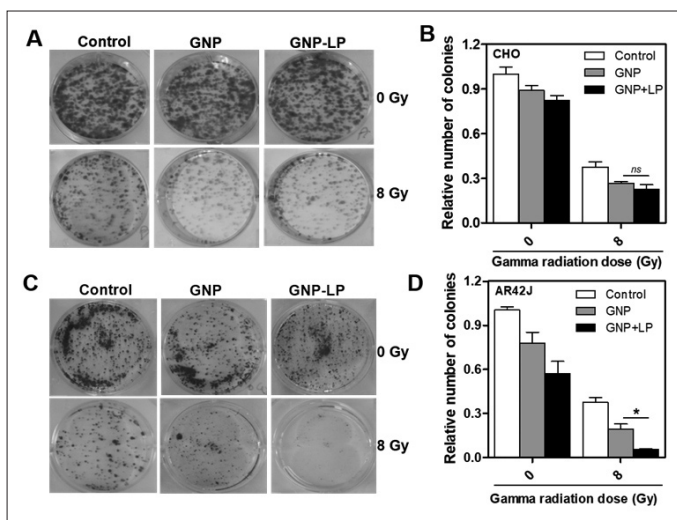


Figure 7. Colony formation assay of CHO and AR42J Cells. Representative images and relative number of colony formation of CHO (A, B) and AR42J (C, D) cells after 10-12 days of gamma irradiation

interactions between the drug and PMNCs (Figure 5b) at mild acid (pH4 and 5). Further, these DOX loaded PMNCs (DOX-PMNCs) under AMF showed much higher cytotoxicity than individual treatments of PMNCs with AMF and DOX-PMNCs alone (Figure 5c). The enhanced toxicity of DOX-PMNCs to tumor cells under an AMF suggests their strong potential for combination therapy. These nanocarriers transformed from a negatively charged to a positively charged form in the acidic environment and promoted cargo release, which could remarkably cause cytotoxicity to cancer cells. Furthermore, these nanocarriers are resistant to protein adsorption under physiological medium. These properties indicate that the creation of magnetic nanocarriers with pH responsive behavior can be applied to design of drug carriers for combining the chemotherapy and hyperthermia.

Magnetic luminescent hybrid nanostructures have also received a great deal of attention in biomedical applications. A bifunctional Fe₃O₄ decorated YPO₄: Eu

hybrid nanostructure was developed by covalent bridging of carboxyl PEGylated Fe₃O₄ and amine coated YPO₄: Eu particles [17]. These nanostructures show good colloidal stability, tunable magnetic and optical properties, and self-heating capacity under an external AC magnetic field. Specifically, the hybrid nanostructure provides an excellent platform to integrate luminescent and magnetic materials into one single entity that can be used as a potential tool simultaneous cellular imaging and therapy. In addition, the high density of functionalized exteriors (free carboxyl and amine groups) on the surface of these hybrid nanostructures can be accessed for further conjugation of drugs/ biomolecules.

Gold nanoparticles have wide biomedical applications because of their exceptional physical and chemical properties. In addition, they also offer a platform for various types of surface modifications. Most importantly, they are promising anti-cancer nanomaterial because of their inherent therapeutic activities such as photothermal and radiosensitizing activities. These properties have been proven to achieve improved anti-cancer activities in various types of cancer cells and tumors. However, cancer cell specific targeting of GNPs to neuroendocrine tumors is still a major challenge. Lanreotide peptide (LP), a synthetic analogue of somatostatin-14 has high affinity towards SSTR2 receptors widely expressed on neuroendocrine tumors as well as has ability in inhibiting malignant forms of breast, prostate and lung cancers. Hence, to target neuroendocrine tumors expressing SSTR2 receptors with GNPs and enhancing their radiosensitization effect, we have developed a LP-decorated GNP system and evaluated their ability to target high SSTR2 expressing cells [13]. Further, we have evaluated the radiosensitization effects of GNP and GNP-LP complexes in high SSTR2 expressing cells (AR42J) under the exposure of gamma radiation. As can be seen from cytotoxicity (Figure 6) and colony formation (Figure 7) assay, the enhanced radiosensitization is evident in SSTR2 expressing cells treated with LP-decorated GNPs and exposed to gamma radiation.

Specifically, this article highlighted various surface functionalization strategies of IONPs and GNPs, and their applications in cancer therapy. The simple conjugation chemistry involved in our surface modification strategies opens the new opportunities for site-specific targeting of drugs and biomolecules. However, there are lots of challenges still lie in development of appropriate surface functionalized NPs to achieve long-term colloidal stability in biological medium. Further, the real time monitoring of NPs inside body and the effect of nanotoxicity should be addressed in near future for their practical applications.

Acknowledgments

Author thanks Dr. A. K. Tyagi, Director, Chemistry Group, BARC for their encouragement.

References

1. K. C. Barick, S. Singh, N. V. Jadhav, D. Bahadur, B. N. Pandey and P. A. Hassan, *Adv. Funct. Mater.* **22**, 4975-4984 (2012).
2. S. Chandra, K. C. Barick and D. Bahadur, *Adv. Drug Del. Rev.* **63**, 1267-1281 (2011).
3. K. C. Barick, S. Rana and P. A. Hassan, *J. Surf. Sci. Technol.* **31**, 60-68 (2015).
4. S. Rana, K. C. Barick and P. A. Hassan, *J. Nanofluids* **4**, 421-427 (2015).
5. S. Rana, K. C. Barick, N. V. Jadhav, B. N. Pandey and P. A. Hassan, *Dalton Trans.* **43**, 12263-12271 (2014).
6. K. C. Barick, Ekta, S. L. Gawali, A. Sarkar, A. Kunwar, K. I. Priyadarsini and P. A. Hassan, *RSC Adv.*, **6**, 98674-98681 (2016).
7. S. Nigam, K. C. Barick and D. Bahadur, *J. Magn. Magn. Mater.* **323**, 237-243 (2011).
8. S. Singh, K. C. Barick and D. Bahadur, *J. Hazard. Mater.* **192**, 1539-1547 (2011).
9. P. Sharma, S. Rana, K. C. Barick, C. Kumar, H. G. Salunke and P. A. Hassan, *New J. Chem.* **38**, 5500-5508 (2014).
10. J. Majeed, K. C. Barick, N. G. Shetake, B. N. Pandey, P. A. Hassan and A. K. Tyagi, *RSC Adv.* **5** 86754-86762 (2015).
11. S. Rana, N. G. Shetake, K. C. Barick, B. N. Pandey, H. G. Salunke and P. A. Hassan, *Dalton Trans.*, **45**, 17401-17408 (2016).
12. K. C. Barick and P. A. Hassan, *J. Coll. Interf. Sci.* **369**, 96-102 (2012).
13. S. B. Shelar, S. L. Gawali, K. C. Barick, A. Kunwar, A. Mohan, I. K. Priyadarsini, P. A. Hassan, *Mater. Sci. Eng.: C* **117**, 111272 (2020).
14. K.C. Barick, S. Singh, D. Bahadur, M. A. Lawande, D. P. Patkar and P. A. Hassan, *J. Colloid Interf. Sci.* **418**, 120-125 (2014).
15. B. Dutta, N. G. Shetake, B. K. Barick, K. C. Barick, B. N. Pandey, K. I. Priyadarsini and P. A. Hassan, *Colloids Surf. B.* **162**, 163-171 (2018).
16. S. L. Gawali, K. C. Barick, N. G. Shetake, V. Rajan, B. N. Pandey, N. N. Kumar, K. I. Priyadarsini and P. A. Hassan, *ACS Omega* **4**, 11728-11736 (2019).
17. K. C. Barick, A. Sharma, R. S. Ningthoujam, R. K. Vatsa, P. D. Babu and P. A. Hassan, *Dalton Trans.* **44**, 14686-14696 (2015).



Dr. S. B. Shelar received Ph.D. degree in Redox Biology from National University of Singapore, Singapore in 2014 and M. Tech degree in Biotechnology and Bioprocess Engineering from Indian Institute of Technology Kharagpur, India in 2009. He has done a postdoctoral research fellowship in Comprehensive Cancer Centre, University of Alabama at Birmingham, USA. In 2018, he has received a prestigious DAE-BRNS KSKRA fellowship. Presently, he is Scientific Officer (D) at Chemistry Division, Bhabha Atomic Research Centre, Mumbai. He has published more than 25 research articles in peer-reviewed international journals. His research interest includes development of targeted drug delivery systems for phototherapy and radiosensitization.



Dr. K. C. Barick obtained his Ph. D Degree in Metallurgical Engineering and Materials Science from Indian Institute of Technology Bombay, India in 2009. He was awarded prestigious DAE-BRNS KSKRA fellowship in 2010 and subsequently joined as a Scientific Officer (D) in Chemistry Division, BARC. He was also a visiting research fellow in the Department of Materials Science and Engineering at Northwestern University, USA under NSF-MWN Program. His research interest includes synthesis, surface functionalization and self-assembly of nanoscale multifunctional oxides, lipids and polymers, and investigation of their potential applications in biomedical and environmental field. Presently, he is Scientific Officer (F) at Chemistry Division, BARC, Mumbai and Assistant Professor in Chemical Sciences at Homi Bhabha National Institute (HBNI), Mumbai. He has more than 80 publications in peer-reviewed international journals and two Indian patents. He has received DAE SSPS Young Achiever Award (2016), DAE Group Achievement Award (2017), and DAE Scientific & Technical Excellence Award (2019) for his outstanding research contribution towards the development of various surface functionalized nanomaterials for healthcare applications. He has been selected as a Member of The National Academy of Science, India (2021).



Dr. P. A. Hassan joined Bhabha Atomic Research Centre (BARC), Mumbai in 1993 and presently serving as Head of Nanotherapeutics and Biosensors Section, Chemistry Division, BARC. He was a visiting researcher at the University of Louis Pasteur, Strasbourg, France in 1995. He pursued his post-doctoral research at the Department of Chemical Engineering, University of Delaware, USA in 2000-2002. He has visited advanced neutron scattering facilities like National Centre for Neutron Research, NIST, Maryland, USA and Institute Lau Langevin, Grenoble, France. He has co-authored more than 170 papers in peer-reviewed journals, 9 book chapters and 1 Indian patent. His current research interests include microstructure and dynamics of self-assembly, polymers, polyelectrolyte-surfactant interactions and nano drug delivery systems. He is an elected fellow of the National Academy of Sciences, India

SOCIETY FOR MATERIALS CHEMISTRY (SMC)
(Reg. No. - Maharashtra, Mumbai/1229/2008/GBBSD)
c/o Chemistry Division
Bhabha Atomic Research Centre, Mumbai 400 085

APPLICATION FOR MEMBERSHIP

Please enroll me as a Life member of the *Society for Materials Chemistry (SMC)*. My particulars are as follows:

Name : _____

Educational Qualifications : _____

Field of Specialization : _____

Official Address : _____

Telephone No. (Off.) : _____

Residential Address : _____

Telephone No. (Res.) : _____

Address for Correspondence : Home/Office (Please tick one of the options)

E-mail Address : _____

Subscription Details

Mode of Payment : Cheque/DD/Cash
(Cheque/DD should be drawn in favor of "*Society for Materials Chemistry*" for Rs. 1000/- payable at Mumbai. For out-station *non-multi-city* cheques, please include Rs.50/- as additional charge for bank clearance.

Number : _____

Dated : _____

Drawn on Bank & Branch : _____

Amount : _____

Place: _____

Date: _____

Signature

Registration Number: _____

(To be allotted by SMC office)

Printed by:

Ebenezer Printing House

Unit No. 5 & 11, 2nd Floor, Hind Service Industries

Veer Savarkar Marg, Shivaji Park Sea-Face, Dadar (W), Mumbai - 400 028

Tel.: 2446 2632 / 2446 3872 Tel Fax: 2444 9765 E-mail: outworkeph@gmail.com

In this issue

Sr. No	Feature Articles	Page No.
1	Glasses and composites based on phosphate and silicate glasses <i>V. Sudarsan</i>	1
2	Intrinsically radiolabeled nanoplateforms for cancer theranostics <i>Rubel Chakravarty</i>	11
3	Synthesis and characterization of metallic nanoparticles using <i>Rheum emodi</i> roots and investigation of its antibacterial and cytotoxic potential <i>Deepika Sharma, Naveen Kumar, Priyanka Pareek and Lalita Ledwani</i>	19
4	Exploring the gravity of tin chalcogenides as potential energy materials <i>Gourab Karmakar, Adish Tyagi and G. Kedarnath</i>	25
5	Electrochemical techniques in evaluation of processes for energy and sensing applications <i>S. Manna Abhishek Sharma, Srikant Sahoo and A. K. Satpati</i>	33
6	Quantum cutting nanomaterials via ionic liquids <i>Pushpal Ghosh</i>	45
7	Development of surface functionalized nanoparticles for cancer therapy <i>S. B. Shelar, K. C. Barick and P. A. Hassan</i>	55

Published by
Society for Materials Chemistry
C/o. Chemistry Division
Bhabha Atomic Research Centre, Trombay, Mumbai 40085
e-mail: socmatchem@gmail.com, Tel: 91-22-25592001